ACUSTICA

VOL. 2 1952 No. 5

THE MECHANISM OF SOUND TRANSMISSION THROUGH SINGLE LEAF PARTITIONS, INVESTIGATED USING SMALL SCALE MODELS

by A. SCHOCH* and K. FEHÉR**

III. Physikalisches Institut der Universität Göttingen

Summary

The paper presents: 1. A qualitative theoretical discussion of sound transmission with regard to the finite area of partitions, 2. A technique of measuring the transmission of sound through partitions by means of small scale models, on the basis of the similarity law relating linear dimensions and frequency, 3. Measurements on homogeneous plates — representing single leaf partitions — with plane waves at varying angle of incidence as well as with diffuse (reverberant) sound. The results show the importance of the "coincidence effect" and the existence of additional "transmitted" waves caused by effects of the boundaries.

Sommaire

La présente note comprend: 1. Une théorie qualitative de la transmission du son établie en tenant compte du fait que les parois ont une surface finie. 2. Un procédé de mesure de la transmission du son à travers des parois à échelle réduite et basé sur les lois de similitude entre les dimensions linéaires et la fréquence. 3. Des résultats des mesures effectués sur des plaques homogènes représentant des parois simples, aussi bien avec des ondes planes sous différents angles d'incidence, qu'avec un son diffus (son de réverbération). Ces résultats mettent en évidence l'importance de l'effet de «coincidence» et l'existence d'ondes «transmises» additionnelles, qui sont dues à l'influence des bords.

Zusammenfassung

Die Arbeit enthält: 1. Eine qualitative theoretische Diskussion der Schallübertragung unter Berücksichtigung der endlichen Fläche von Wänden; 2. Ein Verfahren, die Schallübertragung durch Wände an Modellen in kleinem Maßstab zu messen; es beruht auf dem Ähnlichkeitsgesetz, das lineare Abmessungen und Frequenz verknüpft; 3. Messungen an homogenen Platten — die Einfach-Wände repräsentieren — sowohl mit ebenen Wellen bei verschiedenen Einfallswinkeln als auch mit diffusem Schall. — Die Ergebnisse zeigen die Bedeutung des „Koinzidenzeffekts" und die Existenz zusätzlicher „durchgelassener" Wellen, die von der Wirkung der Ränder herrühren.

I. INTRODUCTION

The first step to an understanding of the mechanism of sound transmission through partitions of any structure must be the study of single leaf walls, because the latter form the basic elements of most structures.

The experimental result that the mass per unit area is the most important factor in the transmission of sound through single leaf partitions, leads to the earlier theories which regarded such partitions simply as mass reactances set in vibration by the differences of the sound pressures on the two surfaces. It is well known that these simple theories failed to give a satisfactory explanation for the measured values of transmission. A rigorous theory of the transmission of plane waves through solid plates (of infinite extent), which had been given by H. REISSNER [1] on the basis of the classical theory of elasticity, should have provided a much better approach to the problem. Unfortunately, the results of this theory were so discouragingly complicated, that it has never been applied to the problem of sound transmission in buildings. In 1942, L. CREMER [2] treated the same problem, using the approximate elementary theory of bending of thin plates, and arrived at a manageable result, which has added considerably to our understanding of the mechanism of transmission.

The restriction of CREMER's theory to plates, the thickness of which is small compared with the wave-

---

* Present address: Institut für theoretische Physik der Universität Heidelberg.

** Present address: Electroacustic G.m.b.H., Kiel.

lengths inside them, is adequate for the plates occurring as partitions in buildings. The assumption of plates of infinite extent may, however, be open to objection. The influence of the boundaries of the plates can be discussed theoretically in a qualitative way, but a quantitative treatment of this problem meets with great difficulties as will be discussed below. Therefore an experimental study of the phenomena in question was attempted.

To permit measurements using plane waves so that the plates themselves and other conditions could be easily changed, relatively small plates and high frequencies have been used in the experiments in such a way, that the plates can be considered as small scale models of partitions of ordinary size. In this report, (i) a theoretical discussion on which experiments were based, (ii) the technique of the model experiments, and (iii) their results are presented.

II. THEORETICAL DISCUSSION

1. Summary of Cremer's results for plates of infinite area

As CREMER's results will be made the starting point of the present investigation, a short summary of them is given.

If a plane wave in air of sound pressure amplitude P_1 strikes the infinite plate at an angle of incidence ϑ (taken as the angle between the normals to the plate and to the wave-front), the transmitted wave is a plane wave of the same direction and, generally, with a reduced sound pressure amplitude P_2. According to CREMER [2] the ratio α of the (complex) amplitudes in the incident and transmitted waves is

$$\alpha = \frac{P_1}{P_2} = 1 - i\frac{\omega d}{2c}\frac{\rho_p}{\rho}\left[(1+i\eta)\left(\frac{v_0}{c}\right)^4 \sin^4\vartheta - 1\right]\cos\vartheta. \tag{1}$$

The "reduction factor", i. e. the ratio of the incident and transmitted acoustic powers, is then given by[1]

$$|\alpha|^2 = \left|\frac{P_1}{P_2}\right|^2 = \left[1 + \eta\frac{\pi f d}{c}\frac{\rho_p}{\rho}\left(\frac{v_0}{c}\sin\vartheta\right)^4\cos\vartheta\right]^2 + \left\{\frac{\pi f d}{c}\frac{\rho_p}{\rho}\left[\left(\frac{v_0}{c}\sin\vartheta\right)^4 - 1\right]\cos\vartheta\right\}^2 \tag{2}$$

where: $\omega = 2\pi f$ = pulsatance; ρ_p = density, d = thickness of the plate ($\rho_p d$ its mass per unit area); ρ = density, c = velocity of sound in air; η = loss factor[2].

v_0 is the velocity of free flexural waves on the plate; it can be expressed in terms of the elastic constants, the thickness of the plate, and the frequency in one of the following equivalent ways:

$$v_0^2 = \sqrt{\frac{E}{\rho_p \cdot 12(1-\sigma^2)}} \cdot 2\pi f d = \frac{\pi \cdot c_l}{\sqrt{3(1-\sigma^2)}} f d, \tag{3}$$

where E = Young's modulus, σ = Poisson's ratio, c_l = velocity of longitudinal waves in a bar of the same material. The attribute "free" is added to indicate that v_0 refers to such flexural waves as propagate from single points or contours of excitation. In contrast to these free waves, the flexural wave forced by an incident plane wave on an infinite plate travels with the velocity of the lines of intersection between the wave planes and the plate, i. e. with the velocity $c/\sin\vartheta$. The most noteworthy deduction from (2) is the appearance of an angle ϑ_0 of maximum transmission, determined by the condition

$$\frac{v_0}{c} \cdot \sin\vartheta_0 = 1. \tag{4}$$

The maximum transmission is total if $\eta = 0$, that is in the absence of dissipative energy losses. Condition (4) expresses "coincidence" of the velocities $c/\sin\vartheta$ and v_0 of "forced" and "free" flexural waves. CREMER emphasized the analogy of this interpretation with the similar relations which hold for the frequency of maximum response of a resonant system to an applied periodic force.

According to (4), a real "coincidence angle" exists for $v_0 > c$ which requires, by (3), that the product of frequency and thickness exceed a certain critical value, depending on the material of the plate:

$$fd > (fd)_{\mathrm{crit.}} = \frac{\sqrt{3(1-\sigma^2)}}{\pi} \cdot \frac{c^2}{c_l}. \tag{5}$$

For fd considerably below the critical value, the formula (2) for the reduction factor reduces to

$$|\alpha'|^2 = 1 + \left(\frac{\pi f d}{c}\frac{\rho_p}{\rho}\cos\vartheta\right)^2 \tag{6}$$

This formula corresponds to the bending stiffness of the plate being neglected. Under this condition, the mass $\rho_p d$ per unit area is the only material property left.

According to (2), total transmission appears also for grazing incidence, $\vartheta = 90^0$. This however, is not exactly true, but is due to limitations in the approximate theory for the bending of plates on which (2) is based. If the rigorous theory for the transmission of sound through plates [1], [3] is applied and is particularised to the case of thin plates, zero transmission for grazing incidence and a maximum for almost grazing incidence is found. Another modification due to these limitations arises in the case of the velocity v_0 of flexural waves. In reality, v_0 can not exceed the velocity of the RAYLEIGH surface waves, and in consequence, the coincidence angle does not decrease below a certain limiting angle. Both these modifications do not seriously restrict the approximation (1), (2).

---

[1] For practical purposes, the reduction factor is commonly given in db as $R = 10 \log |P_1/P_2|^2$ db.

[2] The loss factor η as used in the reports [4] by KUHL and KAISER (usually denoted by Q^{-1} in the American literature) is the ratio of the imaginary to the real part of the complex Young's modulus.

The influence of the loss factor η (which is 10^{-4} to 10^{-2} for building materials [4]) becomes marked only if ϑ is near to the coincidence angle. It reduces the transmission maximum at coincidence. To effect a significant general increase of the reduction factor, an η of 1 or more would be required. Values so high are seldom found in solid materials.

In the usual method of measuring transmission between reverberant rooms, the incident sound field is diffuse. It can be represented as a superposition of plane waves of all directions. For a perfectly diffuse sound field, a uniform distribution over all directions is supposed. If the reduction factor depends on the angle of incidence (as it does according to (2)), the average reduction factor is given by

$$\overline{|\alpha|^2} = \frac{1}{2\int\limits_0^{\pi/2} \frac{\cos\vartheta \cdot \sin\vartheta}{|\alpha(\vartheta)|^2}\, d\vartheta} \qquad (7)$$

The occurrence of a coincidence angle and a transmission maximum above the critical frequency determined by (5) causes a drop in the curve of the average reduction factor against frequency. Such a drop has actually been observed in many cases [5] . . . [8].

2. Free flexural waves on unlimited plates in contact with a surrounding medium

The vibrations of a plate of finite area excited by the sound pressure in the surrounding medium can be described in two different, equivalent ways: They may be represented either as a superposition of the amplitude distributions at the normal modes of the plate (the frequency however being that of the exciting pressure for all modes), or as a superposition of the "forced" flexural wave of the infinite plate on the "free" flexural waves, the addition of which allows for the fulfilment of the boundary conditions [9], [10], [11]. In the latter representation, the disturbance of the forced wave by the change in structure at the boundary may be said to release free waves. This second representation is best suited for the following essentially qualitative discussion.

The free waves in the plate generate sound waves in the surrounding medium, and due to this they will be modified in some way. A rough estimate of the sound field produced and its reaction on the free flexural waves may be derived from consideration of a one-dimensional, progressive wave, travelling in an infinite plate. Then, the amplitude of the plate varies in space and time according to

$$e^{i(kx-\omega t)}$$

and the sound waves generated in the surrounding medium are plane (though generally of the "lateral attenuation" type), the angle ϑ of their direction of propagation being connected with the propagation constant k of the flexural waves by

$$k = \frac{\omega}{c}\sin\vartheta. \qquad (8)$$

In general, k will be complex, $k = k'(1+i\gamma)$, the real part determining the phase velocity v by

$$k' = \omega/v$$

and the imaginary part $k'\gamma$ determining the attenuation by radiation. Writing $\sin\vartheta \equiv z$, and using relation (8), k is obtained from (1) by putting $P_1 = 0$ (no incident wave present). The resulting equation can be written[3]

$$\sqrt{1-z^2}\left[\left(\frac{z}{z_0}\right)^4 - 1\right] = i\,\frac{\rho}{\rho_p}\,\frac{c}{\pi f d}\,. \qquad (9)$$

Here $z_0 = \sin\vartheta_0 = c/v_0$, where ϑ_0 is the coincidence angle defined by (4), and v_0 the velocity of flexural waves on the unloaded plate given by (3). The roots z of equation (9) determine the possible propagation constants of free flexural waves associated with waves in the surrounding medium. They appear in pairs, the two roots in each pair differing in sign only and corresponding to waves of the same type travelling in opposite directions. For a given material, the roots depend on the parameter fd (= frequency-thickness product of the plate), by which also v_0 and z_0 are determined.

Eq. (9) possesses 3 pairs of physically significant roots[4]. We have therefore three branches of curves for the phase velocity v and for the attenuation factor γ of the free waves as functions of fd. The curves are sketched roughly in Fig. 1 for aluminium plates in air. The numerical computation of the roots of (9) is laborious, particularly for $fd < (fd)_{\text{crit.}}$. For this reason the γ-curves given in Fig. 1 are not quite complete. (Other, though also incomplete discussions of the curves, have been given by OSBORNE and HART [12] and by FAY [13].)

---

[3] Substantially the same equation is derived in the report [11] by L. CREMER by an argument based on energy flux relations (Sect. 15, p. 153, eq. (105)).

[4] The physically significant roots must satisfy a condition ensuring "outgoing waves", which requires that the energy flux at the surface of the plate is directed off the plate. This does not imply the condition that the attenuation be positive in the direction of phase propagation (as erroneously supposed in [12], [13]), because in a plate the energy flux may be opposed to the direction of phase propagation.

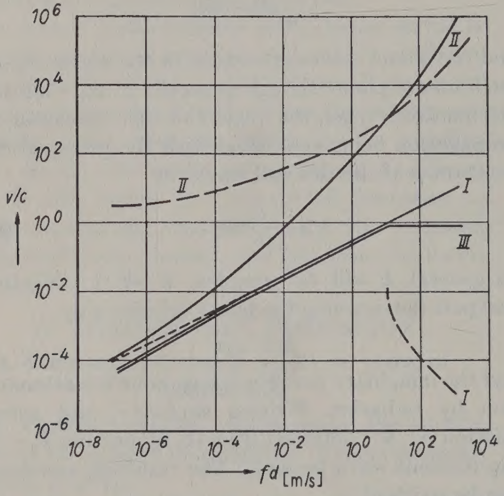

Fig. 1. Phase velocity v and attenuation factor γ (dashed) of free flexural waves on aluminium plates in air.

Branch I belongs to the flexural waves proper; it changes into $v = v_0$, $\gamma = 0$ by putting $\rho = 0$, i. e. by removing the surrounding medium. The reaction of the medium barely affects the velocity, except for very small fd, where $v \sim (fd)^{3/5}$, instead of $v \sim (fd)^{1/2}$ as for the plate in a vacuum. The range of fd, in which this effect occurs, is of no importance for our problem; it may however play a part for plates submerged in liquids. More important is the attenuation of the flexural waves, caused by the radiation of sound waves into the surrounding medium. For fd above the critical value $(fd)_{\text{crit.}}$ a simple approximate expression for the propagation constant is easily derived. In the practical cases which are of interest here the right-hand-side of (9) is very small,

$$\frac{\rho}{\rho_p}\,\frac{c}{\pi fd} \ll 1,$$

and an approximate root is given by

$$z = \pm z_0\left(1 + \mathrm{i}\cdot\frac{1}{4}\cdot\frac{\rho c}{\rho_p \pi fd}\,\frac{1}{\sqrt{1-z_0^2}}\right) \qquad (10)$$

provided also that

$$\frac{1}{4}\cdot\frac{\rho c}{\rho_p \pi fd}\,\frac{1}{\sqrt{1-z_0^2}} \ll 1,$$

i. e. v_0 not near c. For $fd > (fd)_{\text{crit.}}$, this root belongs to branch I. From (10) it follows that $\sin\vartheta \approx \sin\vartheta_0$, which means that the direction of the radiated wave is approximately the same as that of coincidence. Using (6), the attenuation factor γ may, then, be expressed in terms of the reduction factor $|\alpha'|^2$ which the plate would offer if it were perfectly flexible:

$$\gamma = \frac{1}{4|\alpha'|}. \qquad (11)$$

The higher the sound insulation of a plate, the lower the radiation damping of its free flexural waves. It is interesting to compare this attenuation with that caused by a loss factor η due to internal damping of the material of the plate:

$$\gamma_{\text{int.}} = \eta/4.$$

So the quantities to be compared are $1/|\alpha'|$ and η. For a plate with a reduction factor

$$10\log|\alpha'|^2 = 40\ \text{db}, \quad \gamma = 10^{-2},$$

whereas the loss factors of common building materials are in the range $\eta = 10^{-4}$ to 10^{-2}. Therefore radiation usually contributes significantly to the attenuation of flexural waves on plates.

All this holds for $fd > (fd)_{\text{crit.}}$. For $fd < (fd)_{\text{crit}}$ (or $z_0^2 > 1$), z would be real according to (10), and therefore there would be zero attenuation. A more detailed examination of the roots of (9) indicates, however, that for $fd < (fd)_{\text{crit.}}$ the approximate root given by (10) must be ascribed to branch III. Branch I is difficult to compute in this range; but the pertaining waves are attenuated, γ approaching the high value 0.73 ($= \operatorname{tg}\pi/5$) for $fd \to 0$.

The waves of branch II show very high attenuation. This type of wave represents an "edge-effect"; it is important for adjusting the wave motion on the plate to boundary conditions. Due to the high attenuation, its influence is usually marked in the neighbourhood of the boundaries only. For the unloaded plate, branch II changes into $v = \infty$, $\gamma = \infty$, with k then becoming $\mathrm{i}\omega/v_0$, as is well known from the ordinary theory of flexural vibrations of thin plates.

Branch III does not exist for unloaded plates. The relevant waves have a velocity very little below that of the surrounding medium for $fd > (fd)_{\text{crit.}}$. For smaller fd, the velocity almost coincides with that of branch I. The attenuation factor γ is zero for branch III.

3. Transmission through bounded plates

To discuss the case of bounded plates, consider for simplification an infinitely long strip with parallel edges, in a one-dimensional state of vibration, in which the amplitudes depend only on the x-coordinate, the x-axis lying in the plate perpendicular to the edges.

Omitting the influence of a surrounding medium, only the degenerations of the branches I and II in Fig. 1 exist, and the amplitudes of the two types of free waves are uniquely determined by the boundary conditions at the edges of the plate, and by the amplitude of the "forced" wave. As we have with a surrounding medium three types of free waves, their amplitudes can no longer be uniquely determined by these same conditions[5]. In fact the boundary conditions at the edges of the plate have to be supplemented by further boundary conditions holding for the associated waves in the surrounding medium; but the set of waves discussed in the preceding section 2 is far too restricted to permit the adjustment of the wave field to these supplementary conditions as can be seen by trying to solve even simple specified problems in this way. The problem of free waves should preferably be attacked by taking account of the boundary conditions in the surrounding air space from the beginning. This of course means a considerable complication.

It will therefore be necessary not to exaggerate the significance of the special free waves discussed in the preceding section. But it may be expected that the exact vibration of the plate must approach that which would be found without reaction of the medium, provided that the reaction is small, which is true for air. The two modes of free waves with definite amplitudes which appear in this way may be identified afterwards with those modified free waves which show closest correspondence. The correspondence is obvious for the "edge-effect" mode. Due to its high attenuation, the edge effect will, however, give no appreciable contribution to the sound field. It is also obvious that the flexural wave proper should correlate with branch I for $fd > (fd)_{\text{crit.}}$. If $fd < (fd)_{\text{crit.}}$, it seems more reasonable to identify the flexural wave with branch III, because the sound field associated with branch I in this range is rather unlikely near a plate of finite width as is revealed by closer examination. An important consequence of this correlation is the following: For $fd < (fd)_{\text{crit.}}$, free flexural waves do not radiate acoustic energy into the surrounding medium, because $\gamma = 0$ für the branch-III-mode. The sound field associated with branch III has the characteristics of a pure surface wave.

Thus we arrive at the following picture of the transmission of sound through a plate placed tightly in the gap of an impermeable wall (Fig. 2). Firstly, we have a transmitted wave W_1, which is due to the forced flexural wave. If the wavelength amounts only to a fraction of the width of the plate, W_1 leaves the plate more or less as a pencil in the direction of the incident wave, as indicated by dashed wave boundaries in Fig. 2. The amplitude of W_1 is the same as for an infinite plate, and given by CREMER's formula (1). The free flexural waves released from the edges and travelling in opposite directions form a standing flexural wave on the plate. Therefore, their amplitudes are large at resonance frequencies of the plate, and smaller between resonance frequencies. If fd is below $(fd)_{\text{crit.}}$ the free waves do not radiate, so that the transmission does not differ from the infinite plate in this case. But for $fd > (fd)_{\text{crit.}}$, additional waves W_2 and W_3 are radiated at the coincidence angle from each of the two opposite free flexural waves. The amplitudes of W_2 and W_3 must be expected to vary with frequency and to show maxima at resonance frequencies. The amplitudes also depend on the intensity of the "primary" forced flexural wave; they are largest, if the incident wave strikes the plate at the coincidence angle. Under this condition, W_1 and W_2 coincide in direction, and by interference they may sometimes even cancel each other. In summing up all directions, for $fd > (fd)_{\text{crit.}}$ an increase of the energy transmitted per unit area as compared with the infinite plate will be most likely, due to the effect of the free flexural waves.

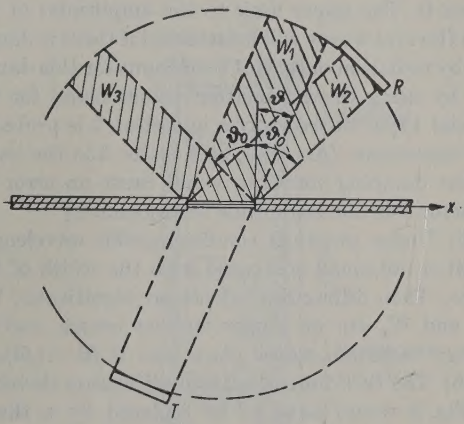

Fig. 2. Waves transmitted by bounded plate in impermeable screen.

A reliable quantitative estimate of the amplitudes of W_2 and W_3 (and thus of the increase of transmitted energy), based on the above conception, is difficult for various reasons:

---

[5] already remarked by FAY [13].

(i) The amplitudes of the free flexural vibrations at resonance frequencies depend on the damping effects of radiation and of the partial absorption of the flexural waves at the edges. Damping by absorption at the edges will usually be of major importance; it depends largely on the fastening of the edges and on the properties of the adjoining walls, and no general predictions can be made about it. The upper limit to the amplitudes of the free flexural waves will be attained if there is damping by radiation only. But to account for this damping by using the attenuation values found for the special types of free waves in section 2 is probably too inaccurate. (An error by a factor 2 in the value of the damping constant would cause an error by a factor 2 in the amplitude at resonance.)

(ii) Under practical conditions, the wavelength is often not small compared with the width of the plate. Then diffraction effects are significant; W_1, W_2 and W_3 are no longer distinct beams, and an energy radiation takes place also if $fd < (fd)_{\text{crit.}}$.

(iii) The two-dimensional simplification sketched in Fig. 2 would have to be replaced by a three-dimensional treatment.

Although the picture here given of the mechanism of sound transmission[6] (because of its complication) reduces the prospects of obtaining theoretical values for the reduction factor, it may nevertheless help in the understanding of more details than before. It leads to the useful conclusion that the reduction factor of a plate cannot on the average exceed the value which the infinite plate would have. To attain this value, suppression of the free flexural waves is necessary; this can be attempted either by a considerable augmentation of the internal damping of the material, or by absorbing the flexural waves by suitably fastening the edges.

To check the above picture — which must be to a certain extent guesswork — the model experiments described in the following sections were carried out.

III. TECHNIQUE OF ACOUSTIC MODEL MEASUREMENTS

4. Similarity relations

The correct basis for acoustic model experiments is a simple similarity relationship between the sound fields in the original and in the model structures.

If all linear dimensions of the structure are reduced by the ratio $1:\mu$ in the model, and if each part of the model consists of exactly the same material as the corresponding part of the original structure, every mode of vibration of the original structure corresponds to a geometrically similar mode of the model, the time scale, however, being reduced also by the factor μ, i. e. the movement of each particle of the model is exactly the same as that of the corresponding particle of the original, except that the frequencies are multiplied by μ in the case of the model. As a consequence, the ratio of the amplitudes in two different points of the structure is the same in the original and in the model, provided that corresponding vibrations have been excited. In particular, the reduction factors of partitions measured in a model with corresponding excitation must agree with those measured at full scale. In the special case of sound transmission through plates, the similarity law is revealed by the appearance, e. g. in formula (1), of frequency and thickness only in the product fd.

The similarity law here pointed out holds as long as effects due to dissipation and gravity may be neglected. It was stated by Lord RAYLEIGH [14]; more recently, C. W. KOSTEN [15] has recommended its application to problems of architectural acoustics. Its validity may be shown by the following reasoning:

In every homogeneous part of a structure, the elastic displacements satisfy the differential equations of elastic theory [16], which are of the second order with respect to the time and to the space variables. Therefore a solution of these equations remains valid, if the time variable as well as the space variables are changed by the same factor μ. This is true also of the solutions pertaining to a composite structure as a whole if the boundary conditions characterizing the coupling between adjacent parts do not contain derivatives with respect to the time (by this assumption viscous forces at the boundaries are excluded).

The argument given is equivalent to the statement, that for the vibration pattern of the structure only the ratios of its linear dimensions to the wavelengths are relevant. As the velocities of elastic waves in non-dissipative media, as well as the elastic constants, are independent of frequency[7], we arrive again at the result that inverse proportionality between linear dimensions and frequency is required to maintain a certain mode of vibration, if the size of the structure is altered.

---

[6] The essential ideas of it are outlined already in CREMER's book [10].

[7] To avoid confusion, it may be emphasized that only the elastic waves, which are possible in the unlimited media, are of importance in this connection; in the case of isotropic solids, there are two fundamental types, density (longitudinal) and shear (transverse) waves. The vibrations occurring in structures of finite extension (like for instance flexural waves in bars and plates) can always be represented by a superpositon of those fundamental types.

With regard to the restrictions imposed on the similarity law by dissipation and gravity effects, the following remarks may be made: Gravity acts only in-so-far as it influences the differential elastic constants which determine the velocities of elastic waves of small amplitude. Because building structures often are loaded with heavy weights, the influence of gravity may be important in some cases[8]. Being a second order effect, it may however be neglected in most cases. The losses of vibrational energy by dissipation are relatively low in ordinary construction materials, such as metals or even concrete, bricks and wood. The propagation of sound waves in structures is therefore mainly determined by the elastic properties and the densities of the materials. Thus the usefulness of model experiments is not too seriously restricted by dissipation effects. Furthermore, the similarity law quoted above is valid also in the case of dissipation, if the dissipation is of a special nature, namely if the loss factor is independent of frequency, and, fortunately, this is approximately true for the materials specified above [4], [17].

5. Dimensions of the models and range of frequencies

It was intended to study first the transmission of plane waves. Experiments with plane sound waves require either large distances from the sound source or sound sources of a high directivity. It was found easier to realize the second alternative by the construction of suitable electroacoustic transmitters. Then the requirement that the diameter of the diaphragm of the transmitter be large in comparison with the wavelength more or less determines the scale of the model arrangement. The transmitters used were adapted to the frequency range from about 2 to 100 kc/s; comparing this with the frequency range of practical measurements of sound transmission in buildings (100 to 3200 c/s) [18] a reduction ratio of 1:20 to 1:30 results for the linear dimensions of the model partitions. Thus a wall with an area of 3×5 m^2 and a thickness of 10 cm should be transformed into an area of at most 15×25 cm^2 and a thickness of 5 mm in the model.

The apparatus used for model measurements in the range of 2 to 100 kc/s is described in the following sections.

6. Electrostatic acoustical transducers

A cross sectional sketch of the electrostatic transducers designed for the model measurements is shown in Fig. 3. The vibrating diaphragm is a paperfoil (thickness 0.008 to 0.012 mm, area 12×12 cm^2) metal coated on its outside, and actuated by an electrostatic force applied through a rigid metal electrode[9]. This electrode is lightly pressed against the back of the paper foil by springs, but the foil is free to vibrate over a pattern of grooves cut into the surface of the electrode. (The grooves are 0.5 mm wide and 0.5 mm deep, and not drawn to scale in Fig. 3; a detailed report on the design and the properties of this type of electrostatic transducer has been given by KUHL [19].) The alternating driving voltage is applied between the back electrode and the metal layer of the foil, together with a direct voltage, which is necessary to produce a component of the driving frequency in the electrostatic force.

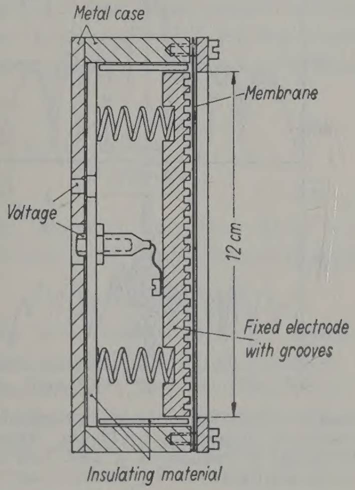

Fig. 3. Electrostatic transducer.

The alternating voltage must be small compared with the direct "polarizing" voltage in order to suppress the double frequency component in the force. In the systems described here, a direct voltage of 180 to 200 V and an alternating voltage of 1 to 20 V is applied.

The same kind of system is used as a receiving transducer. In this case, it represents a highly directive condenser microphone.

---

[8] An example is the reduction of the bending stiffness of a wall under vertical load.

[9] The paperfoil with evaporated metal coating is of the kind used in the manufacturing of condensers. We are indebted for it to Dr. E. TRAUB from the Robert Bosch G.m.b.H. in Stuttgart. Its application for the electrostatic transducers had been suggested by Dr. W. KUHL.

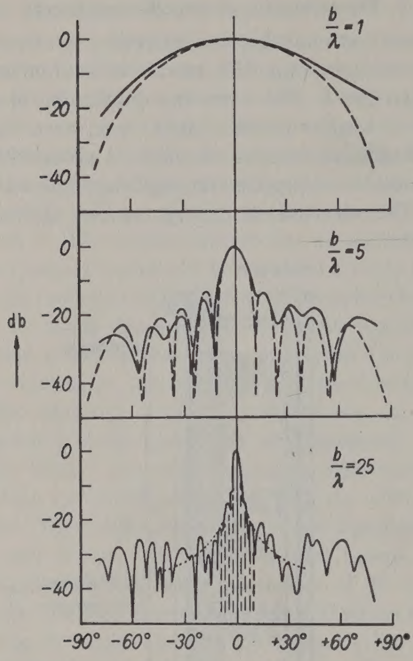

Fig. 4. Angular selectivity of the electrostatic transducers, breadth of diaphragm $b = 12$ cm. Ratios b/λ corresponding to frequencies of 2.83, 14.2 and 71 kc/s;
——— recorded,
— — — computed for piston-like vibration of diaphragm.

Fig. 4 gives examples for the angular selectivity of the transmission through free air between two equal electrostatic transducers as in Fig. 3 at a distance of 1 m. The response in db (with the maximum taken as a reference level) is plotted against the angle between the normal to the transmitting plane and the direction to the receiver. The curves refer to values of the ratio b/λ of 1, 5, and 25 (b = breadth of the square membrane, λ = wavelength in air). The curves are to be interpreted as the angular distribution of the set of plane waves, which — according to Fourier's theorem — is equivalent to the sound field radiated from the transmitter. By using a directive receiver, the sound field is — so to say — analysed into its component plane waves. At a very large distance, i. e. large compared with b^2/λ, the same angular distribution would be found with any receiver. For comparison, the angular distributions computed on the assumption of a piston-like vibration are drawn in Fig. 4 as dotted lines. (Apart from minor deviations, these distributions are given by the function [20]

$$\frac{\sin\left(\pi \frac{b}{\lambda} \sin \Theta\right)}{\pi \frac{b}{\lambda} \sin \Theta},$$

where Θ is the angle between the direction to the receiver and the normal to the transmitter.) They are in fair agreement with the measured curves. This proves that the vibrations of the membrane may be considered piston-like with a good approximation, and that, with the same b/λ, the angular selectivity cannot be greatly improved.

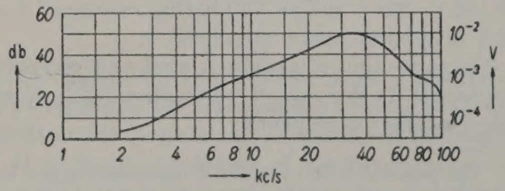

Fig. 5. Transmission between electrostatic transducers (distance 1.2 m). Voltage at receiving system vs. frequency, driving voltage at transmitting system constant (= 4 V).

The dependence upon frequency of the transmission between two electrostatic transducers (in parallel orientation) at constant driving voltage is shown in Fig. 5. There is a flat peak at 35 kc/s, which is due to a resonance of the foil, the air space between the foil and the rigid back electrode contributing to the stiffness. Below the resonance frequency, the slope of the response curve indicates a receiving voltage proportional to f^2 (the resonance curve of the transmitting foil, and the increase of the directivity with frequency contribute one factor f each). Most important for the present work is the smoothness of the response curve, which could not be easily attained with other types of transducers.

The sensitivity of the electrostatic transducers, to which the Figs 3, 4, and 5 refer, is 2 μb per volt driving voltage at a distance of 1 m, when used as transmitter, and 0.4 mV/μb, when used as microphone.

As the electrostatic force is proportional to the square of the voltage, the driving force contains the second harmonic of a sinusoidal driving voltage. The ratio of the amplitude of the second harmonic to the amplitude of the fundamental frequency is $V_{a.c.}/4\,V_{d.c.}$, where $V_{a.c.}$ = the amplitude of the alternating driving voltage and $V_{d.c.}$ = the additional direct voltage. Under the conditions specified above, the second harmonic produced in this way is more than 40 db below the fundamental. Another nonlinear distortion producing undesired harmonics might be suspected to result from restrictions of the free movement of the membrane. An experimental analysis, however, gave values of the harmonic components in the sound wave not exceeding the above estimate. Because of the slope of the response curve (Fig. 5) any harmonic content of the voltage generator appears magnified considerably in the sound pressure. Therefore, in all measurements described in this report interference by harmonic components in the spectrum of sound is prevented by the use of a selective amplifier with a high attenuation for frequencies outside the desired band.

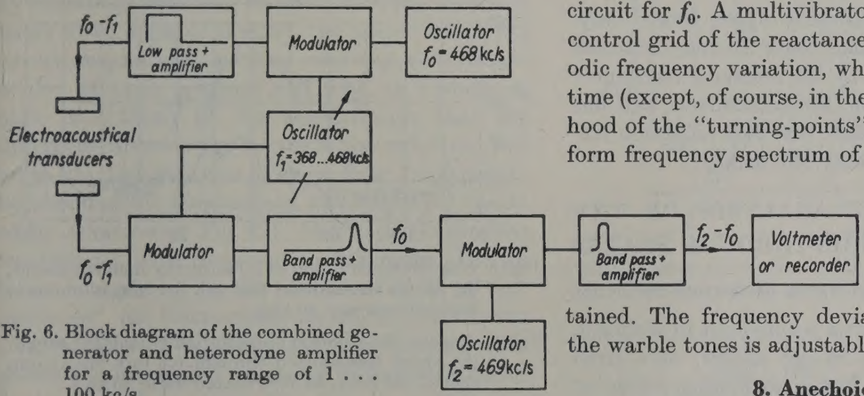

Fig. 6. Block diagram of the combined generator and heterodyne amplifier for a frequency range of 1 . . . 100 kc/s.

7. Driving voltage generator and selective amplifier with automatic tuning

A special electronic measuring set was developed, combining a beat frequency oscillator for the range of 0.1 to 100 kc/s, and a selective heterodyne amplifier for the range of 1 to 100 kc/s[10]. An amplifier with a restricted frequency band is to be recommended for keeping the noise level as low as possible, and for avoiding interference by higher harmonics. To be able to take recordings with continuously varying frequency, a device was desirable which would automatically adjust the pass band of the amplifier to the instantaneous frequency. This was realized by a device as shown in the block diagram Fig. 6. The frequency of the driving voltage for the transmitter is produced as the difference f_0-f_1 of a fixed frequency f_0 and a variable frequency f_1, both well above the required acoustic range. By combining the variable frequency f_1 with the low frequency f_0-f_1 in the modulator stage of the heterodyne amplifier, the fixed frequency is reproduced and can be amplified and selected by fixed filters. By means of a second modulator stage, $f_0=468$ kc/s is shifted to a low frequency $f_2-f_0=1$ kc/s, because it was easier to construct a band pass filter with the necessary sharp cut-off and high attenuation in the stopping band for this low frequency. It furthermore allows the use of a Neumann level recorder for output indication. Two pass bands can be chosen by a switch, the band widths being 50 c/s and 1000 c/s; the latter serves for measurements with frequency-modulated sound ("warble tons"). The amplifying set has a range of 70 to 80 db between the noise level and the limit given by the onset of non-linear distortion.

For frequency modulation of the generator voltage, a reactance tube is provided in the oscillator circuit for f_0. A multivibrator circuit acting on the control grid of the reactance tube produces a periodic frequency variation, which is made linear with time (except, of course, in the immediate neighbourhood of the "turning-points"). By this a fairly uniform frequency spectrum of the warble tone is obtained. The frequency deviation (band width) of the warble tones is adjustable from 0 to 1000 c/s.

8. Anechoic box

The plane wave measurements of sound transmission were carried out in an anechoic box of interior dimensions $1.5\times0.8\times0.8$ m^3. The sound absorbing lining covering the interior surface of the box is of the porous wedge structure type, which had proved particularly efficient for anechoic rooms [21], [22]. As in the present case the range of frequencies extends from 2 to 100 kc/s, the wedges can be made much smaller than usual; the flow resistance of the porous material must, however, be increased in the same proportion to obtain optimum absorption [23]. A lining with wedges 7 cm in length, sawn out from 13 mm fibre board, proved satisfactory. In Fig. 7 are shown the dimensions of the wedges, and the reflection factor r (= ratio of reflected amplitude to incident amplitude) of the lining as a function of frequency for various angles ϑ of incidence. The values for normal incidence, $\vartheta=0$, have been measured in a tube by the standing wave method; the values for oblique incidence in

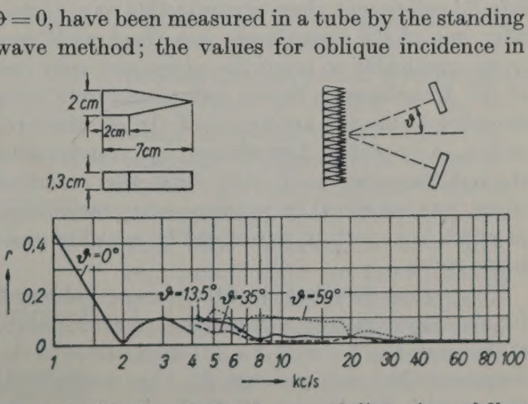

Fig. 7. Amplitude reflection factor and dimensions of fibre board wedges used in the anechoic box.

---

[10] The construction of the amplifier part was performed by Dipl. Phys. H. PRITSCHING.

the anechoic box itself by means of the electrostatic transducers described in section 6, in an arrangement sketched to the right of Fig. 7. Above 2 kc/s, the amplitude reflection factor does not sensibly exceed 0.1. As to the values measured by the second method ($\vartheta = 13.5°$, $\vartheta = 35°$, $\vartheta = 59°$), it must be observed that they represent upper limits only. Particularly at frequencies below 10 kc/s a fraction of the sound picked up by the receiving transducer is due to diffraction from the transmitter, and not to reflection from the wall. The real reflection factors are therefore probably still smaller.

IV. EXPERIMENTAL ANALYSIS OF THE SOUND TRANSMISSION THROUGH PLATES

9. Transmission of plane waves at normal incidence

To check the phenomena pointed out in section 3, rectangular plates, 16×26 cm² in size, were fixed in an aperture in a highly insulating screen of 80×80 cm² in size, consisting of two fibre board plates with a metal sheet sandwiched between. The specimen plates were pressed between soft rubber frames to secure an airtight support at the edges. The area remaining free was 15×25 cm². This support is probably almost equivalent to free edge boundary conditions, so that flexural waves on the plates will experience almost perfect reflection at the edges. An electrostatic transmitter and receiver of the type described in section 6 were arranged as indicated in Fig. 2 by T and R, at distances of about 30 to 60 cm from the plate. Both transmitter and receiver could swing about the centre of the plate (along the circular lines dotted in Fig. 2), to allow adjustment to any angle of incidence, and measurement of the transmitted radiation in any desired direction. Due to the angular selectivity of the receiver, the transmitted sound field can be analyzed into its component plane waves in this way. (Actually, one of the transducers was fixed, as it was more practicable to pivot the screen and only one of the transducers.) Screen and transducers were mounted inside the anechoic box. In all measurements, a possible disturbance by transmission through the screen itself, or by diffraction round its edges, was examined by supplementary recordings, in which the aperture was closed by a highly insulating cover.

The angular distribution of the transmitted sound for aluminium plates, recorded at normal incidence, is shown in Fig. 8 and 9, for different values of the frequency-thickness product *fd*. For comparison, the angular distribution of the incident wave (in the absence of the plate) is also recorded. The critical value is $(fd)_{\text{crit.}} = 12$ (kc/s) mm, and clearly there is practically no change of the primary distribution by transmission in Fig. 8, with $fd = 4$ (kc/s) mm (i. e. considerably below $(fd)_{\text{crit.}}$), a minor change for $fd = 10$ (kc/s) mm in Fig. 9, whereas for $fd = 20$ (kc/s) mm $> (fd)_{\text{crit.}}$ maxima occur at $\vartheta = \pm 53°$, corresponding to the free flexural wave radiations W_2 and W_3 of Fig. 2. The coincidence angle for $fd = 20$ (kc/s) mm is in fact 53° by computation according to (4) (compare also Fig. 15). The intensity of W_2 and W_3 is about 10 db below that of W_1 in this case.

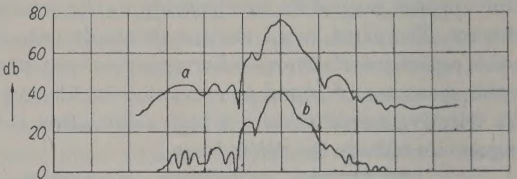

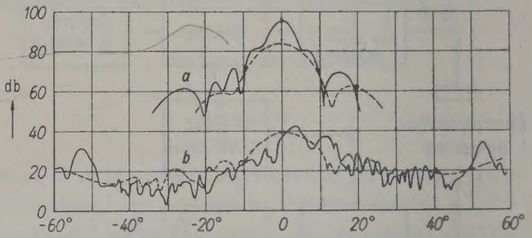

Fig. 8. Angular distribution of (a) normally incident sound, (b) sound transmitted through 0.1 mm aluminium sheet; frequency 40 kc/s.

Fig. 9. Angular distribution of (a) normally incident sound, (b) sound transmitted through 0.5 mm aluminium sheet. Full lines: 40 kc/s, dotted lines: 20 kc/s.

If we fix the receiving system at $\vartheta = 0$, we measure only the wave W_1 (Fig. 2), which should obey the theory for the infinite plate according to section 3. For normal incidence, the formula (2) for the reduction factor changes into the simple formula given by the earlier theories:

$$|\alpha|^2 = 1 + \left(\frac{\pi f d \varrho_p}{c\varrho}\right)^2 \qquad (12)$$

Fig. 10 and 11 show the results of measurements of the reduction factor at normal incidence for aluminium and plexiglass plates as a function of *fd*, obtained by recordings at varying frequency. The curves essentially agree with the dashed lines computed from (12), except for systematic deviations at the low frequency end of the curves, and for occasional peaks which cannot be satisfactorily explained at present. It must be observed however, that in the range in which deviations occur the wavelengths are not much smaller than the dimensions of the plate.

10. Transmission of plane waves at oblique incidence

If we measure the sound transmitted in the direction of the incident beam at oblique incidence, the wave W_2 interferes with W_1 if ϑ coincides or almost coincides with ϑ_0 (compare Fig. 2). This is confirmed by recordings like those reproduced in Fig. 12 which refers to an angle of $\vartheta = 24^0$; the upper and lower curves respectively are the receiving voltages recorded at open aperture and with an aluminium plate ($d = 2$ mm) in the aperture (so that the difference between the curves is the reduction factor in db). One observes (i) an increase in the neighbourhood of the frequency at which $\vartheta_0 = 24^0$ (marked by an arrow in Fig. 12); (ii) fluctuations of the transmission with frequency in this range. The increase is explained by the maximum of W_1 at "coincidence", the fluctuations are due to the varying contributions of W_2 when the free flexural wave passes the successive resonance and antiresonance frequencies of the plate. The frequency difference between successive maxima is in accordance with this explanation.

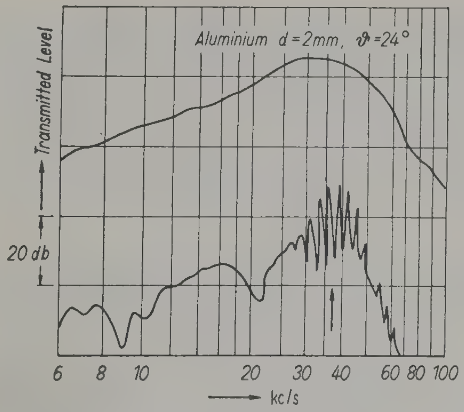

Fig. 12. Transmission recorded in oblique direction (Upper curve: level without plate).

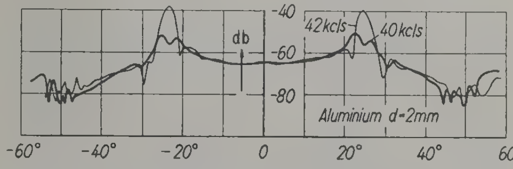

Fig. 13. Effect of resonance on W_1 in dependence on angle of incidence.

The effect of resonance of the free flexural wave on the transmission at the coincidence angle can be shown also by recording the transmission in the direction of the incident wave (i. e. recording W_1 in Fig. 2) at fixed frequencies and varying angles. Two recordings of this kind are given in Fig. 13, referring to the same plate as Fig. 12. The transmission maximum at the coincidence angle is evident, but is considerably dependent on the exact value of the frequency.

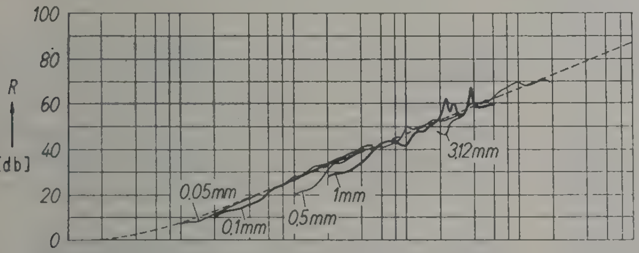

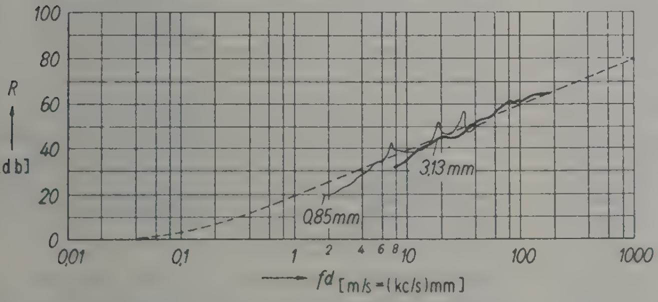

Fig. 10. Reduction factor R as a function of frequency × thickness for transmission of plane sound waves through aluminium plates of various thicknesses at normal incidence.
Dotted: Theoretical curve.

Fig. 11. Reduction factor R as a function of frequency × thickness for transmission of plane sound waves through plexiglass plates of various thicknesses at normal incidence.
Dotted: Theoretical curve.

Outside the neighbourhood of $\vartheta = \vartheta_0$ the curves in Fig. 13 are relatively smooth, because there is no appreciable interference of W_2 with W_1. For this reason, the amplitude of W_1 should be in accordance with Cremer's formula (2), apart from a range near $\vartheta = \vartheta_0$. This is checked in Fig. 14, where recordings of the angular dependence of transmission in the direction of W_1 are compared with curves computed from (2). The curves have been computed for three different values of the loss factor, namely $\eta = 10^{-3}$, 10^{-2}, and 10^{-1} (the value 10^{-1} is considerably higher than the values usually met with in common building materials, compare [4]). It is obvious from Fig. 14 that the influence of damping is restricted to the neighbourhood of the coincidence angle ϑ_0. Apart from intervals around ϑ_0, the recorded curves actually are fairly close to the theoretical curves, also with regard to the absolute values. The coincidence peaks appear less sharp in the recordings. This is, as Fig. 13 has shown, partly due to the interference of W_2 or W_3, and partly due to the restricted angular selectivity of the transmitter and receiver.

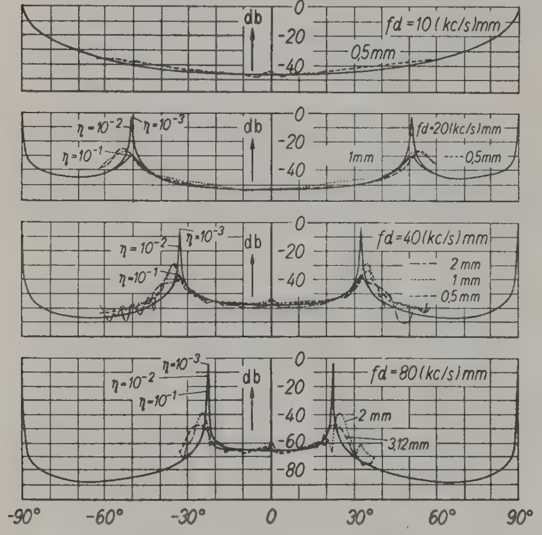

Fig. 14. Intensity of wave W_1 transmitted through aluminium plates in direction of incident wave (in db, with the intensity of the incident wave as a reference level) as function of angle ϑ of incidence, and for various values of *fd*.
Full lines: theoretical. Dashed and dotted lines: recorded.

Especially for large ***fd***, the coincidence peaks are shifted to angles slightly larger than the theoretical angles. This deviation results from the deficiencies of the elementary theory of flexural vibrations which has been mentioned in section 1. Obviously they are of no practical importance for the present problem.

Using the relation (4), the velocity v_0 of free flexural waves can be determined from the measurement of ϑ_0. As the peaks of recordings like those in Fig. 14 are accurately defined, this affords a good method of determining v_0. Results of measurements carried out in this way are shown in Fig. 15, where the square of v_0 is plotted against the frequency-thickness product. For each of a number of materials tested, a straight line is found, in accordance with formula (3). For very large ***fd***, the actual v_0^2 must remain below the straight line, as the velocity of the flexural waves cannot increase indefinitely. For comparison, the straight lines which would be expected for concrete and brickwork (according to [4]) are also drawn in the diagram, to show that in

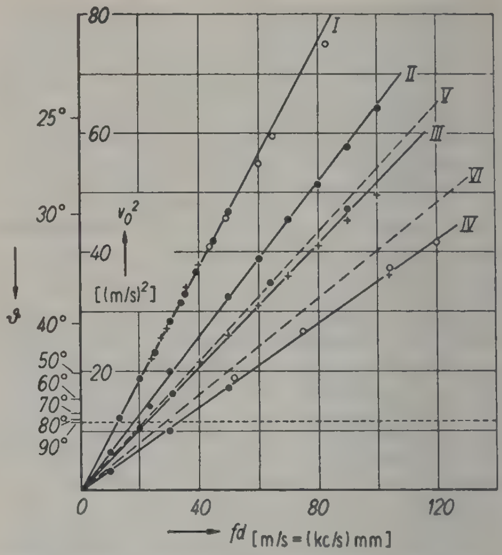

Fig. 15. Square of flexural wave velocity v_0, times 10^{-4}, as a function of frequency × thickness, determined from observed angles of maximum transmission.
I Aluminium (● 750×750×1 mm³, + 260×160×1 mm³, ○ 260×160×2 mm³),
II Brass (260×160×1 mm³), III Pertinax (● 260×160×1 mm³, + 260×160×3.2 mm³),
IV Plexiglas (● 260×160×1 mm³, ○ 260×160×3 mm³, + 260×160×10 mm³,
V, VI Lines to be expected for concrete and brickwork (for comparison).

this respect they fall into the range of the materials used in the model experiments.

At coincidence, the free flexural waves are excited most strongly, and a strong wave W_3, radiated by the reverse free flexural wave, can be observed. This is demonstrated in Fig. 16, where the angular analysis of the transmitted sound is recorded for the case of incidence at the angle ϑ_0, both for a resonance and a non-resonance frequency. The radiation of the reverse flexural wave apparently has the same intensity as the direct transmission.

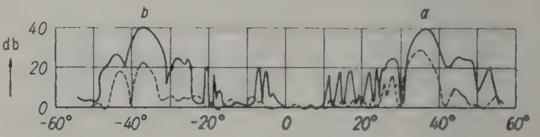

Fig. 16. Angular distribution of sound, transmitted through 1 mm aluminium plate, incident wave striking at coincidence angle. Peak (a) due to direct transmission, (b) due to radiation of reverse flexural wave on the plate. Full line: Excitation in a resonance frequency (36 kc/s); dotted: away from resonance (35 kc/s).

By diminishing the reflection of the flexural waves at the edges, or by providing for sufficient damping, the free flexural waves should be suppressed. In trying to verify this experimentally, it proved difficult to realize a low reflection of flexural waves. There were, however, several successful ways of increasing their attenuation to such a degree that the reverse wave disappeared. An example is given in Fig. 17, which shows the angular distribution of sound transmitted at coincidence through a plate consisting of two sheets of plastic board (Pertinax), sealed together by a thin layer of viscous wax. This compound plate behaves essentially like a homogeneous plate with a somewhat reduced stiffness as regards its flexural wave velocity, whereas attenuation is increased considerably. An arrow in Fig. 17 indicates where the radiation W_3 of the reverse wave should appear if it were present in appreciable intensity.

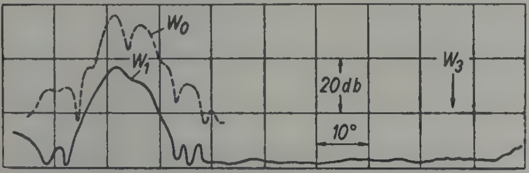

Fig. 17. Angular distribution of sound transmitted through highly damped compound pertinax plate (2 plates, $d = 1$ mm each, sealed together with wax). W_0 angular distribution of incident wave.

A similar damping effect was obtained with partitions consisting of two sheets of aluminium, the interspace (about 1 mm in the model scale) being filled with fine sand.

These observations confirm the statement already made in section 3, that a very high attenuation of the flexural waves — apart from a large mass per unit area — seems to be essential in the design of partition leaves with the highest possible reduction factors. Its effect is twofold: It eliminates the additional radiation of free flexural waves, and it flattens the coincidence peaks.

In principle, attenuation of the flexural waves can also be effected without dissipative losses by giving the plate, instead of a uniform thickness, a periodic structure, for instance by cutting equidistant, parallel grooves into its surface. For a flexural wave travelling perpendicularly to the grooves, this structure behaves like a loaded electrical communication line: If the frequency is within certain "cut-off-bands", there is no genuine propagation of waves, but a high reactive attenuation. The lower limiting frequency of the first cut-off-band is approximately given by the condition that the distance of the grooves be a half wavelength. Experiments with plates of that structure confirmed the existence of pronounced cut-off-bands, and the absence of coincidence peaks in the transmission for frequencies within these bands. This dissipation-free attenuation will probably be of theoretical interest only, because the cut-off-bands are of limited width, and the structure behaves differently for different directions of the flexural waves.

11. Transmission at random incidence

The measurements described in the preceding sections are in accordance with the picture of the mechanism of transmission pointed out in section 3. They disclose that for *fd* smaller than the critical value, the influence of the boundaries and of the flexural stiffness of a plate is negligible. For *fd* above the critical value, the coincidence effect becomes important; furthermore, radiation of free flexural waves adds to the transmission which an infinite plate would have, though the coincidence maximum will be reduced a little due to energy transferred to the free waves.

In the customary measuring technique, for all the above details only an average over many angles of incidence is observed. It seemed worth while to prove that, when using the same model plates measurements at random incidence lead to results of the type known from measurements of single leaf partitions of normal size. For this purpose, two "reverberation chambers", $60 \times 40 \times 30$ cm³ in size, with a common aperture of 15×25 cm² for the test specimens, were constructed. The walls were made from thick glass plates, and care was taken to avoid flanking transmission between the chambers. To facilitate the setting up of a diffuse sound field, special electrostatic transducers were designed, whose radiating (or receiving) surface was of cylindrical shape and had about the same area as the plane wave systems described in section 6.

As the transducers were relatively large, the ratio of the sound energy densities in the transmitting and receiving rooms could not be determined in the usual manner by using the receiving system at first in the transmitting room and subsequently in the receiving room. An uncontrollable alteration of the energy density in the transmitting room would result from the removal of the receiving system. Therefore the following procedure was adopted: One transducer was mounted in the transmitting room, and one in the receiving room. By means of the latter the energy density in the receiving room was measured, at first with the partition to be tested in the aperture, and subsequently with the partition removed. The correction which must be made for the absorption of the rooms is different from that necessary in the usual procedure. If E_2 and E'_2 denote the energy densities in the receiving room 2 with partition, and with partition removed, F (in m^2) the area of the aperture, A_1 and A_2 the absorptions (in m^2) of the transmitting room 1 and the receiving room 2, the reduction factor $|\alpha|^2$ is to be computed from[11]

$$|\alpha|^2 = \frac{E'_2}{E_2}\left(1 + F\frac{A_1+A_2}{A_1 A_2}\right) - F\frac{A_1+A_2}{A_1 A_2}, \qquad (13)$$

or as the rooms 1 and 2 are exactly equal in our experiments:

$$|\alpha|^2 = \frac{E'_2}{E_2}\left(1+\frac{2F}{A}\right) - \frac{2F}{A}. \qquad (14)$$

To examine the uniformity of the angular distribution of the sound energy in the transmitting room, the transmitting room was mounted in the anechoic box, and the sound emerging from plates fixed in the aperture of the room was analyzed by swinging a plane wave receiver about the centre of the plate in the way described in section 9. An example of the recording obtained is reproduced in Fig. 18. It refers to an aluminium plate 0.5 mm in thickness, at a frequency of 40 kc/s (warbletone). The recording paper is that of the Neumann level recorder with a 50 db potentiometer. The coincidence maxima at $\vartheta = \pm 53^0$ are clearly shown. On the whole the distribution corresponds to the curves of Fig. 14, found with plane waves, apart from irregular fluctuations within a range of 10 db about on average curve. From a number of similar recordings it can be concluded that the angular distribution of the incident sound actually is uniform at least down to about 15 kc/s. Below this frequency, the angular selectivity of the receiving system is too unsatisfactory to permit a reliable experimental examination. It may be observed that even for grazing waves ($\vartheta = 90^0$), the level is not appreciably below that at normal emergence. It is true that another maximum should occur near $\vartheta = 90^0$ according to the theoretical formula (2); but it must be borne in mind that the extension of the plate, as seen from the receiver, vanishes at grazing angles, a fact that makes difficult the correct interpretation of the recordings with regard to the distribution of the primary waves near grazing incidence.

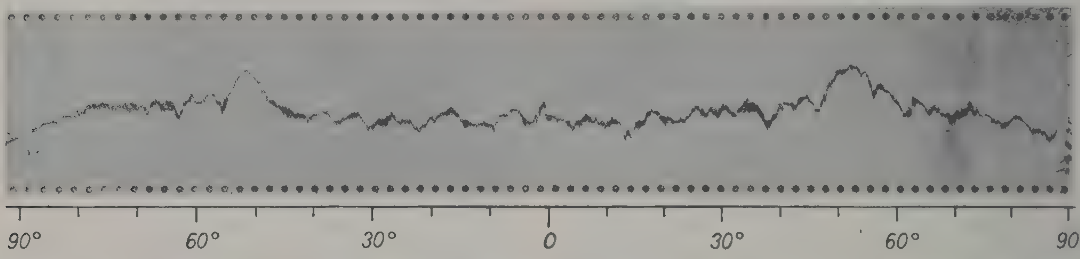

Fig. 18. Angular distribution of sound, emerging from wall of reverberant room; aluminium $d = 0.5$ mm, $f = 40$ kc/s.

A typical example of the recordings of the energy density levels in the receiving room, as obtained in transmission measurements between reverberant rooms, is given in Fig. 19. The upper curve is recorded with partition removed, the lower curve with partition in place. Several recordings taken with varied positions and orientations of the transducers are superposed to show that the curves are fairly independent of these positions, and permit the drawing of reliable average curves.

The absorption A of the model rooms, which must be known for the computation of the reduction factors from the recordings, was determined from the reverberation time T, using Sabine's formula

$$A = 0.162\ V/T$$

(A in m^2, V = volume in m^3, T = Sabine's reverberation time in s). T and A (referring to one room)

---

[11] The formula may be derived as follows: with partition, the acoustical energy flux N radiated from the transmitter, plus the flux coming from room 2, equals the flux absorbed in room 1 and transmitted through the partition. As the flux impinging on the unit area of the walls is $Ec/4$ (uniform angular distribution assumed, E = energy density, c = sound velocity in air), the equality is stated by

$$N = \frac{E_1 c}{4}\left(A_1 + \frac{F}{|\alpha|^2}\right) - \frac{E_2 c}{4}\,\frac{F}{|\alpha|^2}.$$

A similar equation holds for room 2 with $N = 0$:

$$\frac{E_2 c}{4}\left(A_2 + \frac{F}{|\alpha|^2}\right) - \frac{E_1 c}{4}\,\frac{F}{|\alpha|^2} = 0.$$

With partition removed, we have to replace $F/|\alpha|^2$ by F, and have the equations:

$$N = \frac{E_1' c}{4}(A_1 + F) - \frac{E_2' c}{4}F,$$

$$\frac{E_2' c}{4}(A_2 + F) - \frac{E_1' c}{4}F = 0.$$

Elimination of E_1, E_1' and N leads to equation (13) for $|\alpha|^2$.

are plotted against frequency in Fig. 20. T was measured by means of a Neumann level recorder; the single results are marked by points in Fig. 20. Reverberation times below 0.1 s are not measurable with the Neumann recorder, and for this reason there are no values in Fig. 20 above 30 kc/s. Fortunately, however, the correction $2F/A$ in (14) becomes small for the higher frequencies, and can, if necessary, be found by extrapolation.

The value of A, as given in Fig. 20 contains not only the influence of absorption by the walls, but also, to some extent, the absorption in the air itself, which becomes significant at the higher frequencies. It is important that this fact does not restrict the validity of the correction (14) if A denotes the effective absorption, including all influences.

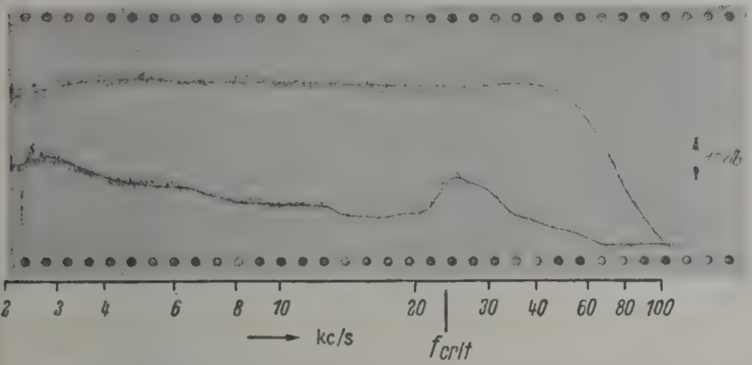

Fig. 19. Recording of sound reduction by plate between reverberant model rooms; aluminium $d = 0.5$ mm, $\Delta f = 1000$ c/s.

The dashed curve in Fig. 20 may be of interest for the judgment of the reliability of the statistical energy flux considerations, on which formula (13) is based. This curve gives the absorption of one of the model reverberation boxes with the aperture open, and the whole box situated in an anechoic room. The open aperture of area $F = 3.75 \times 10^{-2}\ \text{m}^2$ should be expected to add the amount F (at most) to the absorption of the completely closed box. Within an error of about 25%, this actually is the case. (At higher frequencies, there is already considerable absorption with closed aperture, so that the full area of the aperture is not effective.)

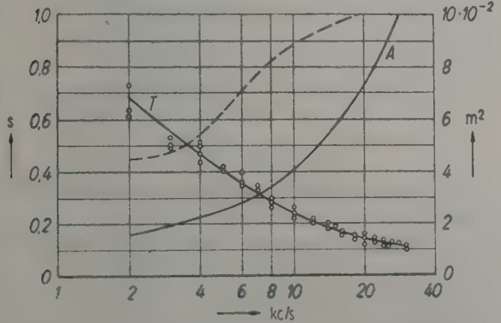

Fig. 20. Reverberation time and absorption of the model reverberation chambers.
(Dashed curve: absorption with aperture of $0.0375\ \text{m}^2$).

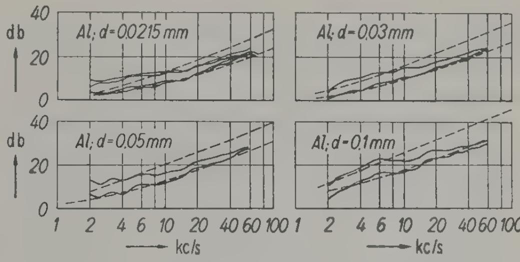

Fig. 21. Reduction factor of plates between reverberant rooms. $f_{\text{crit.}}$ above recorded frequency range.

The diagrams in Fig. 21 and Fig. 22 give the reduction factor, obtained in the model reverberation rooms as a function of frequency for a number of plates. The lower of the full lines always represents the ratio E'_2/E_2 in db, whereas the upper curve is corrected according to (14).

The diagrams in Fig. 21 refer to relatively thin aluminium plates, for which the critical frequency is above the range of frequencies measured. For these plates, the validity of formula (6) should be expected, and curves computed from (6) for normally incident plane waves, and from (6) and (7) for waves incident diffusely with a uniform angular distribution, are represented by dashed lines in the figures. The lower of the dashed lines is that for diffuse incidence.

Apart from an exception in the case of very light plates and at low frequencies, the corrected values lie between the dashed curves, approaching the lower curve for higher frequencies. Rejecting any doubts as to the validity of formula (6) for very thin plates, the conclusion would be that there is preference for smaller angles of incidence (i. e. the angles around normal incidence) at low frequencies.

The thinnest of the plates (0.02 and 0.03 mm) show a tendency towards values above the theoretical at low frequencies. This is in agreement with observations reported by London [7] and confirmed by Fleming [8]. London suggests an explanation by the assumption that some sort of viscous resistance plays a part in addition to the inertia of the plate, and to the internal damping η introduced by Cremer, which has only a negligible effect in the present cases. This assumption, however, is unsatisfactory until a physically plausible cause for such a resistance could be given. One might imagine that the transfer of energy from the forced flexural wave to the free flexural waves, and the dissipation of the energy in the free flexural waves, would result in a resistance of this kind. But a closer examination shows that such transfer is appreciable only at the resonance frequencies of the plate, which are very sharp and are not likely to produce a sufficient resistance on the average.

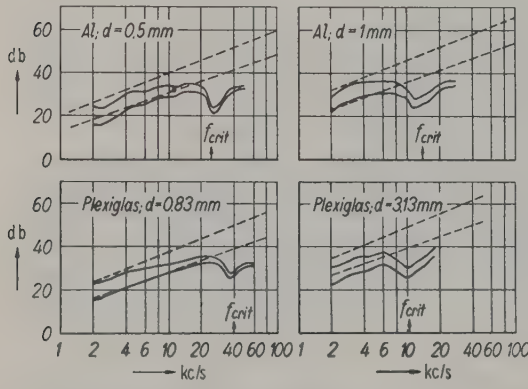

Fig. 22. Reduction factor of plates between reverberant rooms. $f_{crit.}$ within recorded frequency range.

The problem is made still more obscure by the fact that there is no indication of an increase of the reduction factor for very small *fd* in the measurements with plane waves. We would also like to point (although with considerable reserve) to the surprising agreement between the theoretical curves for diffusely incident sound and the uncorrected reduction factors in Fig. 21. The same agreement was found in other measurements of thin plates (plastic and paper foils) not roproduced here. If this is not purely accidental, something is wrong with the correction of the measurements. Now the theory on which corrections like (13) are based is very primitive and might contain deficiencies that become important for low insulations. We are not at present able, however, to propose any alternative theory which would make the uncorrected values more plausible than the corrected.

For thicker plates, where the critical *fd* is within the recorded frequency range, diagrams like those in Fig. 22 are obtained. They are quite similar to the observations made in practical measurements [5] . . . [8] and show the considerable decrease of the reduction factor, compared with the pure mass law (6), due to the coincidence effect and the additional radiation from free flexural waves.

The work described has been carried out as part of a research contract between the Department of Scientific and Industrial Research, London and the University of Göttingen.

(Received 1st July 1951.)

References

[1] Reissner, H., Helvet. phys. Acta **11** [1938], 140.

[2] Cremer, L., Akust. Z. **7** [1942], 81.

[3] Schoch, A., Acustica **2** [1952], 1.

[4] Kuhl, W. and Kaiser, H., Velocity and damping of sound in building materials. Reports to D. S. I. R. of the III. Phys. Inst. Univ. Göttingen, 1950.

[5] Cremer, L. and Eisenberg, A., Baupl. u. Bautechn. **2** [1948], 235.

[6] Gösele, K., Inst. techn. Phys., Stuttgart-Ruit, unpublished.

[7] London, A., Report of the 1948 Summer symposium of the Acoustics Group, Phys. Soc. London [1949], 194.

[8] Fleming, N., Nat. phys. Lab., Teddington, private communication 1950.

[9] Schoch, A., Akust. Z. **2** [1937], 113.

[10] Cremer, L., Die wissenschaftlichen Grundlagen der Raumakustik, Band 3, S. Hirzel Verlag, Leipzig 1950, §§ 60—62.

[11] Cremer, L., Propagation of structure-borne sound, sect. 15. Report to D. S. I. R. of the III. Phys. Inst. Univ. Göttingen. 1950.

[12] Osborne, M. F. M. and Hart, S. D., J. acoust. Soc. Amer. **17** [1945], 1.

[13] Fay, R. D., J. acoust. Soc. Amer. **20** [1948], 620.

[14] Lord Rayleigh, The Theory of Sound II, Macmillan, London 1896, § 381.

[15] Kosten, C. W., Report of the 1948 Summer symposium of the Acoustics Group, Phys. Soc. London [1949], 87.

[16] see for instance: Love, A. E. H., A treatise on the mathematical theory of elasticity, chapter XIII, 4th ed., University Press, Cambridge 1927.

[17] Zwikker, C., Technische Physik der Werkstoffe. Springer-Verlag, Berlin 1942, p. 174.

[18] Code for measurements of air-borne and impact transmission, proposed for international standardisation at London, 1949.

[19] Kuhl, W., Development of condenser microphones for the ultrasonic range. D. S. I. R.-report of the III. Phys. Inst. Univ. Göttingen 1950.

[20] Stenzel, H., Leitfaden zur Berechnung von Schallvorgängen. Springer-Verlag, Berlin 1939.

[21] Meyer, E., Buchmann, G. and Schoch, A., Akust. Z. **5** [1940], 352.

[22] Beranek, L. L. and Sleeper, P. H., J. acoust. Soc. Amer. **18** [1946], 140.

[23] Schoch, A., Report on the 1948 Summer symposium of the Acoust. Group, Phys. Soc. London [1949], 167.

THE VELOCITY OF SOUND IN AIR

by J.M.A. LENIHAN

Western Infirmary, Glasgow

Summary

Measurements have been made of the velocity of sound in free air at a frequency of 13 500 c/s. A small loudspeaker, connected to an oscillator, emitted sound which, after travelling a distance determined by an accurate screw, was received by a microphone. The input waveform of the transmitter and the output waveform of the receiver were passed through pulse-shaping circuits and displayed together on the screen of a double beam oscillograph. Movement of the transmitter, controlled by rotation of the screw, produced relative motion of the two traces on the oscillograph screen and the wavelength of the sound was determined by measuring the distance between successive positions of the transmitter at which the two trains of pulses coincided on the screen. Corrections were applied for the effects of temperature, humidity and a number of less important factors. The final value for the velocity of sound at a frequency of 13 500 c/s in dry air at a temperature of 273.16° K and a pressure of 1013.2 mb was 331.45 ± 0.04 m/s.

Sommaire

On a mesuré la vitesse du son dans l'air libre à la fréquence 13 500 hertz. A cet effet, un petit haut-parleur, relié à un oscillateur, émettait un son qui était reçu par un microphone, après avoir parcouru une certaine distance réglable par une vis micrométrique. L'onde d'entrée dans l'émetteur et l'onde de sortie du récepteur traversaient des circuits formateurs d'impulsions et apparaissaient simultanément sur l'écran d'un oscillographe à deux faisceaux. Le déplacement de l'émetteur réglé par rotation d'une vis, produisait un déplacement relatif des deux traces sur l'écran de l'oscillographe et on déterminait la longueur d'onde du son, par mesure de la distance entre les positions successives de l'émetteur, pour lesquelles les deux trains d'impulsions étaient en coincidence sur l'écran de l'oscillographe. On a appliqué les corrections voulues pour tenir compte de l'influence de la température, du taux d'humidité et d'un certain nombre d'autres facteurs de moindre importance. On a finalement trouvé que la vitesse du son à 13 500 hertz dans l'air sec à la température de 273,16° abs. et sous une pression de 1013,2 mb est 331,45 ± 0,04 m/s.

Zusammenfassung

Die Schallgeschwindigkeit der Luft wurde bei 13,5 kHz im Freien gemessen. Der Abstand zwischen Lautsprecher und Mikrophon ließ sich mit einer Präzisionsschraube sehr genau einstellen. Sende- und Empfangsspannung steuerten je einen Impulsgenerator, und die beiden Impulsfolgen wurden auf einem Zweistrahloszillographen sichtbar gemacht. Ändert man den Abstand zwischen Sender und Empfänger, so verschieben sich auf dem Oszillographenschirm die beiden Impulsfolgen gegeneinander. Man bestimmt die Wellenlänge des Schalles aus dem Abstand zweier aufeinander folgender Senderstellungen, bei denen die beiden Impulsreihen die gleiche Stellung zueinander haben. Für den Einfluß der Temperatur, der Feuchtigkeit und einiger Faktoren geringerer Bedeutung wurden Korrekturen angebracht. Der endgültige Wert der Schallgeschwindigkeit in trockener Luft bei 13,5 kHz, 273,16° K und 1013,2 mbar war 331,45 ± 0,04 m/s.

1. Introduction

During the 250 years which elapsed between the introduction of the pendulum clock and the development of ultrasonic techniques in acoustics many measurements of the velocity of sound in free air were attempted (Table I). Any experiment of this kind must be conducted in a space which has one of its dimensions equal to several wavelengths. If an audible frequency is used a considerable volume of air is necessary and the difficulty of controlling and measuring the temperature and humidity throughout the experimental region imposes a serious limitation on the accuracy which can be obtained. If a frequency in the ultrasonic region is used the dimensions of the apparatus may be reduced to such an extent that constancy of temperature and humidity are readily achieved, though the advantage so gained is partly offset by the necessity of applying substantial corrections for dispersion of velocity and for the error introduced by the proximity of the containing vessel.

The object of the present experiment was to measure the velocity of sound in free air at an audible

Table I: Previous measurements of the velocity of sound in free air

Notes:

1. This table relates to measurements made in the open, or in the laboratory under conditions approximating to those of free air.
2. Most of the experiments were made by timing the sound of gunfire over a known distance; where a different method was used, this is indicated in the table.
3. The results have been recalculated, where necessary, to obtain the velocity in metres per second in dry air at 0° C. Where this conversion has been made from information contained in the original account of the experiment, the temperature is indicated 0*. Where the information provided in the published account has been insufficient to allow of this recalculation, the temperature or humidity columns have been left blank.
4. In compiling the table, an accuracy of ± 1 m/s has been assumed for results obtained before 1800 and of ± 0.1 m/s for later experiments.
5. The date assigned to each experiment is that of publication of the results.

	Name	Place	Date	Baseline [m]	S [m/s]	Temperature °C	Humidity	Remarks
1	Mersenne	Paris	1636	158	316	—	—	Echo method
2	Mersenne	Paris	1636	various	447	—	—	
3	Accademia del Cimento	Florence	1667	1806	361	—	—	
4	Walker	Oxford	1698	100	398	—	—	Echo method
5	Cassini	Paris	1700	2495	356	—	—	
6	Derham	Essex	1708	3219—20012	348	—	—	
7	Flamsteed and Halley	Greenwich	1708	4828	358	—	—	
8	Cassini	Paris	1738	3421—11276	334	0*	—	
9	Cassini	Nimes	1739	26492—43992	338	—	—	
10	Bianconi	Bologna	1744	25813	331	0*	—	
11	Condamine	Cayenne	1745	39428	358	—	—	
12	Condamine	Quito	1745	?	337	—	—	
13	Kästner and Mayer	Göttingen	1778	536—1045	332	0*	—	
14	Müller	Göttingen	1791	2670	338	—	—	
15	Benzenberg	Düsseldorf	1810	4626—9072	334.0	0	—	
16	Benzenberg	Düsseldorf	1812	9069	331.2	0*	—	
17	Espinosa and Bauza	Chile	1817	4496—14082	354.5	0*	—	
18	Arago	Paris	1822	18602	331.2	0*	—	
19	Goldingham	Madras	1823	4247—9006	329.1	0	0	
20	Moll and van Beek	Utrecht	1824	17669	332.0	0	0	
21	Gregory	Woolwich	1824	640—1981	330.1	0*	—	
22	Parry	Canada	1825	878—2636	327.3	0*	—	
23	Parry	Canada	1826	3957	333.7	0*	—	
24	Kendall	Canada	1828	805—1873	340.6	0*	—	
25	Bravais and Martens	Switzerland	1845	9560	332.4	0	0	
26	Regnault	Paris	1868	1447—4891	330.6	0	0	
27	Stone	Cape Town	1872	4873	332.4	0	0	
28	Szathmari	Hungary	1877	—	331.6	0	0	Coincidence method
29	Greeley	Canada	1890	1279	333.3	0*	—	
30	Frot	France	1898	5565	330.7	0	—	
31	Hebb	Chicago	1905	—	331.9	0	0	Stationary wave method
32	Hebb	Chicago	1919	—	331.4	0	0	Stationary wave method
33	Esclangon	France	1919	12600	330.8	0*	0	
34	Angerer and Ladenburg	Belgium and Germany	1919	965—13075	330.8	0	0	
35	Miller	New Jersey	1937	6191	331.4	0	0	
36	Kukkamäki	Finland	1938	1000	330.8	0	0	

References to Table I

[1] MERSENNE, Harmonie Universelle. Paris 1636, book 3, proposition XXI, p. 214.

[2] MERSENNE, De l'utilité de l'Harmonie. Paris 1636, p. 44. (This is one of the tracts contained in Harmonie Universelle.) For further details of MERSENNE's experiments, reference may be made to LENIHAN, Acustica **2** [1951], 96—99.

[3] Accademia del Cimento, Saggi di naturali esperienze fatte nell'Accademia del Cimento, 2nd edition, Naples 1714, p. 245: Essayes of natural experiments made in the Academie del Cimento ... Englished by RICHARD WALLER, London 1684, p. 138.

frequency with an accuracy of one part in 10000, comparable with that of the best ultrasonic measurements.

2. Basis of the method

Consideration of the techniques used in radar for the measurement of short time intervals suggests that the cathode ray oscillograph might be useful in making precise observations. Experiments using this device have, indeed, been made by a number of workers, though with no attempt at great accuracy. Wold and Stephenson [1923] used a loudspeaker connected to an audio-frequency oscillator delivering sound to two tubes placed side by side, each having a microphone at the other end. The output from one microphone was amplified and applied to the X deflecting plate of the oscillograph and the output from the other, after amplification, provided a Y deflecting voltage, thus producing a Lissajous figure on the screen. One tube was adjustable in length and it was possible by observation on the Lissajous figure to find the distance corresponding to a given phase difference between the sound arriving at the two microphones. The wavelength and velocity could then be calculated, though numerical results obtained by this method have not been published.

Patchett's method [2] is essentially similar and uses one microphone which is moved relative to the loudspeaker to produce phase changes. An alternating potential difference which drives the loudspeaker is also applied between the X plates of the oscillograph and the microphone output, after amplification, provided the Y deflection. The procedure used by Patchett is to vary the distance between the loudspeaker and the microphone, observing the positions at which the Lissajous figure is a straight line, corresponding to phase identity. The interval between two successive positions of the microphone at which this occurs is equal to the wavelength of sound at the frequency employed. Patchett quotes only meagre results, but it is not to be expected that either of these methods will give an accurate value for the velocity of sound. The phenomenon on which they depend — the appearance of a particular Lissajous figure — is not very sharply defined and is affected by distortion in the loudspeaker, microphone and amplifiers. A considerable uncertainty in the observations is therefore unavoidable.

A more precise method has been described by Colwell and his collaborators (Colwell, Friend and McGraw [3], [4]; Colwell, Friend and Gibson [5]). Pulses derived from the a.c. main supply are fed to a loudspeaker. The sound which they produce is picked up by a microphone, amplified and applied as a deflecting voltage to the Y plates of an oscillograph. The sweep voltage is derived from the main supply and is therefore syn-

---

[4] WALKER, Philos. Trans. **20** [1698], 433.

[5] CASSINI; Du Hamel, Regiae Scientarium Academiae Historia. Leipzig 1700, contains (p. 169) a description of the experiments made by CASSINI, PICARD and ROEMER in 1677.

[6] DERHAM, Philos. Trans. **26** [1708], 16.

[7] FLAMSTEED and HALLEY; mentioned by DERHAM Philos. Trans. **26** [1708], 16.

[8] CASSINI, Mémoires de l'Academie. Paris 1738, p. 128.

[9] CASSINI. Mémoires de l'Academie. Paris 1739, p. 126.

[10] BIANCONI, De Bononiensi scientarium et artium institute atque academis commentaris. Bologna 1744, vol. 2, p. 365 (a brief description). BIANCONI's experiments are discussed by GOVI, Atti della Reale Accademia dei Lincei (Transunti) 1883, series 3, vol. 7, p. 91.

[11] CONDAMINE, Mémoires de l'Académie. Paris 1745, p. 488.

[12] CONDAMINE, Relation abrégé d'un voyage fait dans l'intérieur de l'Amérique Meridionale ... Paris 1745, p. 205.

[13] KÄSTNER and MAYER, Göttingesche Anzeigen von Gelehrten Sachen. 1778, p. 1145.

[14] MÜLLER, Göttingesche Anzeigen von Gelehrten Sachen. 1791, p. 1593.

[15] BENZENBERG, Ann. Phys. (Gilbert), **35** [1810], 383.

[16] BENZENBERG, Ann. Phys. (Gilbert), **42** [1812], 1.

[17] ESPINOSA and BAUZA, Ann. Chim. Phys. **7** [1817], 93.

[18] ARAGO, Ann. Chim. Phys. **20** [1822], 210.

[19] GOLDINGHAM, Philos. Trans. **113** [1823], 96.

[20] MOLL and VAN BEEK, Philos. Trans. **114** [1824], 424; Ann. Phys. (Poggendorff) **5** [1824], 315, 469.

[21] GREGORY, Phil. Mag. **63** [1824], 481.

[22] PARRY, NIAS and FISHER, Appendix to Captain PARRY's Journal of a second voyage for the discovery of a North West Passage ... London 1825, p. 237.

[23] PARRY and FOSTER, Journal of a third voyage for the discovery of a North West Passage ... London 1826, appendix 4, p. 86.

[24] KENDALL; in FRANKLIN, Narrative of a second expedition to the shores of the Polar Sea in the years 1825, 26 and 27. London 1828, vol. 4, appendix IV.

[25] BRAVAIS and MARTENS, Ann. Chim. Phys. **13** [1845], 5; Ann. Phys. (Poggendorff) **66** [1845], 351.

[26] REGNAULT, Mémoires de l'Académie. Paris **37** [1868], 3.

[27] STONE, Phil. Mag. **43** [1872], 153.

[28] SZATHMARI, Ann. Phys. (Wiedemann) **2** [1877], 418.

[29] GREELEY, Report on the U.S. expedition to Lady Franklin Bay. Wash. 1888; Phil. Mag. **30** [1890], 507.

[30] FROT, Comptes Rendus **127** [1888], 609.

[31] HEBB, Phys. Rev. **20** [1905], 89.

[32] HEBB, Phys. Rev. **14** [1919], 74.

[33] ESCLANGON, Comptes Rendus **168** [1919], 165.

[34] ANGERER and LADENBURG, Ann. Phys., Lpz. **66** [1922], 293.

[35] MILLER, Sound waves, their shape and speed. New York 1937, p. 147.

[36] KUKKAMÄKI, Ann. Phys., Lpz. **31** [1938], 398.

chronised with the microphone pulses, so that a stationary trace appears on the screen. By observing the position of this trace, relative to a reference ruled on the screen, at various positions of the microphone, the wavelength can be found. The trace crosses the reference mark twice if the microphone is moved through one wavelength, since the flyback takes place in the same time as the forward stroke in a sinusoidal sweep. The distance which the microphone moves between alternate transits of the trace across the reference mark is thus equal to the wavelength.

Using 60 c/s mains, the wavelength is about $5^1/_2$ metres and can be accurately measured. The position of the trace on the screen cannot be estimated with the same accuracy because the pulse, if it is originally sharp, is broadened in its passage through the loudspeaker, microphone and amplifier and it becomes difficult to fix exactly the point on the trace corresponding to the beginning of the loudspeaker pulse.

In a modification of this experiment a sinusoidal tone, of various frequencies between 440 c/s and 1760 c/s is used as the source, measurements being made by observing coincidences of the crests of the received waves with the reference marks on the screen. In this way several readings of the wavelength may be obtained on a bench a few metres long. It is, however, difficult to estimate precisely the position of the crest, since a sine wave has almost no slope near its peak. COLWELL and his co-workers made a number of measurements which are of doubtful accuracy, since many important sources of error were not taken into account. One series of experiments (COLWELL, FRIEND and MC GRAW [3]) used sound pulses from a device connected to the 60 c/s main supply, but this frequency was not measured or checked. The temperature was recorded to 0.2°C and the humidity was not measured at all though, at the temperatures prevailing during the experiments, the presence of normal amounts of water vapour in the air would effect the velocity of sound by an appreciable fraction of one per cent. These uncertainties do not, of course, detract from the merit of COLWELL's method, but they are the more regrettable since his final result — 331.54 metres per second — is quoted in a form which implies control of temperature to 0.02°C, measurement of water vapour pressure to 1 millibar and constancy of the frequency of the sound to one part in 30000.

The method now to be described is similar in principle to COLWELL's, but is capable of greater accuracy. An alternating voltage from an audio-frequency oscillator is amplified and fed to a loudspeaker. The output from a movable microphone which picks up the sound is operated on by a pulse-shaping circuit and the pulses obtained are applied to the Y deflecting plate of a cathode ray oscillograph, which may have an internal time base operating at a suitable frequency or may use the oscillator output for its sweep voltage. In either arrangement a stationary pattern is formed on the screen. The wavelength of the sound is found by measuring the distance which the microphone must move between successive positions at which the pulse coincides with an arbitrary reference mark on the screen. To avoid errors of observation due to parallax it is advisable to use a double beam oscillograph in the following way. The microphone pulses are applied to one Y plate, as already described. The loudspeaker voltage is connected to a second pulse shaping circuit and the pulses so formed are used to deflect the second beam of the oscillograph. One of the loudspeaker pulses may then be used as a reference mark; a photograph of the trace obtained in this way is shown in Fig. 1. Measurements may also be made by observing coincidences of the flyback trace with the reference mark. Fig. 2 shows the general arrangement of the apparatus.

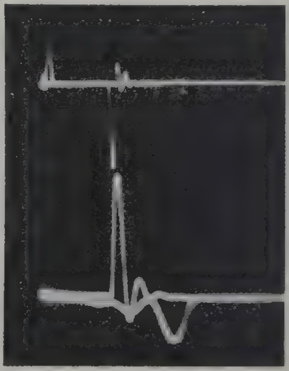

Fig. 1. Appearance of the oscillograph screen. Loudspeaker pulse above, microphone pulse below.

3. Apparatus and equipment

In order to carry out an experiment along these lines with a high degree of accuracy the following requirements must be considered:

a) Location of experiment

After many trials, indoors and out of doors, the apparatus was set up in the Bute Hall of the University of Glasgow, a large room ($35 \times 21 \times 20$ m^3), well insulated from neighbouring buildings.

b) Source of sound

A small moving-coil headphone, 5 cm in diameter, was supplied with alternating current at 13500 c/s from a beat-frequency oscillator and an amplifier. At lower frequencies, reflections from walls and floor were troublesome and at higher frequencies the source and the receiver became inefficient.

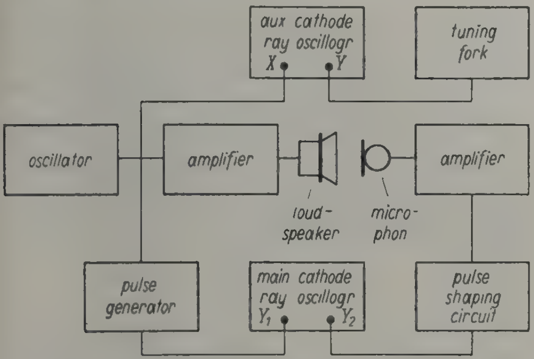

Fig. 2. General arrangement of the apparatus.

c) Control and measurement of frequency

The output of the oscillator was combined with that of a standard 1000 c/s valve-maintained tuning fork to give a Lissajous figure on the screen of a small cathode-ray oscillograph. This figure was examined frequently during the experiment and adjusted when necessary to restore the shape corresponding to a ratio of 27 : 2. After the fork and oscillator had been running for a week, the oscillator frequency drifted very slowly and could be kept constant to one part in 50000 without difficulty.

d) The receiver

A small headphone, identical with the transmitter was connected through a high-gain amplifier to a pulse-shaping circuit, which will be described later.

e) Traversing mechanism

The receiver was moved relative to the transmitter by a simple mechanism based on a steel screw, 1.8 m long and of pitch 1.27 cm (0.5 inch) — actually the lead screw of a lathe, made for the experiment by Noble and Lund of Felling-on-Tyne. The receiver could be moved to within 15 cm of the transmitter or to greater distances up to 165 cm. Its position was recorded by counting the number of whole turns of the screw since the start of the traverse and observing the fractional part on a circular scale divided into 500 units, each representing 0.001 inch.

f) Temperature measurement

Two mercury thermometers, made to British Standard Specification 593 of 1935 (A40C/total), were suspended by threads from the ceiling, their bulbs 5 to 10 cm to the side of the direct path of the sound. The thermometers were graduated in tenths of a degree and had been calibrated at the National Physical Laboratory with an accuracy of 0.02°C. Temperatures were estimated to 0.01°C by observation with a telescope about 2 m away. So that currents near the floor might not affect the temperature in the experimental region, the apparatus was mounted on two boxes about 2 m high.

g) Measurement of humidity

The presence of water vapour in the air affects the velocity of sound by causing a change in the density and a change in the specific heat, C_v. The humidity was measured with a small whirling hygrometer, read at intervals of 30 min during the experiment.

k) Measurement of carbon dioxide content

A portable Haldane apparatus was used and it was found that the proportion of carbon dioxide in the air remained steady at about 0.035%.

i) Electrical circuits

The amplifiers and pulse shaping circuits were of simple design and present no features of especial interest. The voltage available from the microphone was about 100 μV and a gain of about 50000 was sought in the receiver amplifier. Three pentode valves, EF36, were used in cascade with careful decoupling for anodes and screen grids. Since only high audio frequencies were to be dealt with, the coupling condensers between stages were made rather small (0.001 μF) thus reducing the gain for hum and other unwanted signals.

The pulse generating circuits operated as follows. The sinusoidal input voltage was amplified by a succession of valves, biased so as to produce a square wave output in the anode circuit. The final square wave, of amplitude about 100 V, was applied to a ringing circuit consisting of a capacitance and an inductance in series with a variable resistance of 1000 Ω. A momentary disturbance in this circuit, produced for example by the steeply rising front of the square wave, caused a short burst of oscillation at the natural frequency of the ringing circuit. These oscillations decayed at a rate depending on the value of the variable resistance, which could be adjusted to a critical value permitting only one half-cycle of oscillation to occur. This half-cycle burst of current constituted a pulse about a microsecond long and was used to deflect the oscillograph beam. The transmitter pulse generator, which had an input of 20 V from the oscillator, used two stages of amplification and the corresponding circuit in the receiver side had an extra valve to compensate for smaller input voltage.

4. Method of making observations

No readings were recorded until the oscillator and tuning fork had been operating continuously for a week and had settled down at stable frequencies. The detailed procedure in making observations was as follows.

a) The fine frequency control of the oscillator was adjusted until the Lissajous figure on the screen of the auxiliary oscillograph became stationary at the shape corresponding to a ratio of 27:2.
b) The two thermometers were read in turn, through the telescope.
c) The hygrometer was whirled vigorously for about two minutes and its two thermometers were read.
d) The telescope was moved to a position from which it could be used to observe the screen of the double beam oscillograph.
e) The platform carrying the microphone was moved to a position about 1.5 m from the loudspeaker and was then moved forward until the tips of the two pulses coincided on the screen of the oscillograph. The reading of the circular scale was noted.
f) The microphone was moved forward and its position was noted at each of the next four coincidences of the transmitter and receiver pulses on the screen.
g) The microphone was moved forward until the 41st coincidence was reached and, after allowing an interval of about a minute for any turbulence to disappear, its position was recorded.
h) The positions of the next four coincidences were recorded in the same way and it was now possible, by subtracting the first reading from the 41st, the 2nd from the 42nd and so on, to obtain five estimates of a length equal to 40 wavelengths.
i) After checking the frequency of the audio frequency oscillator, the microphone was moved forward about 2.5 cm (two turns) and brought back to position 45, after which the whole process was repeated in the backward direction, until the microphone returned to its original position. A further five values for 40 λ were thus obtained.

The whole cycle of operations was then repeated to find further values for 40 λ. The wet and dry bulb thermometer readings varied only slightly during a period of three or four hours and it was not necessary to record them after each set of ten readings. The hygrometer was operated every half hour and the humidity at intermediate times was found by interpolation.

5. Calculation of the results

In an experiment such as this the final result must be referred to dry air under standard conditions of temperature and pressure, that is, a temperature of 0^0 C and a pressure of one atmosphere.

To assess the various corrections we must first know how the velocity of sound depends on the atmospheric conditions. For sound waves of small amplitude in a gas, the velocity, S, is given by the equation

$$S = \sqrt{\frac{C_p}{C_v} \cdot \frac{K}{d}}$$

where C_p and C_v are the thermal capacities of one mole of the gas at constant pressure and constant volume respectively, K is the bulk modulus of the gas for isothermal changes and d is its density. Using the relations familiar in thermodynamics

$$K = -V\left(\frac{\partial p}{\partial V}\right)_T$$

and

$$\frac{C_p}{C_v} = 1 - \frac{T}{C_v}\left(\frac{\partial p}{\partial T}\right)_V^2 \left(\frac{\partial V}{\partial p}\right)_T$$

we find, following Hardy, Telfair and Pielemeier [6].

$$S = \sqrt{\frac{RT}{M}\left(f + \frac{gR}{hC_{v\infty}}\right)} \qquad (1)$$

where R = gas constant for one mole,
T = temperature on the Kelvin scale,
M = molecular weight of the gas,
$C_{v\infty}$ = specific heat of the gas at constant volume for infinite dilution,
V = volume of one mole,

f, g and h are constants equal to unity for a perfect gas and differing from unity, by an amount depending on the temperature, for a real gas. They are related to the other constants as follows

$$f = \frac{KV}{RT},$$

$$g = \left(\frac{V}{R}\frac{\partial p}{\partial T}\right)_V^2,$$

$$h = \frac{C_v}{C_{v\infty}}.$$

At normal temperature and pressure

$$f = 0.998753,$$
$$g = 1.004503,$$
$$h = 1.000224.$$

The velocity of sound in air is affected by the following factors:

a) The temperature, which produces three separate effects
  1. on the density, which, for a perfect gas, is inversely proportional to the temperature on the Kelvin scale,
  2. on the imperfection of the gas, that is, on the constants f, g and h mentioned above,
  3. on the specific heat, $C_{v\infty}$.

b) The presence of water vapour, which affects
  1. the density of the air,
  2. the specific heat, $C_{v\infty}$.

In the present experiment it is necessary also to correct for

c) the known error of the screw,

d) the known error of the thermometers.

Before any of these corrections are made, it is necessary to define a standard atmospheric pressure, temperature and density and to decide on the values to be adopted for the other physical constants involved in the calculations. The following definitions were made, using the recommendations of BIRGE [7]:

Standard atmosphere = 1013.2 mb (1 mb = 1000 dynes/cm^2); Ice point = 0^0 C = 273.16^0 K.

The following composition was assumed for the atmosphere

	volume [%]	density at N.T.P. [kg/m^3]
Nitrogen	78.04	1.251
Oxygen	20.99	1.429
Argon	0.94	1.783
Carbon dioxide	0.03	1.977

Using this composition, the density of air is found to be 1.29310 kg/m^3.

Corrections for the effect of humidity and temperature on the density and specific heat of the air are tedious and complicated (because many of the correction factors are interdependent), but not unduly difficult; they are set out fully in the original account of this work (LENIHAN [8]). During the course of the experiment the temperature varied between 17^0 C and 19^0 C and the humidity between 13.0 mb and 14.2 mb. It was found convenient to adjust all of the observations to a temperature of 18^0 C and a humidity of 13.6 mb, omitting certain small corrections which could, without loss of accuracy, be applied to the mean value found in this way.

6. Final value for the velocity of sound

Mean value of 40 λ at 18^0 C and 13.6 mb	=	39.9946 inches
correction for effect of humidity on $C_{v\infty}$ — multiply by 1.000472		40.0135
correction for error of screw — add 0.0025		40.0160
effect of temperature and humidity on density — multiply by 0.96618		38.6627
divide by 40 to find λ	=	0.966567
multiply by 13500 to find velocity	=	13048.35 inches/s
multiply by 0.0254001 to find velocity	=	331.437 m/s.

The following corrections may be applied to the final result, following HARDY, TELFAIR and PIELEMEIER [6].

Correction for variation of f, g, and h with temperature	=	—0.032 m/s
correction for variation of $C_{v\infty}$ with temperature	=	+0.046
velocity of sound	=	331.451 m/s

7. Accuracy of this determination

a) Temperature

The calibration of the thermometers left an uncertainty of 0.02^0 C and, in estimating the readings with the telescope, a further uncertainty of about 0.01^0 C was introduced. These errors may partly account for the fact that the readings of the two thermometers usually differed by 0.02^0 C or 0.04^0 C after their known errors had been allowed for. Part of the discrepancy may have been due to an unsuspected temperature gradient in the room but, whatever the reason, it will be wise to allow for an uncertainty of 0.04^0 C in the temperature measurements. The corresponding error in the final result is about 0.025 m/s.

b) Humidity

The readings of the wet bulb depression were reliable only to 0.1^0 C and this uncertainty represents about 0.01 m/s in the velocity.

c) Frequency

The accuracy of the valve-maintained tuning fork was very much better than that of the other components in the experiment and no correction is necessary here. There was, however, a slight uncertainty in the frequency of the audio-frequency oscillator, amounting in the interval between successive checkings to about one part in 50000, or 0.006 m/s in the final result.

d) Carbon dioxide content

The carbon dioxide content of the air as measured with the Haldane apparatus was $3^1/_2$ parts in 10000 with an uncertainty of about 10% of the reading. The difference from the accepted figure of 3 parts in 10000 does not, therefore, require any correction.

e) Electrical circuits

It is difficult to be sure that the delay introduced by the pulse-shaping circuits remained the same for all positions of the receiver, though the following precautions were taken:

1. the circuit of the receiver amplifier was adjusted, after assembly, so that the amplitude and waveform of the output voltage delivered to the pulse shaping circuit was the same whether the microphone was close to the loudspeaker or at the greatest distance allowed by the screw;
2. the pulse generators were adjusted so that the pulse shape remained the same whatever the position of the microphone;
3. the amplifier driving the loudspeaker was adjusted so that its output had a sinusoidal waveform; when distortion was allowed in this amplifier, the pulse shape changed with the position of the microphone.

No change in the shape of the oscillograph traces was detected by the eye as the microphone moved and, since the distribution curve (below) suggests that no large systematic errors have been overlooked, it may be reasonable to conclude that errors introduced by variations in the response of the electrical circuits were not important.

The distribution of the 940 results is shown in Fig. 3 and the standard deviation is found to be 0.044 m/s. This is about the figure expected from consideration of the sizes of the various possible errors discussed above. The normal error curve for this standard deviation is superimposed for comparison and corresponds fairly well with the experimental distribution.

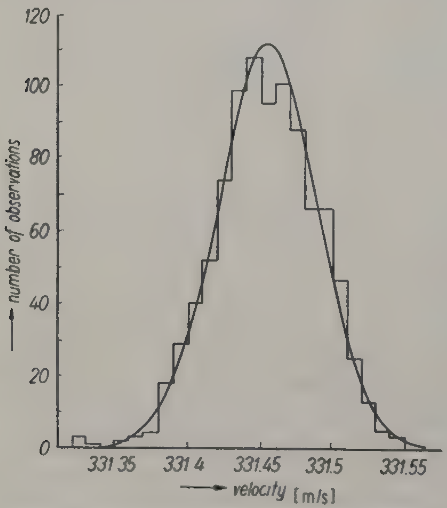

Fig. 3. Distribution curve for the 940 results.

8. Conclusion

Considering all of these factors it seems reasonable to conclude that the velocity of sound at a frequency of 13500 c/s in dry air at a temperature of 0° C and a pressure of 1013.2 mb does not differ from 331.45 m/s by more than 0.04 m/s. This value may be compared with the result of experiments by Hardy, Telfair and Pielemeier [6] at ultrasonic frequencies which gave a result of 331.44±0.05 m/s and with the theoretical calculation of the velocity of sound made by the same authors, which gave 331.45 ± 0.05 m/s.

Acknowledgements

I am glad to have the opportunity of acknowledging the kindly and generous assistance received during the course of this work — as on many other occasions — from my friend and teacher, the late Professor George W. Todd.

The experiment was begun in the Physics Department of King's College, Newcastle upon Tyne, in 1943 and was continued in the Natural Philosophy Department of the University of Glasgow from 1945 till 1948. The acquisition of the necessary apparatus and equipment was made possible by a substantial grant from the Research Committee of King's College and assistance was also given by Noble and Lund, Ltd, Felling-on-Tyne, Fibreglass, Ltd, Glasgow and Stewarts and Lloyds Ltd, Glasgow.

I am grateful to the Senate of the University of Glasgow and to Professor Philip I. Dee for the provision of laboratory facilities.

(Received 1st December, 1951.)

References

[1] Wold, P. I. and Stephenson, E. B., Phys. Rev. **21** [1923], 706.
[2] Patchett, G. N., Proc. phys. Soc. London **55** [1943], 324.
[3] Colwell, R. C., Friend, A. W. and McGraw, D. A., J. Franklin Inst. **225** [1938], 579.
[4] Colwell, R. C., Friend, A. W. and McGraw, D. A., J. Franklin Inst. **227** [1939], 251.
[5] Colwell, R. C., Friend, A. W. and Gibson, L. H., J. Franklin Inst. **230** [1940], 749.
[6] Hardy, H. C., Telfair, D. and Pielemeier, W. H., J. acoust. Soc. Amer. **13** [1942], 226.
[7] Birge, R. T., Rep. phys. Soc. Progr. Phys. **8** [1941], 90.
[8] Lenihan, J. M. A., Ph. D. Thesis, Glasgow 1949.

SCHALLDÄMMUNG DURCH GUMMI- UND STAHLFEDERN

von MARIE-LUISE EXNER

III. Physikalisches Institut der Universität Göttingen

Zusammenfassung

Bei der Untersuchung der Schalldämmung von Gummi- und Stahlfedern im Frequenzgebiet 20...2000 Hz ergab sich eine gute Übereinstimmung zwischen Theorie und Experiment. Die große Materialdämpfung der Gummifedern — der Verlustfaktor ist etwa 10mal so groß wie bei Stahlfedern — wirkt sich im ganzen Frequenzbereich günstig auf die Schalldämmung aus. Neben einfachen Masse-Feder-Systemen werden auch mechanische Drosselketten untersucht, das sind Systeme aus zwei oder mehr Federn, die durch Massen voneinander getrennt sind. Drosselketten sind oberhalb einer kritischen Frequenz den einfachen Systemen überlegen, haben jedoch bei tiefen Frequenzen Nachteile.

Summary

In an investigation on the sound insulation of rubber and steel springs in the frequency range 20 to 2000 c/s good agreement between theory and practice was found. The larger internal damping of rubber springs — the loss factor being about ten times that of steel springs — produces good insulation over the whole frequency range. Beside simple mass + spring systems, mechanical filters were tried, i. e., systems of two or more springs separated by masses. Filters are better than simple systems above a critical frequency but have disadvantages at low frequencies.

Sommaire

On est arrivé à un bon accord entre les résultats théoriques et expérimentaux dans l'étude de l'amortissement du son, dans la gamme 20...2000 Hz, au moyen d'éléments élastiques en caoutchouc et en acier. Le grand facteur de pertes du caoutchouc — qui est environ 10 fois plus grand que pour des ressorts en acier — a un effet favorable sur l'amortissement acoustique, dans toute la gamme de fréquences considérée. En dehors des systèmes élastiques simples, on a également étudié des filtres mécaniques, c'est-à-dire des systèmes constitués par deux ou plusieurs éléments élastiques séparés par des masses. De tels filtres sont supérieurs aux systèmes simples au-delà d'une certaine fréquence critique, mais présentent cependant des inconvénients aux basses fréquences.

1. Einleitung

Seit vielen Jahrzehnten werden Gummi- und Stahlfedern zur Schalldämmung verwendet, und es ist erstaunlich, daß ihre Dämmeigenschaften bisher nur einmal, nämlich von MEYER und KEIDEL [1], in einem größeren Frequenzbereich quantitativ untersucht worden sind. Die vorliegenden Untersuchungen, bei denen das Meßverfahren von MEYER und KEIDEL verwendet wurde, beschäftigen sich hauptsächlich mit den beiden einfachsten Federtypen — prismatischen Gummifedern und Schraubenfedern aus Stahl —, die bei der Messung zu longitudinalen Schwingungen angeregt werden.

2. Schalldämmung durch ein Masse-Feder-System

a) Theorie

Wenn man mit $\bar{K}\, e^{j\omega t}$ die auf eine Masse M ausgeübte Wechselkraft bezeichnet, dann wirkt auf das Fundament eine Kraft $\bar{K}' e^{j\omega t}$, deren Betrag und Phase wesentlich von dem dazwischengeschalteten Dämmelement $\bar{F}$ abhängen (Abb. 1). Wenn man sich nur für die Amplitude der Kraft interessiert, kann man den Zeitfaktor $e^{j\omega t}$ fortlassen und der Phasenverschiebung φ zwischen den beiden Kräften durch einen komplexen Ansatz Rechnung tragen, $\bar{K} = K e^{j\varphi_0}$ und $\bar{K}' = K' e^{j(\varphi_0+\varphi)}$. Als Dämmgrad bezeichnet man den Absolutbetrag des Kraftverhältnisses $\bar{K}/\bar{K}'$ und als Schalldämmung die Größe

$$D = 20 \log |\bar{K}/\bar{K}'| , \qquad (1)$$

die in Dezibel (db) angegeben wird.

Die Theorie der Schalldämmung durch eine beliebig lange prismatische Gummifeder stammt von BÖHME [2]. Er behandelt auf Grund der elektromechanischen Analogien das Schalldämmproblem mit den Hilfsmitteln der elektrischen Leitungs-

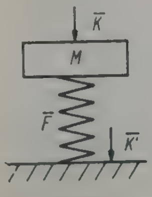

Abb. 1.
Kraftübertragung durch ein einfaches Masse-Feder-System

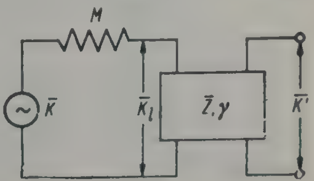

Abb. 2.
Elektrisches Analogieschaltbild zu Abb. 1.

theorie. Benutzt man die elektromechanische Analogie 1. Art, bei der die Kraft der Spannung, die Schnelle (zeitliche Ableitung der Elongation) dem Strom, die Masse der Induktivität usw. entspricht, dann ergibt sich das in Abb. 2 dargestellte elektrische Ersatzschaltbild für das Dämmproblem. Die Feder wird durch eine verlustbehaftete mechanische Leitung der Länge l dargestellt, deren mechanischer Wellenwiderstand (definiert als Quotient aus Kraft und Schnelle bei unendlich langer Leitung) $Z = \rho c q \sqrt{1 + j\eta}$ und deren Ausbreitungskonstante $\gamma = \frac{j\omega}{c\sqrt{1+j\eta}}$ ist (ρ = Dichte, c = Schallgeschwindigkeit, η = Verlustfaktor, q = Querschnitt).

Die Spannung $\bar{K}(l)$ am Eingang der Leitung $(x=l)$ ist mit der Leerlaufspannung[1] $\bar{K}'$ verbunden durch die Gleichung

$$K(l) = K' \cosh \gamma l. \tag{2}$$

Andererseits ist

$$\frac{K(l)}{K} = \frac{W(l)}{j\omega M + W(l)} \tag{3}$$

mit $W(l) = Z \coth \gamma l$.

Hierbei ist $W(l)$ der Eingangswiderstand der offenen Leitung. Für das Kraftverhältnis K/K' ergibt sich[2]:

$$\frac{K}{K'} = \cosh \gamma l + \frac{j\omega M}{Z} \sinh \gamma l. \tag{4}$$

Zunächst soll geprüft werden, ob für $\gamma l \ll 1$ Gl. (4) in die bekannte Formel für die Kraftübersetzung einer kurzen Feder übergeht.

$$\frac{K}{K'} = 1 + \frac{j\omega M}{\rho c q \sqrt{1+j\eta}} \cdot \frac{j\omega l}{c\sqrt{1+j\eta}}. \tag{5}$$

Nach Einführung der Federung (reziproke Federkonstante)

$$F = l/Eq$$

(E = Elastizitätsmodul) und der Eigenfrequenz

$$\nu_0 = \frac{1}{2\pi}\sqrt{\frac{1}{MF}} \quad \text{ergibt sich} \quad \frac{K}{K'} = 1 - \frac{(\nu/\nu_0)^2}{1+j\eta}.$$

Der Dämmgrad der kurzen Feder ist also

$$\left|\frac{K}{K'}\right| = \sqrt{\frac{[1-(\nu/\nu_0)^2]^2 + \eta^2}{1+\eta^2}}. \tag{5a}$$

Er ist gleich 1 für Frequenzen, die klein gegen die Eigenfrequenz sind und für die Frequenz $\nu_k = \sqrt{2}\cdot\nu_0$. In der Umgebung der Resonanzfrequenz tritt eine Resonanzüberhöhung auf, d. h. die von der Feder auf das Fundament übertragene Kraft $\bar{K}'$ ist größer als die erregende Kraft $\bar{K}$. Für $\nu = \nu_0$ ist der Dämmgrad gleich dem Verlustfaktor η, der bei Gummi (unter 100 Hz) etwa 0,1 und bei Stahlfedern nur etwa 10^{-2} ist. Erst oberhalb $\nu_k = \sqrt{2}\,\nu_0$ beginnt das Dämmgebiet. Für hohe Frequenzen $(\nu \gg \nu_0)$ gilt

$$\frac{K}{K'} = \left(\frac{\nu}{\nu_0}\right)^2 \frac{1}{\sqrt{1+\eta^2}}. \tag{6}$$

Der Dämmgrad steigt demnach bei höheren Frequenzen mit dem Quadrat der Frequenz an und ist fast unabhängig vom Verlustfaktor.

Um eine gute Dämmwirkung zu erzielen, macht man die Eigenfrequenz ν_0 kleiner als die niedrigste Störfrequenz. Da es sich nicht immer vermeiden läßt, daß auf das Dämmsystem Kräfte wirken, deren Frequenzen im Resonanzgebiet liegen (z. B. beim Anlaufen von Motoren), muß man Federn mit hohem Verlustfaktor verwenden, um das Auftreten großer Kräfte zu vermeiden. Stahlfedern, deren Materialdämpfung gering ist, benötigen eine zusätzliche Dämpfung, die meist in Form von Reibungsdämpfung mittels eines Flüssigkeitsdämpfers angebracht wird. Das hat den Nachteil, daß bei hohen Frequenzen der Dämmgrad nur mit ν ansteigt und um so kleiner wird, je größer die Reibungsdämpfung ist (vgl. [1]).

Um das Verhalten der Feder bei sehr hohen Frequenzen zu berechnen, muß Gl. (4) herangezogen werden. Beschränkt man sich auf relativ kleine Verlustfaktoren $\eta < 0{,}5$ — diese Bedingung gilt für alle Metallfedern und für Gummifedern bis etwa 2500 Hz — so ergibt sich mit $Z \approx \rho c q$ und

$$\gamma \approx \frac{j\omega}{c}(1 - j\eta/2)$$ [3]

folgende Gleichung für den Dämmgrad:

$$\left|\frac{K}{K'}\right| = \sqrt{\left(\cos\pi\frac{\nu}{\nu_1} - \frac{\nu\cdot\nu_1}{\nu_0^2\pi}\sin\pi\frac{\nu}{\nu_1}\right)^2 + \left[1 + \left(\frac{\nu\cdot\nu_1}{\nu_0^2\pi}\right)^2\right]\sinh^2\frac{\eta}{2}\pi\frac{\nu}{\nu_1}} \tag{7}$$

---

[1] Es wird also angenommen, daß die Eingangsimpedanz des Untergrundes sehr groß gegen den Wellenwiderstand der Feder ist. Messungen der Eingangsimpedanz von Fundamenten, Decken und Wänden sind zur Zeit im Gange.

[2] Diese Formel gilt auch für das Amplitudenverhältnis $\bar{x}/\bar{x}'$, wenn man annimmt, daß das Fundament (s. Abb. 1) mit der Amplitude $\bar{x}\cdot e^{j\omega t}$ schwingt und man sich dafür interessiert, welche Amplitude $\bar{x}'\cdot e^{j\omega t}$ die abgefederte Masse M ausführt. Dieses Problem tritt bei der erschütterungsfreien Aufstellung empfindlicher Apparate auf.

[3] Eine Abschätzung zeigt, daß diese Vernachlässigung einen Fehler von höchstens 2 db im ersten Minimum bedingt. An den übrigen Stellen der Dämmkurve (außer der Masse-Feder-Resonanz) ist der Fehler noch kleiner. Für die Umgebung der Masse-Feder-Resonanz wird weiterhin Formel (5a) benutzt.

In dieser Gleichung steht als neue, für die Welleneigenschaften der Feder charakteristische Konstante, die Frequenz $\nu_1 = \frac{1}{2}\sqrt{\frac{1}{mF}}$, bei der die Feder eine $\lambda/2$-Schwingung ausführt (m=Masse der Feder, F ihre Federung). Die $\lambda/2$-Frequenz ist also unabhängig von der Belastung durch die Masse M, solange die Federung von M unabhängig ist. Die Gl. (7) gilt auch für Schraubenfedern, da bekanntlich auch sie longitudinale Eigenschwingungen ausführen können. Man kann ihnen eine über die Länge gleichmäßig verteilte Masse und Federung zuordnen und wie bei einer kompakten Feder von einer Schallgeschwindigkeit $c = \sqrt{E/\rho} = \sqrt{l^2/mF}$ und einer Wellenlänge $\lambda = c/\nu$ sprechen. Für $\lambda = 2l$ gilt dann wie für die kompakte Feder $\nu_1 = \frac{1}{2}\sqrt{\frac{1}{mF}}$. Selbstverständlich gilt die Annahme der gleichmäßig verteilten Masse und Federung bei Schraubenfedern nicht bis zu beliebig hohen Oberschwingungen, sondern nur, solange die Wellenlänge nicht in die Größenordnung der Windungsabstände kommt.

In welcher Weise die Welleneigenschaften der Feder die Dämmkurve beeinflussen, zeigt am besten eine graphische Darstellung der Gl. (7). In Abb. 3 ist für ein Verhältnis der $\lambda/2$-Frequenz zur Masse-Feder-Frequenz $\nu_1/\nu_0 = 10$ die Dämmung D in Abhängigkeit von der relativen Frequenz ν/ν_0 aufgetragen. Als Parameter dient der Verlustfaktor η. Oberhalb der Masse-Feder-Resonanz steigt zunächst die Dämmung mit $(\nu/\nu_0)^2$ an, wie schon die vereinfachte Dämmformel (6) zeigte. Durch die Eigenschwingungen der Feder wird dieser Anstieg gestört, und zwar liegt der erste Einbruch bei der $\lambda/2$-Frequenz[4]. Ihm folgen bei $n\nu_1$ ($n = 2, 3, 4$) weitere Einbrüche, die jedoch immer schwächer werden. Der Verlustfaktor spielt nur in der Umgebung der Resonanzstellen eine Rolle. Die durch die Eigenschwingungen hervorgerufenen Einbrüche der Dämmkurve stören um so weniger, je größer der Verlustfaktor ist und je weiter die $\lambda/2$-Frequenz von der Masse-Feder-Frequenz entfernt ist, weil dann die Dämmung bei ν_1 an sich schon groß ist. Das Verhältnis

$$\frac{\nu_1}{\nu_0} = \frac{2\pi\sqrt{MF}}{2\sqrt{mF}} = \pi\sqrt{\frac{M}{m}}, \tag{8}$$

das nicht von der Federung abhängt, soll also möglichst groß sein. Man wählt daher bei vorgegebener Last eine möglichst leichte Feder.

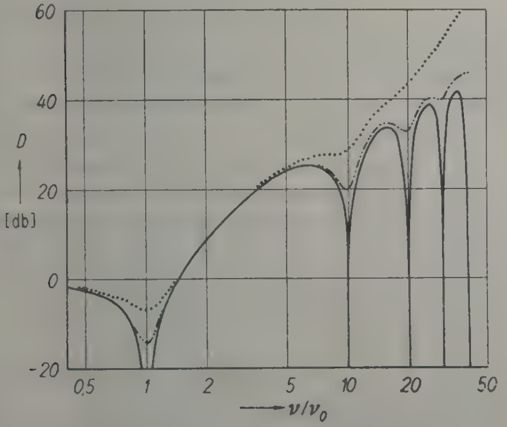

Abb. 3. Theoretische Dämmkurve eines Masse-Feder-Systems für verschiedene Werte des Verlustfaktors; – $\eta = 0$; ·· ·· $\eta = 0,2$; ····· $\eta = 0,5$.

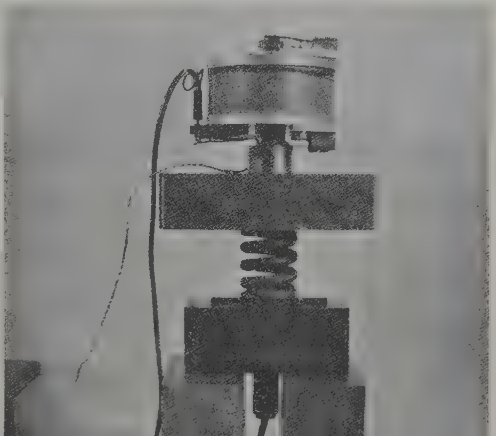

Abb. 4. Versuchsaufbau. Oben der elektrodynamische Sender; unter der Schraubenfeder der piezoelektrische Empfänger.

b) Meßapparatur

Abb. 4 zeigt die praktische Ausführung der Meßapparatur. Das Dämmsystem, bestehend aus Masse und Feder, wird von oben mit einem elektrodynamischen Sender angeregt, der die Kraft $\bar{K}$ ausübt. Die Feder steht auf einem piezoelektrischen Empfänger, dessen Ausgangsspannung der übertragenen Kraft $\bar{K}'$ proportional ist. Da bei der Messung der Dämmung nur das Verhältnis der beiden Kräfte interessiert, ist keine Absolutmessung erforderlich. Man bestimmt die vom Sender ausgeübte Kraft in einem Vorversuch, indem man den Sender direkt auf den Empfänger setzt und die Empfängerspannung U in Abhängigkeit von der Frequenz mißt. Auf diese Weise erhält man eine Kurve für die Dämmung Null, die sog. Nullkurve, auf die alle Messungen bezogen werden. Im Hauptversuch setzt man das zu untersuchende Dämmsystem zwischen Sender und Empfänger und mißt die Empfängerspannung $U' = f(\nu)$. Es gilt dann für den Dämmgrad

---

[4] Bei nicht zu kleinem Massenwiderstand ωM.

$$K/K' = U/U'. \qquad (9)$$

Es zeigt sich, daß die Meßergebnisse nur dann zuverlässig sind, wenn die Nullkurve völlig gerade ist. Unregelmäßigkeiten der Nullkurve deuten auf mechanische Eigenschwingungen des Senders, Empfängers oder Fundamentes, oder auf schlechten mechanischen Kontakt zwischen den einzelnen Teilen des Aufbaus. Alle aufeinander liegenden Flächen müssen völlig plangeschliffen sein und werden am besten durch eine sehr dünne Vaselineschicht, die als akustisches Kontaktmittel dient, miteinander verbunden. Abb. 5 zeigt die Nullkurve der verwendeten Apparatur, die im Bereich von 30...1500 Hz um weniger als ±1 db vom Mittelwert abweicht.

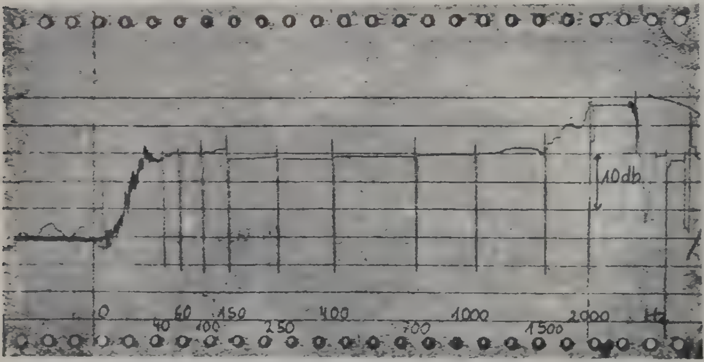

Abb. 5. Nullkurve der Apparatur. (Die senkr. Striche sind Frequenzmarken.)

Ein Blockschaltbild der elektrischen Apparatur ist in Abb. 6 dargestellt. Das elektrodynamische Anregungssystem wird durch einen Schwebungssummer und einen 20 Watt-Verstärker mit konstantem Strom beschickt und übt daher eine konstante Kraft auf das Dämmsystem aus. Die Spannung des Empfängers wird in einem dreistufigen Vorverstärker verstärkt, im Oktavsieb von Störungen befreit und schließlich vom Meßverstärker nach nochmaliger Verstärkung und Gleichrichtung angezeigt. Mit Hilfe der in Dezibel geeichten Eichleitung (Meßbereich 0—140 db) wird die Spannung jeweils soweit geschwächt, daß das Instrument des Meßverstärkers den gleichen Wert anzeigt. Man kann dann an der Eichleitung direkt den Dämmgrad in Dezibel ablesen. Mit Hilfe des Oszillographen wird die Kurvenform kontrolliert.

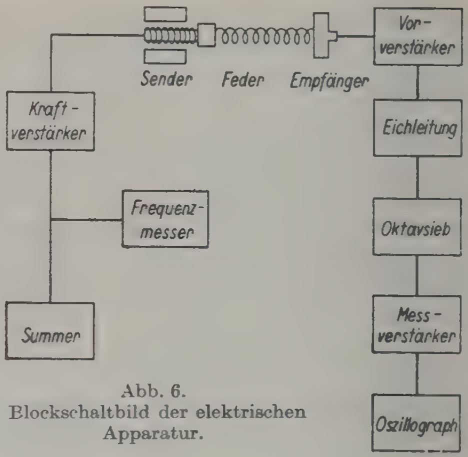

Abb. 6. Blockschaltbild der elektrischen Apparatur.

c) Meßergebnisse

Abb. 7 zeigt die Dämmkurven einer Gummifeder bei zwei verschiedenen Belastungen ($M = 1$ kg und $M = 18$ kg). Die Übereinstimmung der Meßwerte (○○○) mit den berechneten Dämmkurven (———) ist sehr gut. Bei steigender Belastung rückt die Masse-Feder-Resonanz zu tieferen Frequenzen, und die Dämmung wird im ganzen Frequenzbereich um den Faktor 18, das sind 25 db, größer. Die $\lambda/2$-Frequenz liegt bei beiden Kurven an der gleichen Stelle, weil bei kleinen Belastungen die Federung nur wenig von der Last abhängt[5]. Der Verlustfaktor ergab sich zu 0,2 aus der Masse-Feder-Resonanz und zu 0,5 aus der $\lambda/2$-Resonanz. (Mit diesen η-Werten wurden die theoretischen Kurven in Abb. 7 berechnet.) Ähnliche Werte für den Verlustfaktor wurden bei allen untersuchten Gummifedern gefunden. Nach Messungen anderer Autoren, die bei Kuhl und Meyer [3] zusammengestellt sind, ist η bis 100 Hz etwa 0,1 und steigt dann langsam

---

[5] Da Gummi eine sehr große Querkontraktionskonstante $\sigma \approx 0{,}5$ hat, sein Volumen also bei Verformung nahezu konstant bleibt, wird eine Gummifeder bei stärkerer Belastung breiter und damit härter. Die Masse-Feder-Resonanz $\nu_0 = 1/(2\pi\sqrt{MF})$ nimmt wegen der kleiner werdenden Federung nicht proportional $1/\sqrt{M}$ ab, sondern schwächer. In Abb. 8 ist diese Abhängigkeit der Frequenz ν_0 von der Belastung dargestellt (—). Auf der Abszisse ist die dimensionslose Größe $\varkappa = (g/q_0 E)\, M$ aufgetragen (q_0 = Querschnitt der unbelasteten Feder, E = Elastizitätsmodul, g = Erdbeschleunigung). Bei Belastung der Feder mit einer Masse der Größe $q_0 E/g$ erreicht die Eigenfrequenz ein Minimum und steigt bei höheren Belastungen wieder an. Die gestrichelt eingezeichnete Kurve würde für eine Feder gelten, deren Federung nicht von der Belastung abhängt.

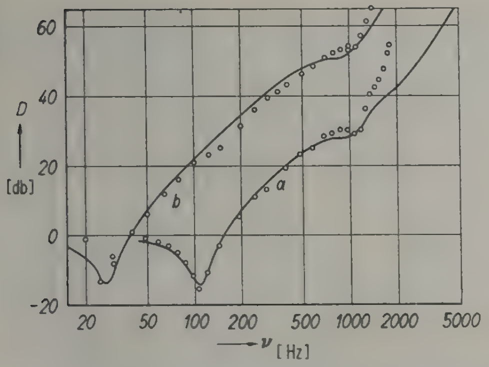

Abb. 7. Vergleich der gemessenen Dämmung (ooo) mit der theoretischen Dämmkurve (——) bei einer Gummifeder für 1 kg (Kurve a) und 18 kg Belastung (Kurve b).

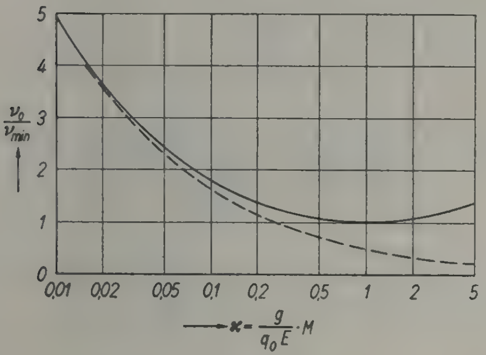

Abb. 8. Abhängigkeit der Grundfrequenz ν_0 einer Feder von der Belastung M in dimensionsloser Darstellung (– – –) Federung unabhängig von der Belastung, (——) Federung abhängig von der Belastung(Gummifeder).

an, um bei 1000 Hz etwa den Wert 0,2 zu erreichen. Bei unseren Messungen war offenbar der Verlustfaktor in der Gegend von 1000 Hz erheblich größer als 0,2, was sich auch in dem sehr steilen Anstieg der Dämmkurve in diesem Gebiet äußert. Diese Erscheinung läßt sich leicht erklären: Voraussetzung für die Dämmformel (7) ist eine eindimensionale Wellenausbreitung. In Wirklichkeit tritt infolge der Querkontraktion auch eine Welle quer zur Anregungsrichtung auf, die besonders stark wird, wenn die Wellenlänge in Gummi vergleichbar mit der doppelten Breite der Feder ist. Diese Querresonanz trägt nichts zur Schallübertragung in longitudinaler Richtung bei, verbraucht aber Schallenergie. Aus diesem Grund verbessern Querresonanzen, ganz im Gegensatz zu Längsresonanzen, die Schalldämmung. (Genaueres über die Erscheinung der Querresonanzen [4]).

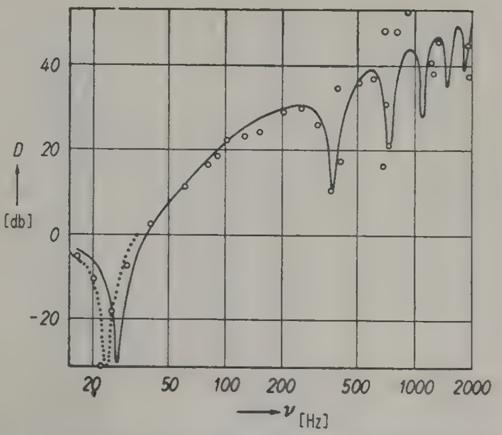

Abb. 9. Vergleich der gemessenen Dämmung (ooo) mit der theoretischen Dämmkurve (——) bei einer Stahlfeder.

Abb. 9 zeigt das typische Dämmverhalten einer Stahlfeder. Wegen der geringen Materialdämpfung (aus der Messung ergibt sich ein Verlustfaktor von höchstens 0,03) bewirken die Eigenschwingungen der Feder sehr tiefe Einbrüche in der Dämmkurve, die die mittlere Schalldämmung erheblich verschlechtern. Die λ/2-Frequenz liegt um den Faktor 2 tiefer als bei der Gummifeder mit der gleichen Federkonstanten (allerdings kleinerer Tragfähigkeit), deren Dämmkurven in Abb. 7 dargestellt sind. Dadurch fallen auf ein bestimmtes Frequenzintervall bei der Stahlfeder doppelt so viele Eigenfrequenzen wie bei der Gummifeder. Die Übereinstimmung zwischen Theorie und Experiment ist auch bei der Stahlfeder recht gut.

Neben prismatischen, nur auf Druck beanspruchten Gummifedern wurden auch konische, zum Teil auf Scherung beanspruchte Hohlfedern untersucht (Abb. 10). Die Dämmkurven dieser komplizierteren Federn haben im wesentlichen denselben Verlauf wie die der prismatischen Federn, für die die Theorie abgeleitet wurde. Wie z. B. Abb. 11 zeigt, steigt die Dämmkurve recht steil an, obwohl sich aus den Minima ein Verlustfaktor von nur etwa 0,2 ergibt. Es wurden Dämmungen über 80 db gemessen, d. h. in dem betreffenden Frequenzgebiet wird nur 0,01% der erregenden Kraft auf das Fundament übertragen. Der sehr scharfe Einbruch der Dämmkurve bei 1300 Hz kann nicht durch eine Eigenschwingung des relativ stark gedämpften Gummis erklärt wer-

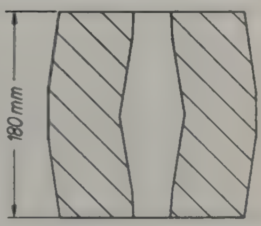

Abb. 10. Schnitt durch die konische Hohlfeder.

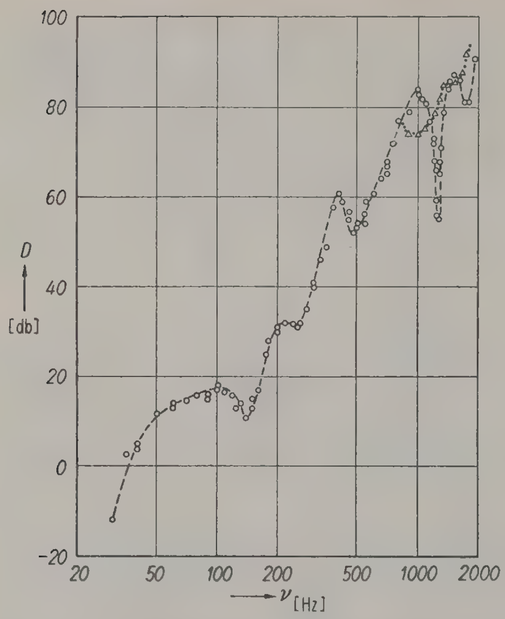

Abb. 11. Dämmkurve der konischen Hohlfeder.

den. Die Vermutung, daß es sich um eine Resonanz der im Puffer eingeschlossenen Luftsäule handelt, wurde dadurch bestätigt, daß der Einbruch verschwand (punktierte Kurve), wenn der Hohlraum mit einem Schallschluckstoff ausgefüllt wurde. Dieser Effekt zeigt, daß es keinen Zweck hat, die Körperschalldämmung beliebig weit zu treiben, wenn nicht die entsprechende Luftschalldämmung vorhanden ist.

Das Ergebnis der Messungen an den oben beschriebenen und einer Reihe anderer Federn ist, daß man das Verhalten eines einfachen Masse-Feder-Systems mit einer für praktische Zwecke ausreichenden Genauigkeit voraussagen kann, wenn man folgende Daten des Dämmsystems kennt:

1. Masse der Feder m,
2. Federung der Feder F,
3. Belastende Masse M,
4. Verlustfaktor des Federmaterials η.

Die Federung von Stahlfedern kann einfach durch Aufsetzen eines Gewichtes und Messen der Längenänderung bestimmt werden. Die Bestimmung der Federung von Gummifedern, die von der Belastung abhängig ist, wird bei KOSTEN [5] ausführlich beschrieben. Die beiden Massen können leicht durch Wägung bestimmt werden. Es ist nur darauf zu achten, daß bei Schwingmetallfedern die Masse des anvulkanisierten Eisens abgezogen wird. Als belastende Masse M gilt nur die wirklich mitschwingende Masse, also nicht Massen, die durch weitere Federn so abgefedert sind, daß sie die Bewegung nicht mitmachen. Der Verlustfaktor η wird meist nicht bekannt sein. Es empfiehlt sich, in diesem Falle für Stahlfedern $\eta = 0{,}01$ und für Gummifedern $\eta = 0{,}1$ einzusetzen.

Wenn man sich nur einen Überblick über die Eigenschaften eines Dämmsystems verschaffen will, ist es zu zeitraubend, die exakte Dämmkurve zu zeichnen. Man kann jedoch leicht aus wenigen Punkten eine Näherungskurve konstruieren, die, wie Abb. 12 zeigt, die Verhältnisse gut wiedergibt.

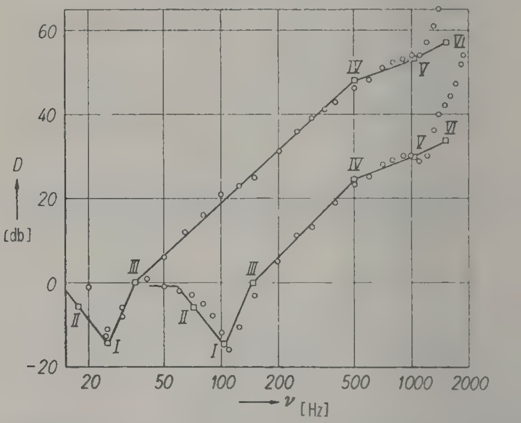

Abb. 12. Vergleich der gemessenen Dämmung (ooo) einer Gummifeder mit der aus der statischen Federung berechneten Näherungskurve (–□–□–). Die römischen Zahlen bezeichnen die berechneten Punkte.

Die Umgebung der Masse-Feder-Resonanz wird durch drei Punkte gekennzeichnet:

$$\text{I.}\qquad \nu_0 = \frac{1}{2\pi}\sqrt{\frac{1}{MF}}\,;\qquad \left|\frac{K}{K'}\right| = \eta,$$

$$\text{II.}\qquad \nu_{II} = \frac{1}{\sqrt{2}}\cdot\nu_0\,;\qquad \left|\frac{K}{K'}\right| \approx 0{,}5,$$

$$\text{III.}\qquad \nu_k = \sqrt{2}\cdot\nu_0\,;\qquad \left|\frac{K}{K'}\right| = 1.$$

Charakteristisch für das Wellengebiet sind die Minima der Dämmkurve, die fast genau bei den Frequenzen $\nu_{V,VII,\ldots} = n\nu_1$ $(n = 1, 2, 3\ldots)$ liegen:

$$\text{V, VII, \ldots}\qquad \left|\frac{K}{K'}\right| \approx \frac{\eta}{2}\,n^2\left(\frac{\nu_1}{\nu_0}\right)^2\sqrt{1+\frac{2}{3}\left(\frac{\eta n\pi}{2}\right)^2}\,.$$

Ferner ist die Schalldämmung leicht für die Frequenzen $\nu_{IV,VI,\ldots} = (n+\frac{1}{2})\,\nu_1$ $(n = 0, 1, 2\ldots)$ zu berechnen: (dies sind nicht genau die Maxima)

$$\text{IV, VI, \ldots}\qquad \left|\frac{K}{K'}\right| \approx \left(\frac{\nu_1}{\nu_0}\right)^2\frac{n+\frac{1}{2}}{\pi}\sqrt{1+[\eta/2\,(n+\tfrac{1}{2})]^2}\,.$$

3. Schalldämmung durch mechanische Drosselketten

Die einfachste mechanische Drosselkette besteht aus zwei Federn, die durch eine Masse voneinander etrennt sind (Abb. 13). Abb. 14 zeigt das zugeörige elektrische Ersatzschaltbild.

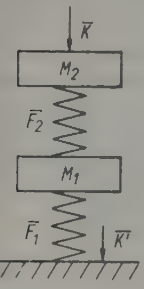

Abb. 13 (links). Kraftübertragung durch eine mechanische Drosselkette.

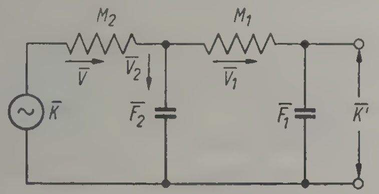

Abb. 14. Elektrisches Analogieschaltbild zu Abb. 13.

Mit Hilfe der Kirchhoffschen Sätze lassen sich ür die Spannungen $\bar{K}$ und die Ströme $\bar{v}$ folgende eziehungen aufstellen:

$$v = v_1 + v_2, \quad K = j\omega M_2 v + \frac{1}{j\omega F_2} \cdot v_2 \qquad (1),\ (2)$$

$$\text{mit } F = \frac{F}{1 + j\eta},$$

$$0 = j\omega M_1 \bar{v}_1 + \underbrace{\frac{1}{j\omega \bar{F}_1} \cdot \bar{v}_1}_{K'} - \frac{1}{j\omega F_2} \cdot \bar{v}_2. \qquad (3)$$

ieraus erhält man den gesuchten Dämmgrad:

$$\left|\frac{K}{K'}\right| = \sqrt{\frac{[\mu\alpha^4 - (1+\varphi)\,\alpha^2 + (1-\eta^2)\,\varphi]^2 + \eta^2\,[\alpha^2(1+\varphi) - 2\varphi]^2}{\varphi^2(1+\eta^2)^2}}. \qquad (4)$$

s ist: $\alpha = 2\pi\nu\sqrt{F_1(M_1+M_2)}$ ein Frequenzparameter, $= M_1/(M_1+M_2)$ ein Maß für die Massenverteilung nd $\varphi = \frac{F_1}{F_2} \cdot \frac{M_1+M_2}{M_2}$ ein Federungsparameter.

Bei Abwesenheit von Verlusten ($\eta = 0$) geht For-el (4) in die einfachere Formel (5) über

$$\frac{K}{K'} = \frac{\mu\alpha^4 - (1+\varphi)\alpha^2 + \varphi}{\varphi}. \qquad (5)$$

iese Funktion ist in Abb. 15 für $M_1 = M_2$ und $_1 = F_2$, d. h. $\mu = 0{,}5$ und $\varphi = 2$ dargestellt. Sie zeigt en für gekoppelte Schwingungen typischen Ver-uf: Es treten zwei Resonanzstellen auf, die zu eiden Seiten der Frequenz $\nu_0 = \frac{1}{2\pi}\sqrt{\frac{1}{MF}}$ der unekoppelten Kreise liegen. Für die Schalldämmung edeutet das, daß der Dämmbereich erst bei höheen Frequenzen beginnt. Im Dämmbereich steigt doch die Schalldämmung sehr stark an, und zwar it ν^4 gegenüber ν^2 bei der Einzelfeder. Charakte-stisch für die Grenze zwischen dem Übertragungsgebiet und dem Dämmgebiet ist offenbar die Frequenz ν_k, bei der die Dämmkurve die Gerade $|K/\bar{K}'| = 1$ ($D = 0$) schneidet. Gelingt es, diese Frequenz so niedrig zu machen, daß sie unter der kleinsten Störfrequenz liegt, dann wird mit der Drosselkette eine erheblich bessere Schalldämmung zu erreichen sein, als mit einem einfachen Masse-Feder-System (gestrichelt eingezeichnet). Die kritische Frequenz ν_k läßt sich aus Formel (5) leicht berechnen

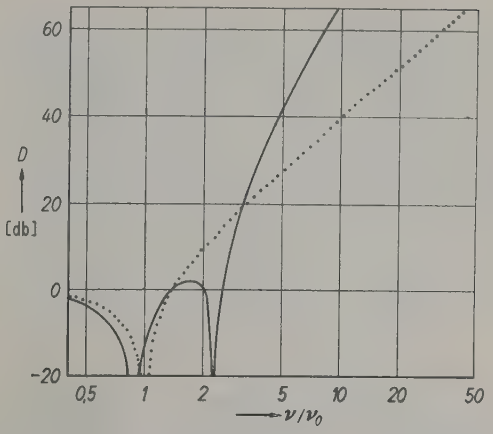

Abb. 15. Theoretische Dämmkurve (——) für eine Drosselkette aus zwei gleichen, verlustfreien und masselosen Federn und zwei gleichen Massen. (.....) Berechnete Dämmkurve für das einfache Masse-Feder-System, das entsteht, wenn man die obere Feder der Drosselkette entfernt.

$$\nu_k = \frac{1}{2\pi}\sqrt{\frac{1}{M_1F_1} + \frac{1}{M_2F_2} + \frac{1}{M_1F_2}} \qquad (6)$$

oder

$$\nu_k = \sqrt{\nu_{11}^2 + \nu_{22}^2 + \nu_{12}^2}. \qquad (7)$$

ν_{12} ist dabei die Eigenfrequenz der mittleren Masse mit der oberen Feder. Um ν_k möglichst klein zu halten, ist es sicher günstig, ν_{11} ungefähr gleich ν_{22} zu machen, denn der größere der beiden Werte beeinflußt ν_k am stärksten. Das Produkt aus Masse und Federung ist damit festgelegt, nicht aber das Verhältnis M_1/M_2. Das Glied ν_{12} wird klein, wenn M_1 größer als M_2 und dafür F_2 größer als F_1 ist. Es genügt jedoch, $M_1/M_2 = 3$ zu wählen, da eine weitere Vergrößerung des Verhältnisses ν_k nur noch unwesentlich beeinflußt.

In Abb. 16 ist die Dämmkurve einer mechanischen Drosselkette aus zwei gleichen Stahlfedern aufgezeichnet. Die ausgezogene Kurve wurde nach Gl. (5) berechnet. Bei tiefen Frequenzen stimmt sie mit den als Kreisen eingezeichneten Meßwerten recht gut überein. Im Wellengebiet muß sie natürlich versagen, da sie nur für Federn berechnet worden ist, die klein gegen die Wellenlänge sind. Man

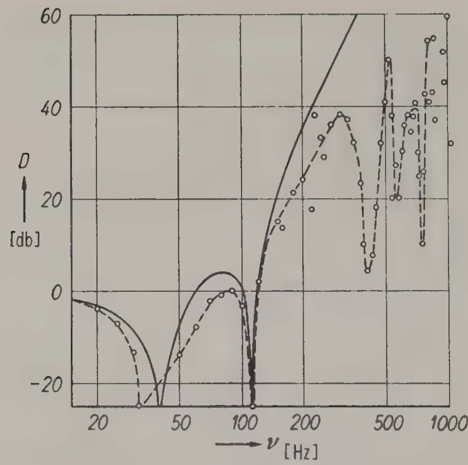

Abb. 16. Dämmung einer mechanischen Drosselkette aus zwei gleichen Stahlfedern (——) berechnet, (—o—) gemessen.

kann jedoch die Lage des ersten Einbruches der Dämmkurve aus der λ/2-Frequenz der einzelnen Federn berechnen. Diese liegt nach (Abb. 9) bei 410 Hz, und denselben Wert findet man auch in der Meßkurve für die Drosselkette.

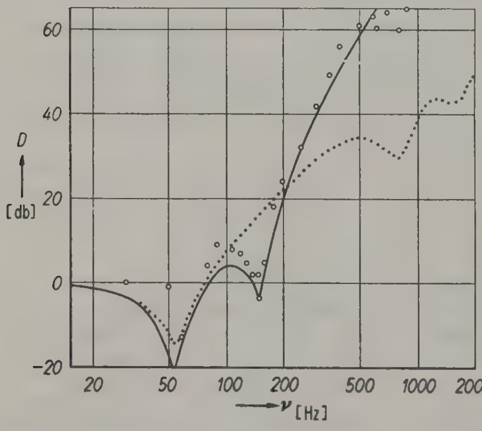

Abb. 17. Dämmung einer mechanischen Drosselkette aus zwei gleichen Gummifedern. (——) berechnet, (ooo) gemessen, (......) Dämmkurve bei herausgenommener oberer Feder.

Ein Beispiel für eine Drosselkette aus zwei gleichen, verlustbehafteten Federn zeigt Abb. 17. Die ausgezogene Kurve wurde nach Gl. (4) für $\eta = 0{,}1$ berechnet. Man sieht bei dieser Drosselkette, deren λ/2-Frequenz erst bei 800 Hz liegt, sehr schön den Anstieg der Dämmung mit ν^4 oberhalb der kritischen Frequenz ν_k, die also auch bei Systemen mit Dämpfung ihre Bedeutung als Anfangspunkt des Dämmgebietes behält, obwohl sie der Einfachheit halber für $\eta = 0$ berechnet wurde. In Abb. 17 ist punktiert die Dämmkurve eingezeichnet, die das System hätte, wenn man die obere Feder herausnähme und die beiden Massen direkt aufeinander setzte. Man sieht an dieser Gegenüberstellung die Vorzüge und Nachteile der Drosselketten: Erst bei Frequenzen, die oberhalb der kritischen Frequenz liegen, ist eine Drosselkette dem entsprechenden einfachen Masse-Feder-System überlegen, bei tiefen Frequenzen ist das einfache System besser. Die gleichen Verhältnisse findet man z. B. bei der Dämmung von Luftschall durch Doppelwände.

4. Gegenüberstellung von Gummi- und Stahlfedern

Gummi- und Stahlfedern unterscheiden sich in zwei Punkten grundsätzlich: 1. in ihrer Eigendämpfung und 2. in ihrem elastischen Verhalten. Gummifedern haben einen etwa zehnmal so großen Verlustfaktor wie Stahlfedern. Diese große Dämpfung bedeutet bezüglich der Schalldämmung einen wesentlichen Vorteil im gesamten Frequenzgebiet. Die geringe Eigendämpfung der Stahlfedern kann durch eine zusätzliche Reibungsdämpfung vergrößert werden. Man erreicht dadurch zwar eine Verringerung der gefährlichen Resonanzüberhöhung in der Umgebung der Masse-Feder-Resonanz, verschlechtert jedoch die Dämmung bei höheren Frequenzen.

Das elastische Verhalten von Gummifedern, die auf Druck beansprucht werden, wird von der Volumenkonstanz des Gummis bestimmt. Bei Belastung wird der Querschnitt der Feder größer und damit ihre Federung kleiner; sie wird härter. Nimmt man dem Gummi die Möglichkeit, seitlich auszuweichen, so ist die Feder außerordentlich hart und für Dämmzwecke unbrauchbar. Bei Stahlfedern ist die Federung innerhalb der zulässigen Belastungsgrenzen von der Belastung unabhängig. Die tiefste Eigenfrequenz ν_0, die mit einer gegebenen Feder erreicht werden kann, ergibt sich aus der zulässigen Spannung des Federstahls bzw. aus der Einfederung, bei der alle Windungen aufeinander liegen.

Da bei einer Gummifeder die Federung bei zunehmender Belastung kleiner wird, hat ihre Eigenfrequenz bei einer bestimmten Belastung ein Minimum, das mit keiner noch so großen Last unterschritten werden kann. Mit der vom Hersteller angegebenen zulässigen Belastung von 8 kp/cm² kommt man bei den üblichen Gummisorten bis auf den Faktor 1,3 an diese tiefstmögliche Eigenfrequenz heran. Die Tatsache, daß die Eigenfrequenz in einem gewissen Bereich von der Belastung unabhängig ist, gibt Gummifedern einen Vorteil gegenüber Stahlfedern, wenn es sich um die Abfederung stark wechselnder Lasten handelt (z. B. beladener und unbeladener Wagen).

Bei der Abfederung kleiner Massen ($M<10$ kg) lassen sich mit Gummidruckfedern keine genügend niedrigen Eigenfrequenzen erreichen. Man wird deshalb bei kleinen Massen Gummifedern verwenden, die auf Zug oder Schub beansprucht werden.

Herrn Prof. Dr. E. MEYER danke ich für die Anregung zu dieser Arbeit und für viele wertvolle Ratschläge. Ferner möchte ich Herrn cand. phys. K. HELBIG für seine Hilfe bei der Durchführung der Untersuchungen danken.

(Eingegangen am 9. Februar 1952.)

Schrifttum

[1] MEYER, E. und KEIDEL, L., Zur Schalldämmung von Federn und Dämmstoffen. Z. techn. Phys. **18** [1937], 299.

[2] BÖHME, H., Dynamisches Verhalten von Schalldämmstoffen. Akust. Z. **2** [1937], 303.

[3] KUHL, W. und MEYER, E., Dynamische Eigenschaften von Gummi und gummiartigen Stoffen in einem großen Frequenzbereich. Unveröffentlichter Bericht. Auszug in: Report of the 1948 Summer Symposium of the Acoustics Group. S. 181. The Physical Society, London.

[4] CZERLINSKY, E., Über die Ausbreitung von Ultraschallwellen in Drähten. Akust. Z. **7** [1942], 12.

[5] KOSTEN, C.W., Berechnung von Federungselementen aus Gummi. Z. VDI **86** [1942], 535.

ASPECTS OF THE CONCENTRATION OF ULTRASONIC ENERGY

by ALFONSO BARONE

Istituto Nazionale di Ultracustica „O. M. Corbino", Roma

Riassunto

Dopo aver esaminati i vantaggi offerti dai concentratori a riflessione rispetto alle lenti acustiche, nelle applicazioni delle elevate potenze ultrasonore, si descrivono due tipi di concentratori applicabili direttamente ai normali supporti dei quarzi ad emissione verticale. Vengono inoltre fatte considerazioni qualitative sulla struttura dei campi ultrasonori ottenuti mediante i sistemi descritti.

Sommaire

On indique les avantages que présente, pour la production d'ultra-sons intenses, la concentration par réflexion en comparaison à la concentration par lentilles acoustiques; on décrit deux façons de concentrer les ultra-sons, qu'on peut adapter aux supports de quartz employés habituellement pour faire une émission verticale. On étudie ensuite qualitativement la structure du champ ultrasonore ainsi produit.

Zusammenfassung

Bei der Herstellung hoher Ultraschallintensitäten hat die Fokussierung mittels Reflexion Vorteile gegenüber der Fokussierung mit akustischen Linsen. Es werden zwei Konzentrierungsmethoden beschrieben, bei denen man die üblichen Quarzhalterungen für vertikale Abstrahlung verwenden kann. Es folgt eine quantitative Betrachtung der Struktur des Ultraschallfeldes, das mit diesen Systemen erhalten wird.

Summary

The advantages offered by reflecting concentrators as compared with acoustic lenses in producing ultrasonics at high power are discussed and two types of concentrators capable of direct application to the usual quartz holders for vertical emission described. There follows a qualitative consideration of the structure of the ultrasonic field obtained by these systems.

1. Introduction

To produce most of the physical, chemical and biological effects of ultrasonics, it is necessary to use ultrasounds of high intensity.

It is always difficult to attain high values of the specific power in the direct field generated by the electroacoustic transducer because of the limitations imposed by its electrical and mechanical characteristics to the electric power supply (whether the transducer is piezo-electric or magneto-strictive in principle), and in a liquid, of the liability to produce cavitation in the immediate vicinity of the emitting surface.

The possibility of concentrating the ultrasonic energy emitted by a transducer, by reflecting or refracting systems analogous to those used for optical radiation, has been studied in numerous researches.

In the field of refracting systems, the first suggestion came from HOPWOOD [1]. Subsequently BEZ BARDILI [2] constructed converging lenses of aluminium, but these have low efficiency because of the characteristic impedance of aluminium being very high in comparison with that of the liquid.

With the same object GIACOMINI [3] and later POHLMANN [4] made lenses of a hollow solid envelope surrounding another liquid, but such lenses are difficult to construct. According to an observation of ERNST [5], some plastic materials have characteristic impedances near that of liquids and accordingly lend themselves to the purpose involved. Following these ideas, SETTE [6] has attained refracting systems which by the accuracy of their construction give an optimal concentration of the ultrasonic energy. Unfortunately such plastic materials have a high absorption, especially at high frequencies, and the dissipation of energy which follows causes, at large intensities, high internal temperatures which rapidly destroy the lens.

The use of plastic lenses is limited to low powers and to optical ultrasonics.

The problem of the refracting system for ultrasonics is accordingly only solved in part.

As to reflecting systems it is common practice in laboratories to use concave metallic mirrors. An exhaustive study of such reflectors has been made by GRIFFIN [7] and FOX [8]. The use of simple concave reflectors however presents the inconvenience that a vessel with a large liquid capacity must be used to satisfy geometric considerations.

It is to be noted also that certain ultrasonic transducers have been made to concentrate the radiation emitted directly. The first of these, conceived by GRÜTZMACHER [9], consists of a slice of quartz of concave shape. Such transducers are however costly and have not had many applications in this field. More recently concave transducers [10] have been made up from piezo-electric ceramics of barium titanate which, although able to concentrate the energy into a small space, are not able to produce large energy densities because the emission per unit area of source (ca. 2 W/cm²) is much inferior to that which one can get from quartz, for example (ca. 40 W/cm²).

In view of these considerations, we have thought of constructing two types of concentrating reflector with a view to the elimination of the inconveniences aforesaid and we propose in what follows to give a detailed account of these. It is the intention that such apparatus shall be capable of direct application to the normal holders for giving vertical emission from quartz generators forming part of ultrasonic apparatus of medium and large power.

The reflecting surfaces are made of metal blocks having as high a specific impedance as possible to get a maximum of reflected energy.

In the first part of what follows we shall suppose that the dimensions of the source are large compared to the ultrasonic wavelength so that we can with good approximation apply the laws of rectilinear propagation to the compressional waves; later we shall indicate the limits of this approximation.

2. The biconical concentrator

The object of this apparatus is to concentrate as much energy as possible into a region of given area. Fig. 1. shows a transverse section of a cavity of the shape of two conical frustra joined end-to-end by their smaller apertures. A beam of plane ultrasonic waves enters in an axial direction from the lower end of radius R. The central portion of the beam, having radius r, travels through the concentrator axially without deflection, while the outer annular portion of the beam, being reflected on the sides, forms a beam of conical waves which passing through the constriction of radius r is again reflected on the confines of the upper cone towards a zone distant $H+h_1$ from the base of the bi-cone. Here it produces a considerable augmentation of energy density. For simplicity of treatment we shall refer first to a model made of plane reflectors of section shown in Fig. 1. For the greatest output, all the energy passing the throat should have been reflected once only on the lower inclined surface; then the rays incident on the middle of the inclined surface will pass through the centre of the hole, as shown. Under these conditions:

$$r = R\,\frac{k-1}{k+1}\,,\quad \left(k = \frac{\tan\gamma}{\tan\gamma/2}\right) \qquad h_1 = \frac{R+r}{\tan\gamma}\,. \qquad (1), (2)$$

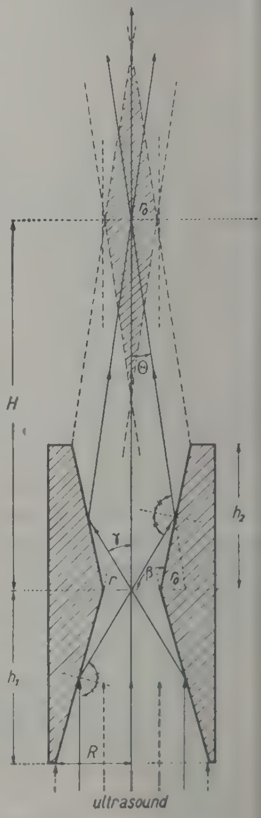

Fig. 1. Diagram of biconical concentrator.

It follows from (1) that the ratio R/r, on the square of which the gain of intensity depends, is greater for small values of the angle γ and tends to a maximum of 3. For a given semi-angular aperture γ of the exit beam and radius R of the entry, it is possible to determine the dimensions of the lower part of the apparatus.

Simple geometric consideration of the form of the upper frustrum leads easily to a relation that links the distance H (at which the lateral beams come together into the central beam) for a given angle γ and the unknown angle β, as follows:

$$\frac{H}{r} = \frac{\sin\beta}{\cos(\beta-\gamma)} \cdot \frac{\sin(2\beta-2\gamma)}{\sin(2\beta-\gamma)} \,. \qquad (3)$$

The solution is notably simplified if we trace loci in which H/r is given as a function of β for discrete values of γ. Then we have a family of curves each characterised by a value of γ (Fig. 2). The region of convergence indicated on Fig. 1 has a maximum diameter $2r_0$ where $r_0 = -H\tan(2\beta-\gamma) - r$.

The gain of intensity is: $G = \dfrac{R^2 + r_0^2 - r^2}{r_0^2}$.

So it is possible to plan a concentrator filling given conditions corresponding to values of the parameters, e. g. the distance of the focussing zone, the gain of intensity and consequently the size of the region in which a desired energy density (or specific power) shall be produced.

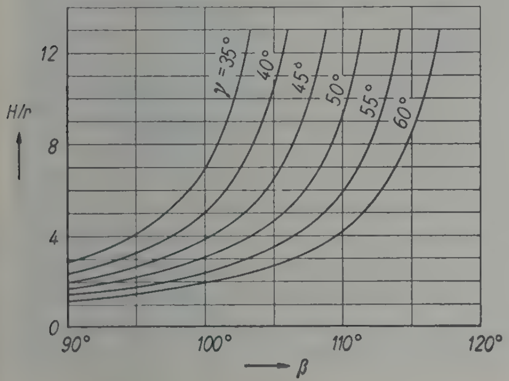

Fig. 2. Curves to determine H/r.

Besides the energy density, the form of the ultrasonic field in the „focus“ should be considered. We have three beams of plane waves which will interfere. The zone of interference is readily computed by the principle of superposition. Immediately after leaving the concentrator the two lateral beams will interfere with the central one; interference bands result directed along the bisectrix of the two beams which meet at an angle Θ. Their separation D is given by $D = \dfrac{\lambda \sin\Theta/2}{2}$, λ being the ultrasonic wavelength in the liquid. This is seen in Fig. 3a which is a photograph of the ultrasonic field at 4 Mc/s taken by the „Schlierenmethode“ in a demonstration model of plane reflecting walls. The clear strips represent the zones of maximum pressure. Fig. 3b shows the field at double this frequency (8 Mc/s). Evidently the actual concentrator has circular symmetry in relation to the central axis and therefore the zones of interference have the form of circular coronae of width equal to that of the bands here observed. Fig. 4a and 4b show a practical realisation of a bicone made in two pieces to attain variable distances of convergence as desired. Some openings are cut on the base of the concentrator so that the liquid from the outside takes the place of that inside, which is continually forced up under the action of the strong radiation pressure.

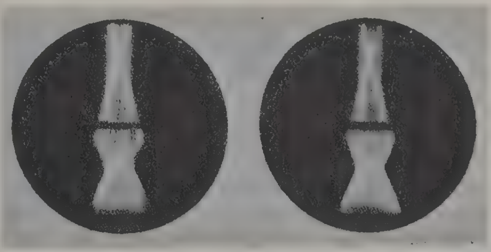
(a) (b)

Fig. 3. Ultrasonic field in model bi-conical concentrator; (a) frequency 4 Mc/s, (b) Frequency 8 Mc/s.

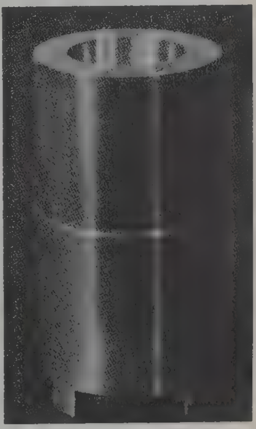

Fig. 4a. Bi-cone.

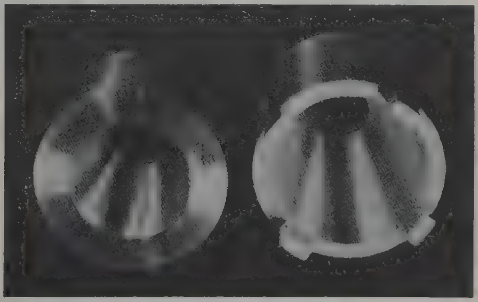

Fig. 4b. Bi-cone.

Now let us examine the conditions under which the laws of rectilinear propagation can (as in light) be applied to the system. If the wavelength is not negligible compared to the source of diameter d the ultrasonic beam will diverge to an extent depending on the ratio λ/d in accordance with $\sin\alpha = 1.22\,\lambda/d$, where α is the semiangle of the beam. In consequence of diffraction, the ultrasonic beam debouching from the internal constriction will be modified as to wavefront in the peripheral zone. All this results in a divergence from the gain as calculated by the simple geometric theory. With the size of sources and frequencies commonly used (order of Mc/s) such divergencies anyway rigorously computable may be neglected in practical applications.

3. The parabolic concentrator

Also with this type of concentrator, it is proposed to plan an apparatus readily applicable to the quartz holder but capable of focussing in this case all the energy into a restricted region on the vertical axis of the crystal. Let us consider a beam of plane waves reflected on surfaces, in the first place, for simplicity of treatment, taken to be plane and cylindro-parabolic according to the section shown in Fig. 5. The parabola having focus at F and being tangent to the (vertical) Y-axis, let the part of an ultrasonic beam first reflected from the plane (inclined at 45° to the vertical) fall on the parabolic surface in a (horizontal) direction parallel to its axis so that after this second reflection the rays converge to F. It is clear that the parabola must be so disposed that the rays reflected by it miss the top of the plane mirror. Suppose the point P on the former has co-ordinates $y = H$ and $x = f - HR/h$. Such values substituted in the equation of the parabola $y^2 = 2px$ enable the parameter p to be determined for given values of R and the focal distance h of the concentrator.

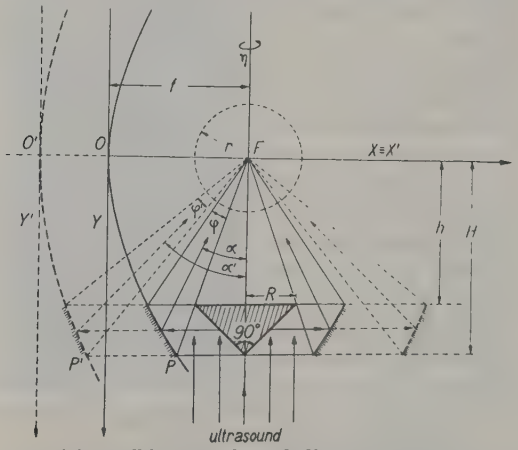

Fig. 5. Diagram of parabolic-concentrator.

By rotating the section indicated about the axis η, one obtains a mirror in the form of a cone surrounded by a paraboloidal surface. For demonstration purposes, as with the bicone, we figure an apparatus with plane and cylindroparabolic surfaces. Results obtained at two frequencies, 4 Mc/s (Fig. 6a) and 8 Mc/s (Fig. 6b) show clearly how optical conditions of propagation are approached at higher frequencies. Fig. 7 shows a practical example of such a concentrator.

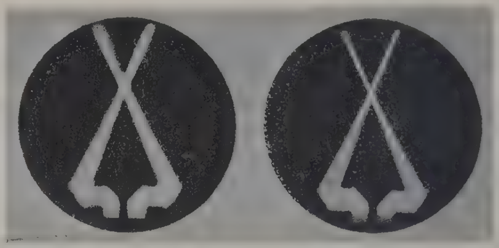

(a) (b)

Fig. 6. Ultrasonic field in model parabolic concentrator; (a) Frequency 4 Mc/s, (b) Frequency 8 Mc/s.

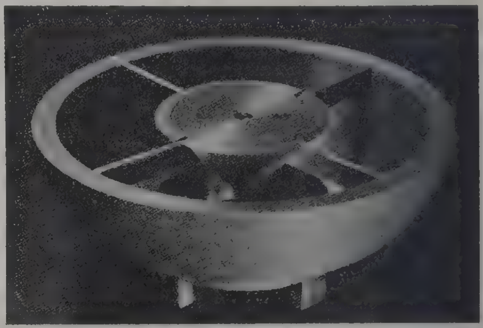

Fig. 7. Parabolic concentrator.

The gain of intensity can be calculated according to the formula of Fraunhofer for the optical case.

The "focal spot" is a central zone surrounded by peripheral concentric rings in which the intensity gradually diminishes outwards. As the wavelength diminishes so does the diameter of the central zone so that the efficiency of such a system increases notably with the frequency.

In practice, for frequencies of the order of megacycles one can, with generators of medium power, reach focal intensities of hundreds of watts/cm².

An observation on the concentrator here described which may have a certain interest relates to the gradient of intensity towards the focus. At a distance r therefrom (Fig. 5) the total energy is distributed over an area;

$$S = 4\pi r^2 \sin\alpha \sin\varphi/2.$$

As a first approximation $\tan\varphi/2 = \dfrac{R}{H+h}\cos\alpha$ and at $\varphi < 20^0$ (which is effectively true in practice) we can put $\tan\varphi/2 \approx \sin\varphi/2$ and so:

$$S = \frac{2\pi R}{H+h}\, r^2 \sin 2\alpha.$$

If W is the total power emitted by the source, we have for the intensity J:

$$J = \frac{W}{S} = \frac{(H+h)\,W}{2\pi R r^2 \sin 2\alpha}$$

and for its gradient with respect to r

$$\frac{\mathrm{d}J}{\mathrm{d}r} = -\frac{(H+h)\,W}{\pi R \sin 2\alpha} \cdot \frac{1}{r^3}\,.$$

As we see, the gradient of intensity diminishes as α augments up to a value $\alpha' = 45^0$. Under these conditions, higher values of J or of $\mathrm{d}J/\mathrm{d}r$ are attained at much smaller distances from the focus. So an increase in the diameter of the paraboloid causes a diminution in the specific power near the focus. Such a possibility may be useful especially in therapy, where one wishes to work at a depth in a restricted zone without having great intensity in the surrounding tissue.

On Fig. 9 and 10 we exhibit the effect of the concentrators described. The radiation pressure at the surface of the liquid, suitably adjusted to the height of the focus, produces the characteristic fountain. This shows quite different forms for the two types. The focal region of small dimensions in the case of the parabolic concentrator produces a compact jet. In the case of the bicone the jet is more diffuse and formed of droplets projected to great distances. This is due to the large pressure in the interference zones.

For comparison Fig. 8 shows the effect of the ultrasonic beam without concentrations.

I wish to thank Professor A. GIACOMINI for his friendly interest and advice.

(Received 4th April, 1952.)

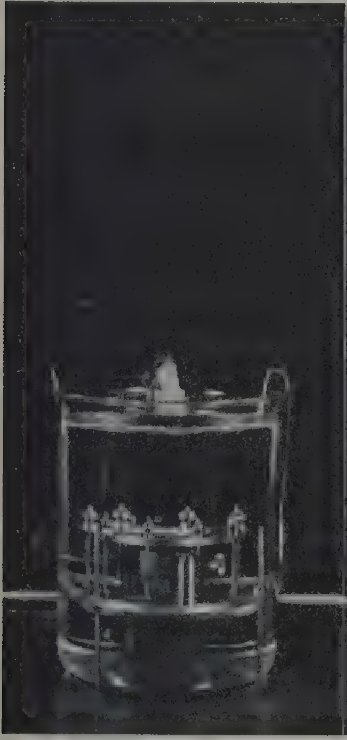

Fig. 8.
Ultrasonic radiation (unconcentrated).

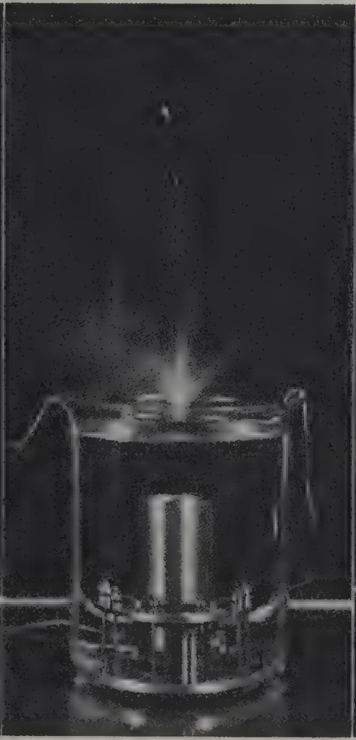

Fig. 9.
Ultrasonic radiation in bi-cone.

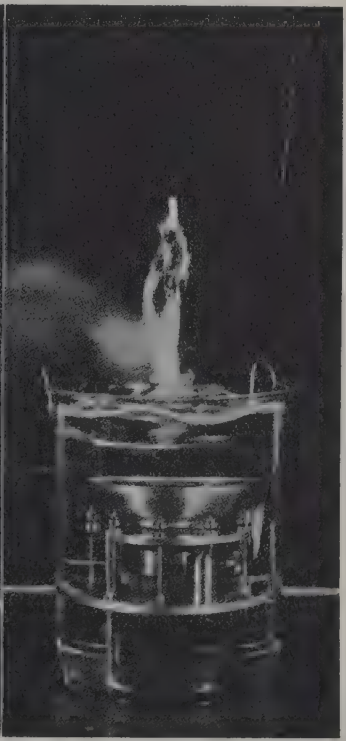

Fig. 10.
Ultrasonic radiation in parabolic concentator.

References

[1] HOPWOOD, F. L., Nature **128** [1931], 748; J. sci. Instrum. **23** [1946], 63.
[2] BEZ BARDILI, W., Phys. Z. **36** [1935], 20.
[3] GIACOMINI, A., Alta Frequenza. **7** [1938], 384.
[4] POHLMAN, R., Z. Phys. **113** [1938], 697.
[5] ERNST, P., J. sci. Instrum. **22** [1945], 238.
[6] SETTE, D., J. acoust. Soc. Amer. **21** [1949], 375.
[7] GRIFFIN, V. and FOX, F. E., J. acoust. Soc. Amer. **21** [1949], 348.
[8] FOX, F. E. and GRIFFIN, V., J. acoust. Soc. Amer. **2** [1949], 352.
[9] GRÜTZMACHER, J., Z. Phys. **96** [1935], 342.
[10] JAFFE, H., Industr. engng. Chem. **42** [1950], 264.

ON THE DIRECTIVITY OF SPHERICAL MICROPHONES*

by WALTER KUHL**

III. Physikalisches Institut der Universität Göttingen

Summary

The directivity patterns of microphones with circular plane diaphragms on the surface of a sphere have been measured for ten frequencies and are compared with the directivity patterns of point-like microphones on the surface of a sphere, as computed exactly by SCHWARZ. The directivity patterns for two frequencies have been calculated approximately for the microphone investigated. It is possible to get exactly the same response for all angles of incidence by adding the absolute values of the voltages of two point-like identical microphones situated on opposite points of a sphere. This does not hold for actual microphones with finite dimensions. Finally the frequency response curve of a microphone without any directivity is calculated, viz. a spherical microphone the diaphragm of which covers the whole surface.

Sommaire

Les caractéristiques de directivité de microphones à membrane plane circulaire à la surface d'une sphère, ont été relevées pour dix fréquences et ont été comparées avec les caractéristiques de directivité d'un microphone ponctuel à la surface d'une sphère qui ont été calculées rigoureusement par SCHWARZ. La caractéristique de directivité du microphone étudié a été calculée d'une manière approximative pour deux fréquences. Il est possible d'obtenir une sensibilité presque constante à tous les angles d'incidence en ajoutant les valeurs des tensions de deux microphones ponctuels identiques situés sur des points diamétralement opposés d'une sphère. Ce procédé n'est pas valable si les microphones ont une dimension finie. Enfin on a calculé la courbe de réponse en fréquence d'un microphone sans aucune directivité, c'est-à-dire d'un microphone sphérique, dont la membrane couvrirait toute la surface.

Zusammenfassung

Die Richtcharakteristiken von Mikrophonen mit kreisförmiger, ebener Membran auf der Oberfläche einer Kugel wurden für zehn Frequenzen gemessen und werden mit den exakt von SCHWARZ berechneten Richtcharakteristiken eines punktförmigen Mikrophons auf der Kugeloberfläche verglichen. Für zwei Frequenzen wurde die Richtcharakteristik des untersuchten Mikrophons näherungsweise berechnet. Durch die Addition der Beträge der Spannungen von zwei gleichen punktförmigen Mikrophonen auf entgegengesetzten Punkten einer Kugel kann eine fast konstante Empfindlichkeit für alle Winkel erzielt werden. Dies gilt aber nicht für Mikrophone endlicher Größe. Schließlich wird die Frequenzkurve eines Mikrophons ohne jegliche Richtwirkung berechnet, nämlich eines kugelförmigen Mikrophons, dessen Membran die gesamte Oberfläche bedeckt.

For the purpose of transmitting, recording, and measuring airborne sound in the audible frequency range, microphones of very different directional characteristics have been developed. A microphone of a not too low sensitivity perfectly independent of the direction of incident sound, i. e. a microphone in which the sensitivity varies in direction by no more than a few per cent, has proved difficult to design in this range. This may be illustrated by a numerical example. If at a frequency of 10 kc/s a maximum variation of 3 db in sensitivity in any direction is permitted, the diameter of a microphone of spherical outer shape must not exceed 6—7 mm. If a maximum variation of 5 or 10 db is tolerated, the maximum diameter is 12 or 27 mm, respectively. Microphones of cylindrical shape require still smaller diameters. These figures show that for structural reasons and on account of the decrease in sensitivity it would be impossible to design a nondirectional microphone for up to 100 kc/s or still higher frequencies merely by reducing the dimensions of the types hitherto employed. In the case of probe-tube microphones the low dependence of the sensitivity on the angle of incidence, owing to the small diameter of the probe-tubes, is allied with a low sensitivity. In order to avoid resonance effects in the tube, which would result in considerable dips of the frequency response curve, the propagation of sound in the tube has to be attenuated; this, however, causes a further decrease of sensitivity with frequency.

By combining two or more microphones, arranged on the surface of a sphere and facing different direc-

---

* This work was supported by the Department of Scientific and Industrial Research, London.

** Now at the Rundfunktechnisches Institut, Nürnberg.

tions, it is possible to obtain a less dependence on the direction of the incident sound for given dimensions. In order to avoid interference effects, the absolute values of the microphone voltages have to be added, i. e. the microphone voltages have to be separately amplified and rectified, and the direct currents have to be added.

The directivity patterns of some arrangements of microphones were investigated by calculation as well as by experiment. These were:

1. a point-like microphone at the surface of a sphere,
2. two such microphones, the absolute values of their voltages being added,
3. a cylindrical microphone, $2r$ in diameter, with a spherical cover of radius R, R being three times r (Fig. 1),
4. two microphones of this size arranged in a sphere, the absolute values of the voltages being added.

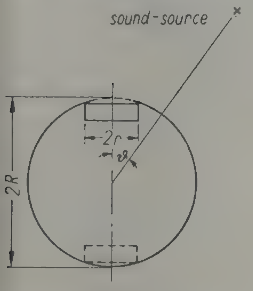

Fig. 1. Scheme for the arrangement of one or two cylindrical microphones with spherical cover.

The calculations have been based upon a paper by L. Schwarz [1] who had calculated the amplitudes and the phases of the pressure distribution as well as their real and imaginary parts using the exact solution of the diffraction problem with an accuracy of 10^{-5}. The calculations have been carried out for various values of the ratio of the circumference $2\pi R$ of the sphere to the wavelength λ namely 1, 2, 3 ... 10, and for 5^0 increments of the angle of incidence ϑ. The ratio of the pressure p at the point considered to the pressure p_0 of the incident plane wave, calculated by Schwarz, has been plotted against angle of incidence for $2\pi R/\lambda = 1, 2, 3, 4, 5, 6, 8$, and 10 in Fig. 2...4 (full lines) and Fig. 5...6 (curves "a"). They represent the directivity patterns of a point-like microphone at the surface of the sphere.

As a measure of the directivity of this and other systems of microphones, the ratio of the maximum and minimum sound pressures observed when the microphone system is rotated about an axis perpendicular to the direction of incident sound has been chosen, i.e. for $\vartheta = 0 ... \pm 180^0$. For a point-like microphone arranged on a sphere this ratio has been plotted as curve "a" in Fig. 7 in a db-scale; it is 4.2 db for $2\pi R/\lambda = 1$ and rises up to 19 db for $2\pi R/\lambda = 10$.

By arranging two microphones at opposite points of a sphere and adding the absolute values of their voltages as described above, an arrangement is obtained the sensitivity of which shows but little variation with the angle of incidence. This case is illustrated by curve "d" in Fig. 7. The variation of the sensitivity is 2.0 ... 2.8 db only. If these two microphones are connected in parallel or in series,

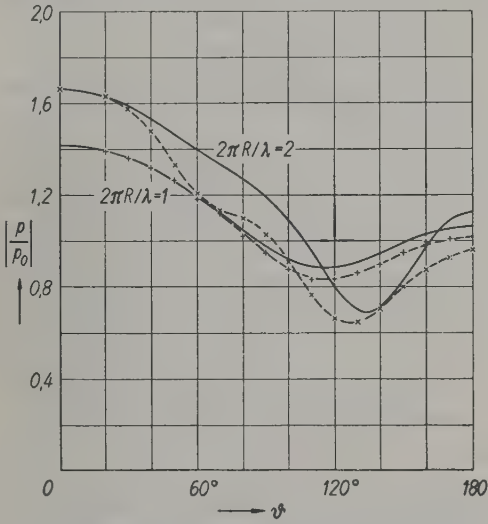

Fig. 2. Dependence of the ratio of pressure on the surface of a sphere (radius R) to the pressure of the incident sound wave on the angle of incidence. $2\pi R/\lambda = 1$ and 2. Full lines: for a point of the sphere (computed), broken lines: integrated over the diaphragm of a microphone (radius r; $R/r = 2.8$) (measured).

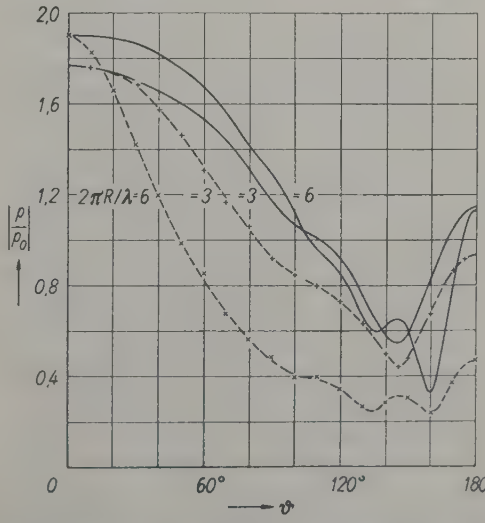

Fig. 3. Dependence of the ratio of the pressure on the surface of a sphere (radius R) to the pressure of the incident sound wave on the angle of incidence. $2\pi R/\lambda = 3$ and 6. Full lines: for a point of the sphere (computed), broken lines: integrated over the diaphragm of a microphone (radius r; $R/r = 2.8$) (measured).

i. e. their voltages added with respect to amplitude and phase, the variation is 19 db for $2\pi R/\lambda=10$ owing to the interference of the voltages, just as in the case of a single microphone.

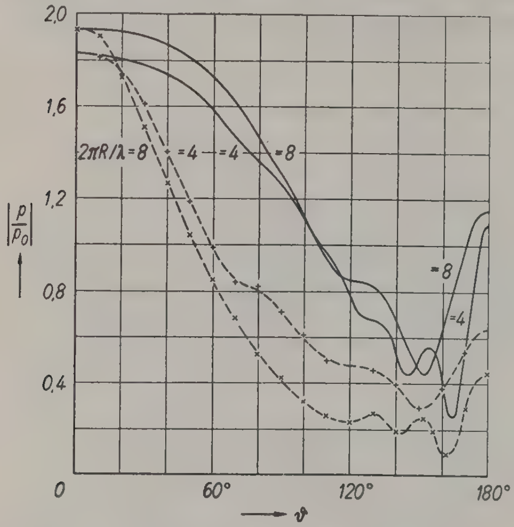

Fig. 4. Dependence of the ratio of the pressure on the surface of a sphere (radius R) to the pressure of the incident sound wave on the angle of incidence. $2\pi R/\lambda = 4$ and 8. Full lines: for a point of the sphere (computed), broken lines: integrated over the diaphragm of a microphone (radius r; $R/r=2.8$) (measured).

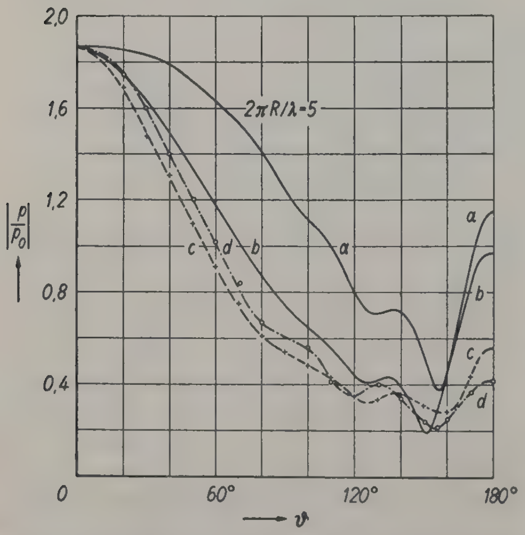

Fig. 5. Dependence of the ratio of the pressure on the surface of a sphere (radius R) to the pressure of the incident sound wave on the angle of incidence. $2\pi R/\lambda=5$. a) for a point on the sphere (computed), b) integrated over a section of the sphere (radius r; $R/r=3$) (computed), c) integrated over the diaphragm of a microphone (radius r; $R/r=2.8$) (measured).

The conditions are widely different for the case when the microphone mounted in the spherical surface is not point-like. Then the directivity patterns of one or two identical microphones no longer coincide with the pressure distributions at the spherical surface. The directivity patterns for actual microphones will be considered for a condenser microphone constructed in this Institute for an upper cut-off frequency of 25 kc/s. It has a diaphragm diameter $2r=12.5$ mm and the diameter of the spherical cover is $2R=35$ mm so that $R/r=2.8$ which is usual for microphones of this type. The cylindrical boring in the spherical body is 18 mm diameter. The diaphragm, of an effective diameter of 12.5 mm, is arranged about 1 mm below the plane of the edge of the boring. Thus the distance between the diaphragm and the centre of the sphere is smaller by 4 mm than the radius of the sphere. For the approximate calculation, however, the pressure distribution over the diaphragm has been assumed to be equal to that of the corresponding area of the spherical surface having an equal diameter, i. e. a segment subtending an angle of ±20° at the centre of the sphere. The directivity patterns of this microphone have been approximately calculated for $2\pi R/\lambda=5$, and 10, respectively, and with $R/r=3$.

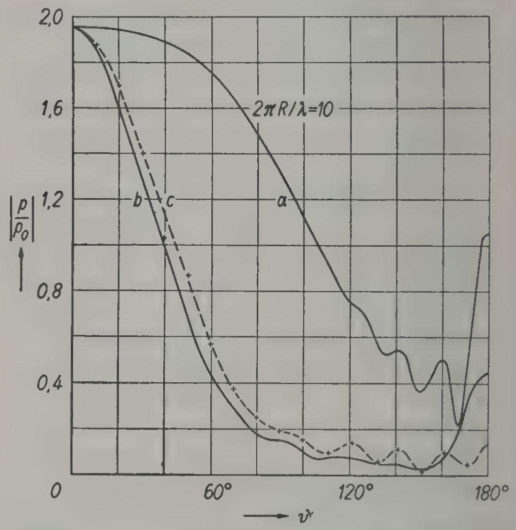

Fig. 6. Dependence of the ratio of the pressure on the surface of a sphere (radius R) to the pressure of the incident sound wave on the angle of incidence. $2\pi R/\lambda = 10$. a) for a point on the sphere (computed), b) integrated over a section of the sphere (radius r; $R/r = 3$) (computed), c) integrated over the diaphragm of a microphone (radius r; R/r 2.8) (measured).

A further approximation is made in the method of integration. An exact integration of the sound pressure over the spherical surface being impossible, the circular area with the diameter of the diaphragm has been divided into eight strips of "constant" angle of incidence for $2\pi R/\lambda=5$, and into ten such strips for $2\pi R/\lambda=10$. The breadth of each strip corresponds to angles of 5^0 and 4^0, respectively, at the centre of sphere. The total pressure acting upon these partial areas is obtained in the following way. The pressure per unit area acting upon the centre of the strip as calculated by SCHWARZ is multiplied by the area of the strip. These eight or ten partial pressures have been added, the real and imaginary parts separately, and the absolute value has been formed from the sums. The angle of incidence ϑ has been varied by steps of 5^0, and 4^0, respectively, and the partial pressures calculated for each angle and then added. For instance for $2\pi R/\lambda=10$ the angles of incidence of the centres of the ten individual partial areas are $\vartheta\pm 2^0$, $\vartheta\pm 6^0$, $\vartheta\pm 10^0$, $\vartheta\pm 14^0$, and $\vartheta\pm 18^0$. The small variations of the sound pressure along the length of the strips, corresponding to angles at the centre of the sphere from ± 7.5 to $\pm 20^0$ in the perpendicular direction are disregarded in order to simplify the approximate calculation.

The directivity patterns of "spherical diaphragms" thus approximately calculated have been plotted in Fig. 5 and 6 as curves "b". The deviations from the associate directivity patterns of the point-like microphones are considerable. In the case of $2\pi R/\lambda=10$ a wavelength along the circumference of the sphere nearly equals the assumed diameter of the diaphragm. Hence we have a cancelling effect when averaging over the area of the diaphragm for angles of incidence between about 100^0 and 160^0 (see Fig. 6).

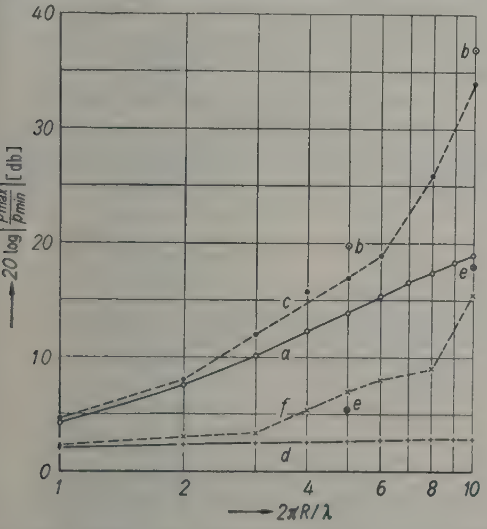

Fig. 7. Dependence of the ratio of the maxima and minima of the directional characteristics of one microphone or two combined microphones on the surface of a sphere (radius R), on $2\pi R/\lambda$. a) one point-like microphone ($r \ll R$), computed. b) one microphone ($R/r = 3$), computed approximately. c) one microphone ($R/r=2.8$), measured. d) two combined point-like microphones ($r \ll R$), computed. e) two combined microphones ($R/r=3$), computed approximately. f) two combined microphones ($R/r=2.8$), measured.

For $\vartheta=0$ in both cases ($2\pi R/\lambda=5$ and 10) the pressure integrated over the area of the diaphragm equals that at a point of the spherical surface with an accuracy of less than 0.5 per cent. The pressure transformation at a sphere calculated by BALLANTINE and others is, therefore, also valid for microphones of finite dimensions with a spherical cover up to $2\pi R/\lambda=10$ for zero angle of incidence. It would, however, be erroneous to apply these simple calculations also for other angles of incidence as is often done for microphones of spherical or other shape in the acoustical literature.

The ratio of the maximum to the minimum value of the curves "b" has been plotted for $2\pi R/\lambda=5$ and 10, respectively in Fig. 7. The plots have also been marked by "b" in this figure. The variations of sound pressure amount to 19.8 and 38 db, respectively. The values calculated for the combination of two microphones of equal size ($R/r=3$) have been denoted by "e". By combining two microphones the variations can be reduced to 5.5 db for $2\pi R/\lambda = 5$; for $2\pi R/\lambda=10$, however, they can only be reduced to 18 db.

For comparison with the calculated values, and to complete the work, the directivity patterns of the above-mentioned condenser microphone have been measured in an anechoic chamber. The clearance between the absorbing wedges at the walls (consisting of soft wood fibre material) was $80\times 80\times 150$ cm³. At normal incidence the reflection factor is smaller than 10 per cent above 1.8 kc/s, whereas this applies at oblique incidence even above a somewhat lower frequency. The measurements have been taken with $2\pi R/\lambda = 1, 2, 3, 4, 5, 6, 8,$ and 10, i. e. in the frequency range from 3.1 to 31 kc/s. The high quality of the anechoic chamber can be seen from the fact that the directivity patterns have been found perfectly symmetrical up to $\pm 90^0$. The discrepancies between the corresponding measured values at the left and right hand remained below ± 1.5 per cent of the sound pressure of the incident wave. The values measured for angles between $\pm 90^0$ and $\pm 180^0$ deviate from the expected ones by the fact that the maximum values at the rear side are in all cases shifted by 8^0 from 180^0. This fact can be explained by assuming that the air gap of the condenser microphone, measuring 0.015 mm on average, is not constant over the whole area of the diaphragm, thus causing an asymmetry of the microphone. In order to be able to compare the measured and the calculated values, the shift of the rear part of the directional characteristic has been equalized by calculation. The sound pressure at $\vartheta = 0^0$ has been put equal to the value calculated by SCHWARZ for this point of the sphere, with the exception of the cases $2\pi R/\lambda = 5$ and 10. The deviation from the true value is below the accuracy of measurement. In the cases $2\pi R/\lambda = 5$ and 10 the measured pressure was put equal to the value gained by integrating over the surface of the diaphragm.

The measured values, averaged for positive and negative angles of incidence, have been plotted in Fig. 2 ... 6 (broken lines). The figures show the deviations between the directivity patterns of a point-like microphone and those measured for $R/r = 2.8$ at various frequencies. The deviations of the measured patterns from those approximately calculated for $R/r = 3$ and $2\pi R/\lambda = 5$ and 10 are greatest in the case of the maximum value at $\pm 180^0$, (denoted in optics as the "bright spot"), the measured maximum values being considerably smaller than the calculated ones. Having regard to the degree of approximation, the agreement between the measured and calculated curves can be considered good. In the case of $2\pi R/\lambda = 5$ the directional effect is more pronounced and for $2\pi R/\lambda = 10$ it is less pronounced than it ought to be according to the calculation. In these two cases, only, the directivity patterns were also measured for a condenser microphone of the same size but with a solid dielectric. The deviations from the measured curves were nearly the same as for the microphone with air as a dielectric.

The ratios of the maximum and minimum values of the sound pressure which can be read from the curves of Figs. 2 ... 6 for a single microphone, and for two microphones with added absolute values of the voltages, have also been drawn in Fig. 7 (curves "c" and "f"). They agree within 1.5 to 3 db with the calculated plottings b (one microphone) and e (two microphones).

By means of the curves given in Fig. 7, we are able to determine the size of microphone for the different arrangements with given directivity requirements. In the introduction a numerical example has been given. Since the considerable reduction of the directivity by combining two microphones is only valid for point-like microphones, and not for the microphones used in practice, only little improvement can be obtained by combination. For a frequency of 10 kc/s and a permitted pressure variation of 3 db, the maximum diameter of the sphere can be enlarged from 6.5 mm with one microphone to 22 mm with two microphones combined. In the latter case the diameter of the diaphragms should be 7.5 mm. The measurements of MULLER, BLACK and DAVIS [2], however, showed that the pressure variations of a rotating cylindrical microphone of this diameter (7.5 mm) without the spherical cover did not exceed 4.4 db. The slight improvement from 4.4 to 3 db, obtainable in practice by using two equal microphones and a two-channel amplifier, does not pay.

A complete independence of direction can be attained at arbitrary high frequencies only by extending the diaphragm of a spherical microphone with a solid dielectric. Such a microphone, however, suffers from the disadvantage that with growing frequency various regions of the spherical surface counteract one another, thus reducing the sensitivity of the microphone.

An approximate calculation of the frequency response curve has been carried out. The surface has been subdivided into circular zones each of 5^0 in latitude. The real and imaginary parts valid for the middle of each circular zone have been calculated and multiplied by the area of the respective zone. The individual values have been plotted against the surface of the sphere from $\vartheta = 0^0$ to $\vartheta = 180^0$. In the case of $2\pi R/\lambda = 10$ the curves so plotted already show 8 transitions through the zero axis. The pressure distribution has been obtained by graphical integration of the curves, the values being given by the integrals of the real and imaginary parts. The integral over the total surface of the

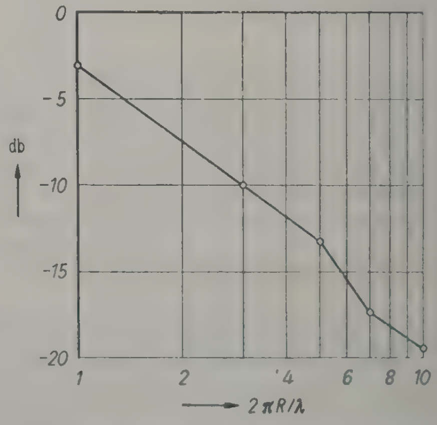

Fig. 8. Frequency response curve of a condenser microphone with a spherical diaphragm covering the whole surface of the sphere (radius R) (computed approximately).

sphere valid for low frequencies is chosen as unit. These calculations have been carried out with $2\pi R/\lambda = 1, 3, 5, 7$, and 10. The frequency response curve of the microphone so obtained is shown in Fig. 8. The calculation is based upon the assumption that the natural frequency of the microphone is very high, i. e. that at all frequencies in question the capacity varies as the pressure per unit area. The sensitivity decreases by 19.4 db from low frequencies up to $2\pi R/\lambda=10$, i. e. with a diameter of 11 mm up to 100 kc/s. At this frequency a cylindrical microphone of a maximum pressure variation of 3 db in the range from 0^0 to 180^0 should have a diameter of 0.5 mm. The same holds for the diameter of the tube of a probe microphone. If the spherical microphone must be chosen larger for technical reasons, the sensitivity decreases correspondingly. The thermal noise level is also reduced owing to the increased capacity. It may be mentioned that by shunting this condenser microphone by a resistor the response curve can easily be flattened electrically.

(Received 10th August, 1951.)

References

[1] SCHWARZ, L., Zur Theorie der Beugung einer ebenen Schallwelle an der Kugel. Akust. Z. **8** [1943], 91.

[2] MULLER, G. G., BLACK, R. and DAVIS, T. E., The diffraction produced by cylindrical and cubical obstacles and by circular and square plates. J. acoust. Soc. Amer. **10** [1938], 6.

ANALYSE DE MOUVEMENTS VIBRATOIRES DANS UN TUYAU SONORE

DISCONTINUITÉS VENTRALES

par J. GUITTARD

Institut Catholique de Toulouse

Sommaire

Il s'agit d'une méthode d'analyse du mouvement vibratoire de l'air dans un tuyau sonore ou autre cavité fermée, au moyen de fines poussières d'amidon. Cette méthode est applicable, d'une part, aux dérivations, aux variations de section ou autres déformations du tuyau, d'autre part, à des phénomènes de circulation et des phénomènes tourbillonnaires engendrés par de petits obstacles placés dans le tuyau.

Zusammenfassung

Das Schallfeld in einem luftgefüllten Rohr oder einem anderen geschlossenen Hohlraum wird mit Hilfe von feinem Stärkestaub analysiert. Die Methode läßt sich einerseits anwenden, um den Einfluß von Querschnittsänderungen des Rohres zu studieren und andererseits, um die Umströmung kleiner Hindernisse und die dabei auftretende Wirbelbildung zu beobachten.

Summary

This is a method of analysis of the vibratory movement of the air in a sounding pipe or other closed cavity, by means of fine dust. The method may be applied on the one hand to derivations, section variations or other deformations of the cylindrical column, on the other hand to phenomena of circulation and vortex production in the pipe by small obstacles.

1. Introduction

Un tuyau sonore fermé à ses deux extrémités, a son mouvement vibratoire entretenu par un téléphone dépolarisé branché sur le secteur. Le mouvement vibratoire de l'air est analysé au voisinage du ventre, unique, de ce tuyau.

Différentes discontinuités peuvent se présenter: on peut ouvrir le tuyau au droit du ventre et mettre en communication avec un volume, soit infini (atmosphère), soit fini (tuyau de longueur variable). A ces phénomènes se rattache l'ouverture d'un petit trou dans la paroi terminant le tuyau à l'opposé du téléphone, ainsi que l'introduction d'un corps de volume et de position variables.

Dans tous ces cas, il y a modification d'amplitudes et de phases, facilement mesurables et indiquant que l'onde n'est plus stationnaire.

L'introduction au ventre d'obstacles de volume négligeable ne modifie le mouvement vibratoire que dans leur voisinage immédiat. L'analyse par de fines poussières d'amidon montre l'existence de zones tourbillonnaires et de circulations, liées aux obstacles et bien déterminées.

2. Matériel et méthodes d'observation

Les différents tuyaux sonores utilisés sont en laiton, de diamètre 4 cm, d'épaisseur 1 mm. Des glaces convenables sont disposées pour l'observation ou la photographie; enfin, le tuyau comporte tous les ajutages nécessaires.

On peut modifier sa longueur au moyen de deux coulisses dont l'une porte le téléphone.

La température variant au cours des expériences, la longueur d'onde du son change; il faut modifier la longueur du tuyau. Pour une variation de température de 10 degrés, la longueur d'un tuyau comprenant une demi-longueur d'onde doit augmenter ou diminuer de près de 4 cm; d'où la nécessité d'un réglage au début de chaque séance de travail.

Le téléphone, dépolarisé, est alimenté sous 110 V par l'intermédiaire d'un transformateur et de résistances ou rhéostats. On mesure l'intensité du courant qui peut varier de 10 à 200 mA. Toutes choses égales d'ailleurs, l'amplitude dans le tuyau n'est pas proportionnelle à l'intensité, mais croît plus vite que celle-ci. En effet, lorsque les amplitudes du mouvement de la plaque du téléphone augmentent, la distance moyenne plaque-électroaimant diminue; l'action de l'électroaimant augmente. Le tableau suivant donne quelques correspondances:

Intensités	10	15	20	25	30	35	40	45	mA
Amplitudes	0,05	0,07	0,14	0,27	0,30	0,40	0,55	0,70	mm

Le contrôle de la fréquence du courant a montré que ses variations ne dépassent pas 2 pour cent, c'est l'ordre de grandeur de la précision des mesures.

Au moyen d'une petite poire en caoutchouc on injecte au voisinage du lieu d'observation de la poudre d'amidon. Les grains qui la composent ont une dimension qui ne dépasse pas 2 microns; ils reproduisent fidèlement le mouvement de l'air pour une fréquence inférieure à 1000 p/s.

Ces poussières peuvent être observées, dans une direction opposée à celle de l'éclairage par le dispositif suivant, bien centré autour d'un axe perpendiculaire à celui du tuyau (Fig. 1). Une lentille L donne du court filament S d'une lampe (6 V, 100 W) une image au voisinage de l'axe du tuyau à travers la glace F. Les poussières qui s'y trouvent envoient de la lumière par diffraction à travers la glace G vers l'objectif à long foyer (3 à 4 cm) d'un microscope. L'écran E, placé près de la lentille L, dimensionné pour le diaphragme D de l'objectif du microscope, empêche la lumière, venant directement de S et non diffractée, d'atteindre l'objectif et d'aveugler l'observateur. Les poussières sont vues comme des points brillants sur fond noir quand l'air ne vibre pas et sous forme de bâtonnets ou d'ellipses quand le téléphone est alimenté.

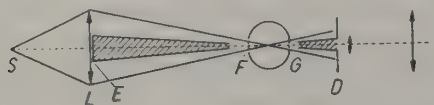

Fig. 1.

Les mesures directes se font au moyen d'un oculaire micrométrique; elles sont rendues pénibles par le déplacement des poussières qu'il faut réduire au minimum: étanchéité absolue du tuyau et éclairement modéré (sauf à l'instant des photographies).

Celles-ci s'obtiennent en adjoignant au microscope une chambre noire. Une pose de 0,015 s est suffisante pour une fréquence de 100 p/s.

Lorsqu'on observe ou photographie des ellipses dont on veut connaître le sens de parcours, il faut une lentille convergente supplémentaire donnant une image réelle de S, qu'on peut éclipser périodiquement au moyen d'une lame vibrante. Celle-ci est alimentée par le courant ordinaire que l'on peut déphaser dans un sens connu au moyen d'une self.

Beaucoup de mesures sont complétées par l'observation au moyen de capsules manométriques actionnant un miroir. Elles sont mises en communication avec le tuyau sonore par un tube dont la longueur est telle que le branchement ne modifie pas le mouvement vibratoire. Chaque capsule porte en son centre un petit cône de moelle de sureau qui agit sur une légère feuille de papier, mobile le long de sa ligne d'attache et qui porte le miroir (Fig. 2). Les déformations de la membrane sont ainsi amplifiées. La sensibilité de ce système demande que le point d'application du sommet du cône soit près de la ligne d'attache. Mais, d'autre part, il faut que ce point soit aussi approximativement au centre de percussion. Il faut prendre un miroir de petites dimensions (2 ou 3 mm) pour qu'il puisse être assez près de l'axe (ligne d'attache du papier).

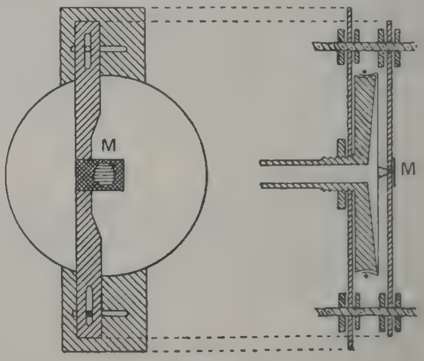

Fig. 2.

Une source lumineuse ponctuelle est vue dans une lunette après réflexion sur le miroir sous forme de bâtonnet perpendiculaire à l'axe du miroir; la longueur de ce bâtonnet est proportionelle à l'amplitude des variations de pression au lieu de branchement. Avec deux capsules disposées de telle sorte que les axes des miroirs soient perpendiculaires, la source apparaît, après deux réflexions, sous la forme d'une ellipse de Lissajous qui donne les amplitudes des deux mouvements et leur différence de phase φ par la relation:

$$\sin \varphi = ab/AB,$$

a et b sont les axes de l'ellipse, A et B les amplitudes des mouvements vibratoires (côtés du rectangle dans lequel est inscrite l'ellipse). La détermination précise de φ est faite par le spectroscope à lame vibrante.

De même lorsque les poussières forment des ellipses on peut dire que le mouvement de l'air qu'elles représentent est dû à deux composantes rectangulaires dont on a facilement les amplitudes et la différence de phase.

3. Branchement latéral

Parmi les discontinuités étudiées, je parlerai seulement d'une dérivation branchée au ventre et des obstacles solides ventraux.

Pour le branchement, disons d'abord que l'angle n'intervient pas; les phénomènes sont les mêmes pour une dérivation en T ou pour une dérivation en Y (Fig. 3 et 4).

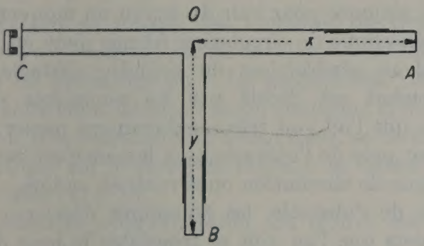

Fig. 3.

On fait varier les longueurs des deux branches. Pour tracer une courbe (phase ou amplitude) on donne à x = OA une valeur paramétrique constante et l'on fait varier y = OB. On recommence pour d'autres valeurs de x.

La différence de phase φ entre A et B varie au moins de + 120° à — 120° suivant la Fig. 5 où φ sert de paramètre ou de côte pour les courbes dites de niveau. On voit qu'il y a concordance de phase lorsque les longueurs x et y sont égales; A et B sont alors en opposition de phase avec C (téléphone). Lorsque A et B ne sont plus en phase, la différence entre A et B se partage suivant les signes entre A et C d'une part, B et C d'autre part.

Il existe dans l'ensemble du tuyau une onde quasi-stationnaire, unique entre C et O, qui se divise entre OA et OB. Si l'une des branches OA ou OB a une longueur trop différente d'un quart de longueur d'onde, le mouvement a lieu entre OC et OA ou entre OC et OB exclusivement, suivant les cas.

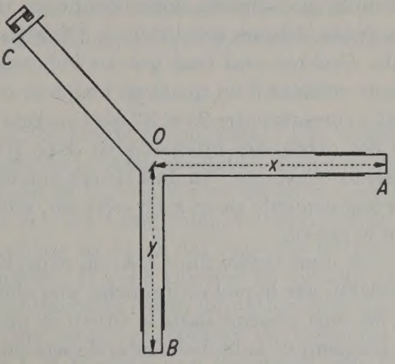

Fig. 4.

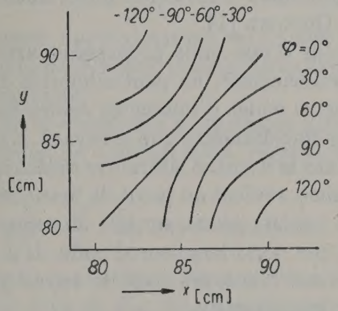

Fig. 5.

Les mesures d'amplitudes montrent un changement rapide de la répartition des intensités; par exemple, l'amplitude diminue dans le rapport de 19 à 12 pour la branche OA lorsque la longueur de OB varie seulement de 2 cm, ce qui représente pour l'énergie une diminution de 361 à 144, soit de plus de moitié. Il s'en suit que si l'une des longueurs OA ou OB s'éloigne de quelques centimètres seulement d'un quart de longueur d'onde, l'autre gardant cette valeur, la quasi totalité de l'énergie se trouve dans la deuxième. La branche latérale joue le rôle de filtre.

Cependant, une ouverture au ventre avec adjonction d'une cheminée, ne devrait pas permettre à l'air contenu dans celle-ci d'entrer en vibration, puisqu'au point de branchement il n'y a pas de variation de pression (ventre). En réalité, l'ouverture n'est pas ponctuelle et intéresse une longueur trop grande pour admettre en face de l'ouverture tout entière l'absence de variations de pression. Et aussi l'onde n'est certainement pas stationnaire pure. On se rapprocherait des conditions idéales avec une intensité beaucoup plus faible, mais alors les mesures ne sont plus possibles.

L'ensemble se comporte donc comme un résonateur: pour un volume total donné, l'énergie reste constante. Ceci est vrai tant que les longueurs OA et OB sont voisines d'un quart de longueur d'onde. Pour x et y compris entre 85 et 87 cm l'énergie totale (somme des carrés des intensités en A et B) reste sensiblement constante. Au delà de ces valeurs, elle diminue rapidement; pour $x=y=80$ cm, elle n'est plus que le quart.

Si au lieu d'un tuyau fini COA, on considère un tuyau indéfini sur lequel on branche une cheminée fermée, les sons passant dans le tuyau et pour lesquels la longueur de la branche latérale sera un quart de longueur d'onde, seront supprimés dans la suite du tuyau principal. C'est l'effet filtre, mentionné et réalisé par QUINCKE [1].

Dans le cas d'une onde progressive arrivant au point de branchement, on peut admettre qu'elle se divise en deux ondes d'intensités égales (si la cheminée a le même diamètre que le tuyau). L'onde qui a pénétré dans la branche latérale se réfléchit au fond de la cheminée, revient au point de branchement où elle rejoint l'autre, ayant sur elle un retard correspondant à une demi-longueur d'onde. Il n'y a plus de mouvement vibratoire dans le tuyau principal à partir du branchement.

4. Obstacles ventraux

Il s'agit toujours du même tuyau sonore, sans branchement latéral, dont les distances OC et OA sont telles que l'amplitude donnée par une capsule branchée en A soit maxima et que l'on ait un ventre au lieu d'observation (maximum de longueur des bâtonnets). L'ouverture au ventre, utilisée précédemment, est fermée de façon étanche par un bouchon portant les différents obstacles que l'on veut y placer. Il est possible, de l'extérieur, d'orienter convenablement l'obstacle et de le mettre à la hauteur voulue.

Ces obstacles sont cylindriques, les génératrices étant perpendiculaires à l'axe du tuyau de manière que le phénomène soit à deux dimensions: l'axe du tuyau et une direction perpendiculaire à celui-ci et à la direction d'observation.

Ils sont assez petits par rapport au diamètre du tuyau pour ne pas modifier sensiblement l'état vibratoire.

J'ai successivement étudié: des fils métalliques rectilignes dont le diamètre variait de 0,1 à 1,6 mm; des demi-cylindres pleins ou creux; des lames à section rectangulaire, l'épaisseur variant de 0,15 à 25 mm; des obstacles en forme de V ou de U; une grille à fils parallèles; une fenêtre rectangulaire; etc.

Pour une amplitude assez grande — pour fixer les idées, supérieure à 0,5 mm — au voisinage de toute discontinuité, assez marquée, créée par l'obstacle, les poussières décrivent des ellipses fixes, que nous appellerons stationnaires; cela, parce qu'elles persistent fort longtemps, immuables comme forme et comme position, dans le champ du microscope. Elles sont toutes égales entre elles et alignées le long d'une génératrice qu'elles touchent presque par une de leurs extrémités. Pour une injection abondante d'amidon, on en voit un très grand nombre qui se projettent l'une sur l'autre, ce qui rend l'observation très difficile. Il suffit alors de donner un coup sec sur le tuyau pour en détacher quelques unes; elles reviennent peu à peu, mais il est possible d'observer et de photographier tant qu'il n'y a qu'une poussière pour former l'ellipse stationnaire. Il n'est pas rare que plusieurs poussières s'agglutinent en une seule particule plus grosse dont la trajectoire est alors plus lumineuse et convient bien à la photographie. Il s'agit d'une véritable agglutination de mobiles et non pas de leur poursuite le long d'une même trajectoire.

Le sens de parcours des ellipses, sur l'arc le plus voisin de l'obstacle, va du corps de l'obstacle vers l'arête ou vers la génératrice du cylindre qui en tient lieu.

Au mouvement vibratoire engendré par le téléphone, s'ajoute pour l'air du tuyau un mouvement non périodique de circulation fermée dans un plan normal au génératrices du cylindre obstacle. Ce mouvement est décelé par les poussières elles-mêmes que l'on voit très régulièrement passer puis repasser près de l'obstacle sans jamais s'arrêter sur leur ligne de circulation ou revenir en arrière.

Loin de l'obstacle, les poussières décrivent des bâtonnets que l'on voit se translater le long de la ligne de circulation. Plus près, la trajectoire périodique est une ellipse (non stationnaire) qui se translate également.

La circulation peut se définir par des ovales, emboîtés les uns dans les autres, qui passent tous entre l'ellipse stationnaire et l'obstacle, où ils forment un réseau de lignes très denses; tandis que, loin de l'obstacle, les lignes laissent entre elles un plus grand intervalle. Conséquemment, la vitesse de circulation est plus petite au loin, très grande entre l'ellipse stationnaire et l'obstacle, où ni bâtonnets ni ellipses ne sont visibles. L'ellipse stationnaire semble la ligne limite de circulation, ligne périodique celle-là. Aucune poussière n'est visible à l'intérieur; celles qui s'y trouvent accidentellement sont entraînées sur l'ellipse et s'y agglutinent à la poussière qui s'y trouve déjà.

Le grand axe des ellipses stationnaires est égal ou upérieur à la longueur des bâtonnets. Il en résulte que ces ellipses sont placées en un point où l'amplitude du mouvement (ou de la vitesse) est maximum.

Les ellipses, au voisinage d'obstacles sont dûes à 'existence d'une onde diffractée. Le cas le plus simple est celui d'un fil à section circulaire. Le problème est à deux dimensions. Prenons comme coordonnées polaires la trace, dans le plan d'observation, de l'axe du fil et une parallèle à l'axe du tuyau sonore [2].

Le potentiel complexe correspondant à l'onde diffractée doit satisfaire à l'équation aux dérivées partielles:

$$\frac{1}{a^2}\frac{\partial^2\psi}{\partial t^2}=\frac{\partial^2\psi}{\partial r^2}+\frac{1}{r}\frac{\partial\psi}{\partial r},$$

a étant la vitesse du son dans le tuyau. Si l'on pose:

$$\psi=\psi_1\,e^{ikat} \text{ où } k=2\pi/\lambda=2\pi N/a,$$

ψ_1 doit vérifier l'équation:

$$\Delta\psi_1+k^2\psi_1=0.$$

Enfin, si ψ_1 est décomposé en série de Fourier, série de cosinus à cause de la symétrie du phénomène, on aura pour les différents coefficients B_n de cette série les équations différentielles:

$$\frac{d^2B_n}{dr^2}+\frac{1}{r}\frac{dB_n}{dr}+\left(k^2-\frac{n^2}{r^2}\right)B_n=0,$$

qui s'intègre au moyen des fonctions de Bessel. Celles-ci s'exprimeront par un développement limité suivant les puissances de r. Le potentiel de l'onde stationnaire étant donné de façon analogue, la détermination des constantes d'intégration se fera en écrivant que sur le cercle de rayon c, la vitesse est tangentielle ($V_r=0$).

En première approximation, on trouve comme expressions des composantes de la vitesse:

$$\frac{1}{k}V_r=-2\left(1-\frac{c^2}{r^2}\right)\cos\theta\sin kat,$$

$$\frac{1}{k}V_\theta=-2\left(1+\frac{c^2}{r^2}\right)\sin\theta\sin kat.$$

Ce résultat fait retrouver les composantes de la vitesse pour un écoulement continu, de vitesse uniforme au loin et égale à $2k$, avec un obstacle constitué par un cylindre circulaire immergé. Ces formules ne conviennent pas: pas d'ellipses et pas de maximum pour la vitesse $V=\sqrt{V_r^2+V_0^2}$.

Il est certain que les expériences sont faites dans des conditions trop éloignées de celles des petits mouvements et, par conséquent, on ne peut se limiter aux premiers termes. Pour une amplitude de 0,2 mm, celle des pressions est de 500 baryes, celle de la vitesse de 125 mm/s.

Dans le cas d'un écoulement constant avec un obstacle cylindrique, on fait intervenir le nombre de Reynolds:

$$R=Vc/\nu,$$

V étant la vitesse de l'écoulement, ν le coefficient cinématique de viscosité du fluide. Pour une vitesse d'écoulement de 12,5 cm/s, $c=0{,}05$ cm et $\nu=0{,}14$ C.G.S., on a $R=4{,}3$. Cette valeur est trop grande pour que l'on puisse se servir des formules de première approximation. Il y a à l'arrière du cylindre (alternativement des deux côtés) formation de deux tourbillons. Pour avoir un nombre de Reynolds plus petit que 1, il faudrait une amplitude plus faible, pour laquelle d'ailleurs, il n'y a pas d'ellipses stationnaires.

En deuxième approximation, on trouve des formules donnant des ellipses, mais inutilisables à cause de leur complexité.

En partant des formules de première approximation, les lignes de courant sont représentées par l'équation:

$$V_0\left(r-\frac{a^2}{r}\right)\sin kat=\text{constante}.$$

Ces lignes sont symétriques par rapport à l'axe polaire comme dans la Fig. 6A. L'expérience montre qu'il y a dissymétrie comme l'indique la figure suivante 6B. La ligne passe plus près de l'obstacle du côté où le fluide l'aborde que du côté où le fluide s'en éloigne. Pour le mouvement vibratoire et pour son effet permanent, il faut superposer les deux sortes de lignes, ce qui donne la Fig. 6C; des deux côtés de l'obstacle, les lignes séparées dessinent une courbe fermée sur laquelle la circulation a le sens observé dans les ellipses stationnaires. L'inertie des poussières entraînées est assez grande pour transformer en ellipse la courbe à deux rebroussements.

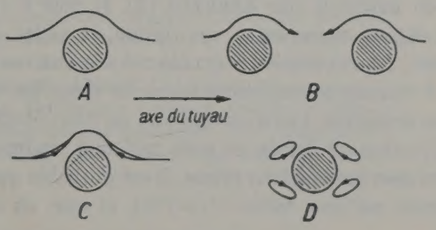

Fig. 6.

Il reste que, pour obtenir une expression mathématique du potentiel complexe et des lignes de courant il faut faire intervenir un tourbillon à l'emplacement de chaque ellipse stationnaire. Pour que les lignes de courant rendent compte de la forme de l'obstacle, on utilise une représentation conforme convenable.

5. Autres circulations

Des fils cylindriques parallèles, disposés sur le fond du tuyau, perpendiculairement à l'axe, donnent eux aussi des ellipses stationnaires et les mêmes phénomènes de circulation. Il n'y a pas de différence essentielle entre ces «rides artificielles» et les rides de Kundt.

Dans ce dernier cas, l'origine de ces entassements sélectifs peut être attribuée à un maximum de poussières accidentellement réalisé. Au contact de la paroi du tuyau le mouvement de l'air est nul; à une petite distance (2 mm au plus) [3] il est le même qu'au voisinage de l'axe. Il suffit de la présence d'un obstacle pour donner naissance à des mouvements tourbillonnaires dont les rides sont la manifestation.

On obtient des rides à partir des fils cylindriques parallèles sur le fond du tuyau au moyen de poussières de moelle de sureau. Les rides restent sur les fils, même pour des amplitudes correspondant à un écartement plus grand. Lorsque l'espacement qu'auraient les rides si elles étaient libres s'approche du double de la distance des fils, une ride sur deux disparait. Il y a donc une grande tolérance pour l'espacement des rides.

Les mouvements des poussières de sureau sur les rides ne sont pas périodiques mais participent à une circulation analogue à celle déjà étudiée. Un potentiel convenable peut en rendre compte: série de tourbillons et leurs images par rapport au fond du tuyau.

Lord Rayleigh, dans sa «Theory of Sound» [4], se basant sur des équations de propagation faisant intervenir la viscosité de l'air, trouve pour un tuyau contenant de l'air en vibration un terme correspondant à une circulation générale non périodique, allant des ventres aux noeuds le long des parois et en sens inverse le long de l'axe. Cette circulation a été mise en évidence par Andrade [5]. Il doit y avoir une relation entre cette circulation et celles déjà étudiées. La circulation Rayleigh-Andrade est difficile à retrouver expérimentalement dans les conditions actuelles. Les mouvements de l'air, étudiées par injection de fumée ne sont pas nets, malgré de nombreuses précautions prises. Il est probable que la fréquence est trop faible ($N=100$), et que, en conséquence, la longueur de la circulation (85 cm) trop grande.

Une circulation analogue s'établit facilement entre deux couronnes ayant un diamètre extérieur égal à celui du tuyau, placées perpendiculairement à l'axe, au voisinage du ventre. Ces couronnes ont 3 mm de largeur; leur écartement, variable, peut aller jusqu'à 10 cm sans que la circulation disparaisse. L'espace qui les sépare comporte deux tronçons égaux. La circulation va du milieu de cet espace vers les couronnes le long de la paroi et en sens inverse le long de l'axe. Il se peut que dans le cas d'une trop grande longueur comme c'est le cas pour notre tuyau, la circulation de Rayleigh se fractionne en plusieurs parties.

L'appareillage mentionné permet une analyse détaillée du mouvement vibratoire dans un milieu sonore. L'emploi simultané de photographies de poussières d'amidon et de capsules sert à comparer les résultats, à peu près toujours concordants.

Il serait possible d'étendre ce genre de recherches à d'autres volumes contenant de l'air en vibration et à d'autres fréquences.

On met en particulier en évidence par cette méthode les différentes circulations apériodiques dans un milieu en vibration. Ces phénomènes montrent que la théorie élémentaire n'est pas suffisante pour des intensités non très petites et pour un fluide non parfait[1].

(Reçu le 11 Février 1952.)

---

[1] Dans un article dont nous n'avons eu connaissance qu'après la rédaction de ce mémoire, G. D. WEST étudie (Proc. phys. Soc. **64**B [1951], 483) des phénomènes de circulation se produisant autour d'une lame vibrante, et qui se rattachent à ceux traités par CARRIÈRE et par ANDRADE; sur ces points particuliers, ses résultats sont analogues aux nôtres. (Note ajoutée le 20 Juin 1952.)

Références

[1] QUINCKE, G., Ann. Phys. (Poggendorf) **128** [1866], 177.

[2] LORD RAYLEIGH, Theory of sound. Macmillan, London 1929, Vol. II, p. 340.

[3] CARRIÈRE, Z., Analyse ultramicroscopique des vibrations aériennes. J. Phys. (6) **10** [1929], 198.

[4] LORD RAYLEIGH, Theory of sound. Macmillan, London 1929, Vol. II, p. 297.

[5] ANDRADE, E. N. da C., Roy. Soc. phil. Trans. A **230** [1932], 413; Roy. Soc. Proc. A **134** [1931], 445.

International Electro-acoustics Congress 1953 in the Netherlands

This Congress, under official sponsorship of the International Commission on Acoustics, has first been announced in Acustica 2 [1952], 96. A brochure has just been published, giving the organizational outlines and a description of the 7 sections and their scope.

Copies of this leaflet will be sent on request.

The organizing secretary
P. A. de Lange
Mijnbouwplein 11, Delft, Netherlands